

DETECTION, MAPPING AND CLASSIFICATION OF CRUDE OIL IN DRILL CORE USING HYPERSPETRAL IMAGERY

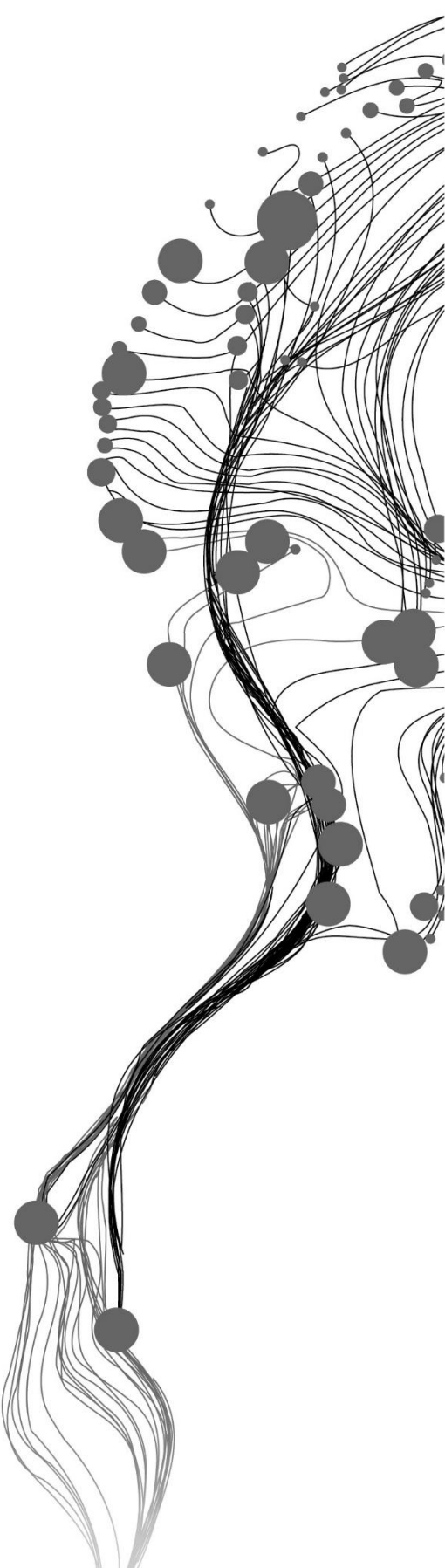
SHANAN D'SILVA

July 2024

SUPERVISORS:

Dr. Frank van Ruitenbeek

Wim H. Bakker MSc



DETECTION, MAPPING AND CLASSIFICATION OF CRUDE OIL IN DRILL CORE USING HYPERSPPECTRAL IMAGERY

SHANAN D'SILVA

Enschede, The Netherlands, July 2024

Thesis submitted to the Faculty of Geo-Information Science and Earth Observation of the University of Twente in partial fulfilment of the requirements for the degree of Master of Science in Geo-information Science and Earth Observation.

Specialization: Applied Remote Sensing for Earth Sciences

SUPERVISORS:

Dr. Frank van Ruitenbeek

Wim H. Bakker MSc

THESIS ASSESSMENT BOARD:

Dr. Harald van der Werff (Chair)

Dr. Fred Beekman (External Examiner, Utrecht University)

DISCLAIMER

This document describes work undertaken as part of a programme of study at the Faculty of Geo-Information Science and Earth Observation of the University of Twente. All views and opinions expressed therein remain the sole responsibility of the author, and do not necessarily represent those of the Faculty.

ABSTRACT

Oil, a complex mixture of hydrocarbons, is a crucial energy resource and industrial commodity with a wide range of applications, from powering transportation to serving as the foundation for various chemical products. Understanding its spatial distribution within drill cores is essential for optimizing drilling strategies and targeted exploration efforts, such as horizontal drilling and hydraulic fracturing. Beyond exploration, mapping the oil concentration in drill cores provides valuable insights into the porosity and permeability of different lithologies, which is critical for enhancing fluid flow in geothermal reservoirs. Additionally, identifying impermeable caps in hydrocarbon reservoirs is vital for effective carbon storage. Previous studies on oil in drill cores have primarily focused on the Alberta region of Canada, known for bituminous oils. These studies use uncemented drill cores containing heavy, viscous oil and minerals such as smectite, quartz, and clays, which have non-overlapping absorption features with oil. This study, however, addresses the detection, mapping, and classification of oil and minerals in drill cores from Dutch hydrocarbon reservoirs, which contain lighter oils and minerals such as clays, carbonates, and evaporites, whose absorption features overlap with those of oil.

Two datasets were utilized in this study. The first dataset comprised pure oil samples, which served as a training set to determine the spectral properties of oil in the VNIR, SWIR, and TIR ranges. The second data set consisted of two drill cores, differentiated based on their mineral composition and the type of oil they contain. The first drill core contains transparent oil with minerals like kaolinite, gypsum, calcite, quartz, and hematite, while the second drill core contains heavy oil along with minerals like kaolinite and quartz. The understanding obtained from measuring and comparing the spectra of the oil samples was then applied to detect, map, and classify oil and minerals within the drill core. Oil detection was achieved independently through the UV fluorescence property of oils, confirming the presence of oil in both the drill cores. Furthermore, the mapping of oil and minerals in a drill core was achieved using techniques like Hydrocarbon Index, Spectral Angle Mapper, and Minimum Wavelength Mapper. The existing Hydrocarbon Index was modified to include another significant oil feature, resulting in improved accuracy and reduced noise. The Spectral Angle Mapper and Minimum Wavelength Mapper were applied over specific wavelength ranges, differing from previous studies that applied SAM over the full range. The ranges of 1.65 μm to 1.85 μm and 2.3 μm to 2.36 μm were identified as optimal for mapping oil in the drill core. These specific ranges highlighted by this study helped to better map the spatial distribution of the oil and minerals. Additionally, the mapping techniques used also reflected the relative concentration of oil within the drill cores.

This study also aimed to classify the oil in the drill cores based on the functional groups present in the oil. Hydrogen and carbon are the most abundant elements in oil, making their absorption features more prominent compared to those of nitrogen, oxygen, and sulphur. The functional groups formed by these elements are best differentiated in the TIR range, while the SWIR and VNIR range only show major absorption features due to C-H bonds and minor absorption features due to the O-H and N-H bonds. When present in a drill core, these minor absorption features of oil are masked by the other minerals or water present. Thus, the study reveals that classifying the oil in the drill core based on the functional groups is not possible from the VNIR and SWIR spectra. Lastly, this study provides a prototype workflow to detect and map the oil and minerals in a drill core.

Keywords: Oil concentration, functional groups, wavelength mapping, UV fluorescence, transparent oil

ACKNOWLEDGEMENTS

The journey I have undertaken has been a profound blend of personal growth and scientific discovery. I am immensely thankful for the chance to explore the vast expanse of knowledge. I deeply appreciate the inspiration, support, and guidance of all those who have played a pivotal role in completing this research.

I extend my heartfelt gratitude to my supervisors, Frank van Ruitenbeek and Wim Bakker, for their support and guidance throughout this year-long journey, which has been instrumental in successfully completing my MSc research. I would also like to thank my chair, Harald van der Werff, for his support and generously providing knowledge and expertise during the proposal defence and mid-term presentation, both of which were crucial to the completion of this research. Special thanks go to ITC Geoscience laboratory assistants Kathrin Zweers-Peter and Camilla Marcatelli for their help with the various laboratory measurements.

Lastly, I would like to thank my parents and my sister. Their faith in me has sustained my spirit and motivation throughout this process. I am also grateful to everyone else who, in various ways, supported this research. It is with immense pleasure and deep gratitude that I acknowledge the help of these individuals.

TABLE OF CONTENTS

1.	Introduction.....	1
1.1.	Background.....	1
1.1.1.	Crude Oil Formation and Importance	1
1.1.2.	Importance of understanding Oil distribution in Drill Cores.....	1
1.1.3.	Classification of Crude Oil	2
1.1.4.	Spectral Properties of Crude Oil	2
1.1.5.	Crude Oil Reservoirs in the Netherlands.....	4
1.2.	Research Gap	5
1.3.	Research Problem.....	6
1.4.	Research Objectives	7
2.	Datasets and Methodology.....	8
2.1.	Datasets	8
2.1.1.	Crude Oil Samples	8
2.1.2.	Drill Cores.....	9
2.2.	Methodology	11
2.2.1.	Oil Samples	11
2.2.2.	Drill Core.....	16
3.	Results.....	19
3.1.	Measurements of the Oil Samples.....	19
3.1.1.	TIR Measurements	19
3.1.2.	VNIR-SWIR Measurements	21
3.1.3.	Measurements with respect to Thickness of Oil layer	23
3.1.4.	Comparing the Spectra of Oil and Minerals.....	26
3.1.5.	UV Fluorescence Measurements.....	31
3.1.6.	VNIR-SWIR Imaging Measurements.....	32
3.2.	Measurements on the Drill Cores.....	34
3.2.1.	UV Fluorescence Measurements.....	34
3.2.2.	VNIR-SWIR Point Spectral Measurements	35
3.2.3.	VNIR-SWIR Imaging Measurements.....	36
3.2.4.	TIR Measurements	49
4.	Discussion.....	50
4.1.	Characterization of the Oil Samples	50
4.2.	Influence of the Oil Layer Thickness	52
4.3.	Comparing the Spectra of Oil and Minerals	52
4.4.	Composition of the Drill Cores	53
4.5.	Techniques to map the Oil and Minerals in the Drill Core	54
4.6.	Comparison of Mapping Methods	57
4.7.	Implications for the Prototype Workflow	58
5.	Conclusion	62
5.1.	Conclusion	62
5.2.	Recommendations.....	63
6.	Ethical Considerations, Risks and Contingencies.....	64
	List of References	65
	Appendix.....	70

LIST OF FIGURES

Figure 1.1 Absorption spectrum of light crude oil, highlighting the absorption regions of the C-H bond overtones and combination tones in the SWIR range (Source: Alves & Poppi, 2015).	3
Figure 1.2 Distribution of oil and gas fields in the Netherlands. The black circle marks the area from where the drill core used in this study has been obtained, which lies in the Broad Fourteens Basin (Source: de Jager & Geluk, 2007)	5
Figure 2.1 The three oil samples that were used in this study.	8
Figure 2.2 Photograph of Drill Core 1	9
Figure 2.3 Photograph of Drill Core 2.	10
Figure 2.4 Setup of the VNIR-SWIR Point Spectroscopy	12
Figure 2.5 Diagrammatic representation of the light ray recorded by the spectrometer after interacting with the oil, glass and white reference. Here I- incident ray, L- reflected ray, T- transmittance and R- reflectance, o- oil, g- glass and wr- white reference.	13
Figure 2.6 Spectra of the glass (petri dish) and oil recorded over a white reference (WR) and dark surface (DR).....	13
Figure 2.7 Setup used to record the fluorescence spectra.	15
Figure 2.8 Setup of the oil-soaked sandstones and the unsoaked sandstone which were then scanned by the Specim cameras. The black and yellow squares mark the region from which the spectra were taken in section 3.2.3.....	15
Figure 2.9 Relation between the absorption feature minimum at B and the two shoulders at A and C that is used to generate the Hydrocarbon Index (HI) (modified from Kühn et al. (2004))......	17
Figure 3.1 TIR spectra of the three oil samples.	19
Figure 3.2 VNIR-SWIR spectra of the three oil samples.	21
Figure 3.3 Spectra of the very light oil with increasing thickness.....	23
Figure 3.4 Graph showing the thickness vs depth relation of the very light oil at a)1.724 μm and b) 2.308 μm	24
Figure 3.5 Spectra of the light oil with increasing thickness.	25
Figure 3.6 Graph showing the thickness vs depth relation of the light oil at a)1.724 μm and b) 2.308 μm	25
Figure 3.7 Graph showing the interpolated minimum wavelength of the four deepest absorption features in the range of 1.100 μm to 1.650 μm	26
Figure 3.8 Graph showing the interpolated minimum wavelength of the four deepest absorption features in the range of 1.650 μm to 1.850 μm	27
Figure 3.9 Graph showing the interpolated minimum wavelength of the four deepest absorption features in the range of 1.850 μm to 2.100 μm	27
Figure 3.10 Graph showing the interpolated minimum wavelength of the four deepest absorption features in the range of 2.100 μm to 2.500 μm	28

Figure 3.11 Spectral Angle Matrix showing the spectral angle similarity of the minerals and oil in the range of 1.100 μm to 1.650 μm .	29
Figure 3.12 Spectral Angle Matrix showing the spectral angle similarity of the minerals and oil in the range of 1.650 μm to 1.850 μm .	29
Figure 3.13 Spectral Angle Matrix showing the spectral angle similarity of the minerals and oil in the range of 1.850 μm to 2.100 μm .	30
Figure 3.14 Spectral Angle Matrix showing the spectral angle similarity of the minerals and oil in the range of 2.100 μm to 2.400 μm .	30
Figure 3.15 Fluorescence spectra of the unsoaked sandstone and the sandstone soaked with the three oil samples, with the inset focusing on the unsoaked sandstone and very light oil.	31
Figure 3.16 Photograph of the unsoaked sandstone (S) along with the sandstone soaked with very light oil (VO), light oil (LO) and heavy oil (HO).	31
Figure 3.17 Spectra of the oil soaked sandstone recorded by the Specim camera in the SWIR range. The thinnest line represents 0.25 ml, the medium thick line represents 0.5 ml, and the thickest line represents 1.0 ml of oil in the sandstone.	32
Figure 3.18 Spectra of the oil soaked sandstone recorded by the Specim camera in the VNIR range. The thinnest line represents 0.25 ml, the medium thick line represents 0.5 ml, and the thickest line represents 1.0 ml of oil in the sandstone.	33
Figure 3.19 Fluorescence Spectra of (a) Drill Core 1 and (b) Drill Core 2.	34
Figure 3.20 Spectra of the oil (A), gypsum (B), kaolinite (C) and hematite (D) present in Drill Core 1 as revealed by point spectral analysis.	35
Figure 3.21 Spectra of the oil (B) and kaolinite (A and C) present in Drill Core 2 as revealed by point spectral analysis.	35
Figure 3.22 VNIR spectra of Drill Core 1 showing the broad absorption features of hematite.	36
Figure 3.23 VNIR spectra of Drill Core 2 showing the absorption due to quartz (A and D) and oil (B and C).	36
Figure 3.24 SWIR spectra of Drill Core 1 showing the mix spectra of oil (A), gypsum (B), kaolinite (C), and hematite (D).	37
Figure 3.25 SWIR spectra of Drill Core 2 showing the mix spectra of oil (B and C) and kaolinite (A and D).	37
Figure 3.26 Hydrocarbon Index applied to Drill Core 1 at 1.7 μm and 2.3 μm .	38
Figure 3.27 Hydrocarbon Index applied to Drill Core 2 at 1.7 μm and 2.3 μm .	38
Figure 3.28 SAM rule image of Drill Core 1 in the range of 1.1 μm to 1.65 μm .	39
Figure 3.29 SAM rule image of Drill Core 1 in the range of 1.65 μm to 1.85 μm .	39
Figure 3.30 SAM rule image of Drill Core 1 in the range of 1.85 μm to 2.1 μm .	40
Figure 3.31 SAM rule image of Drill Core 1 in the range of 2.1 μm to 2.4 μm .	40
Figure 3.32 SAM rule image of Drill Core 2 in the range of 1.1 μm to 1.65 μm .	41

Figure 3.33 SAM rule image of Drill Core 2 in the range of 1.65 μm to 1.85 μm	41
Figure 3.34 SAM rule image of Drill Core 2 in the range of 1.85 μm to 2.1 μm	42
Figure 3.35 SAM rule image of Drill Core 2 in the range of 2.1 μm to 2.4 μm	42
Figure 3.36 Minimum wavelength map of Drill Core 1 in the range 1.1 μm to 1.65 μm	43
Figure 3.37 Minimum wavelength map of Drill Core 1 in the range 1.65 μm to 1.85 μm	43
Figure 3.38 Minimum wavelength map of Drill Core 1 in the range 1.85 μm to 2.1 μm	44
Figure 3.39 Minimum wavelength map of Drill Core 1 in the range 2.1 μm to 2.4 μm	44
Figure 3.40 Minimum wavelength map of Drill Core 1 in the range 2.185 μm to 2.225 μm	45
Figure 3.41 Minimum wavelength map of Drill Core 1 in the range 2.3 μm to 2.36 μm	45
Figure 3.42 Minimum wavelength map of Drill Core 2 in the range 1.1 μm to 1.65 μm	46
Figure 3.43 Minimum wavelength map of Drill Core 2 in the range 1.65 μm to 1.85 μm	46
Figure 3.44 Minimum wavelength map of Drill Core 2 in the range 1.85 μm to 2.1 μm	47
Figure 3.45 Minimum wavelength map of Drill Core 2 in the range 2.1 μm to 2.4 μm	47
Figure 3.46 Minimum wavelength map of Drill Core 2 in the range 2.185 μm to 2.225 μm	48
Figure 3.47 Minimum wavelength map of Drill Core 2 in the range 2.3 μm to 2.36 μm	48
Figure 3.48 TIR spectra of the powdered samples from Drill Core 1.....	49
Figure 3.49 TIR spectra of the powdered samples from Drill Core 2.....	49
Figure 4.1 Flowchart of the workflow to detect (step 1) and map (step 2) the oil in drill cores.....	59

LIST OF TABLES

Table 1.1 Fundamental vibrations, first overtones, and second overtones of the vibrational bonds of molecules present in crude oil and its associated functional groups. The ranges in blue correspond to TIR spectra, those in yellow to SWIR spectra, and the ranges in green to VNIR spectra (Modified from: Asemani & Rabbani, 2020; Kiefer & Corsetti, 2017; Smith, 1998).	4
Table 2.1 Instruments used and their wavelength range.	11
Table 3.1 Maximum wavelength of the absorption features of the three oil samples and the corresponding functional group that causes the absorption features in the infrared range.	20
Table 3.2 Minimum wavelength of the absorption features of the three oil samples and the corresponding vibrational bonds that cause the absorption features in the SWIR range. c refers to combination, while 1o and 2o refer to the first and second overtone.	22
Table 4.1 Summary of the methods used to map the spatial distribution of oil in a drill core. Green indicates suitable for mapping while red indicates not suitable for mapping for the given method, wavelength range, oil concentration and drill core mineral composition. Yellow indicates the suitability needs to be tested, which was not covered in this study.	61

ABBREVIATIONS

API	American Petroleum Institute
ASD	Analytical Spectral Devices
ASTER	Advanced Spaceborne Thermal Emission and Reflection
ATR	Attenuated Total Reflectance
DC1	Drill Core 1
DC2	Drill Core 2
FTIR	Fourier Transform Infrared
HI	Hydrocarbon Index
H.Oil	Heavy Oil
HypPy	Hyperspectral Python
L.Oil	Light Oil
SAM	Spectral Angle Mapper
SWIR	Short Wave Infrared
TBC	Total Bitumen Content
TIR	Thermal Infrared
UV	Ultraviolet
V.Oil	Very Light Oil
VNIR	Visible and Near Infrared

1. INTRODUCTION

1.1. Background

1.1.1. Crude Oil Formation and Importance

Crude oil, also referred to as petroleum or black gold, is a type of fossil fuel. It is formed through the decomposition of organic matter, such as algae and plants residing in shallow seas, which mixes with sediments and, when subjected to high pressure and temperature, gradually transforms into fossil fuels over millions of years (Tissot & Welte, 1984). Since its commercial utilization in the 19th century, oil has played an important role in shaping modern civilisation (Altawell, 2021). Society relies on oil for its economic, social, and environmental progress (Hall et al., 2003).

The global consumption of oil is dominated by the transportation sector, with significant usage also observed in the manufacturing industry, power generation, residential and commercial heating, and the petrochemical industry (EIA, 2023). With the ongoing energy transition, crude oil plays an important role as a transitional resource by acting as a bridge to facilitate a smooth and sustainable shift from fossil fuels to renewable energy sources, ensuring energy security and economic stability during this transformative period. However, it is essential to note that despite advancements in renewable energy, crude oil remains irreplaceable in certain sectors due to its unique properties and established infrastructure (Insights, 2023).

1.1.2. Importance of understanding Oil distribution in Drill Cores

The importance of drill cores in oil exploration cannot be overstated, given the critical role of crude oil in various industries. Information derived from drill cores is indispensable for the extraction and production processes. Understanding the spatial distribution of oil within a drill core is crucial for identifying optimal drilling locations and guiding targeted exploration efforts, such as horizontal drilling and hydraulic fracturing (Canadian Association of Petroleum Producers, 2019). These techniques not only facilitate efficient extraction but also contribute to reducing the overall costs associated with oil exploration.

Hyperspectral imaging emerges as a valuable tool for analysing oil-bearing drill cores. It is a relatively cost-effective and non-destructive technique that enables rapid visual assessment of the spatial distribution of oil in the core (Linton et al., 2023). Beyond its direct implications for crude oil exploration, the mapping of oil in the subsurface has broader applications in geothermal exploration and carbon storage.

The presence or absence of oil within the layers of an oil-bearing drill core serves as an indicator of the porosity and permeability of various lithologies. This information is crucial for understanding fluid movement within geothermal reservoirs, particularly with the increasing repurposing of Abandoned Oil and Gas Wells (AOGW) for geothermal utilization and carbon storage (Ashena, 2023; Kang et al., 2023; Nian & Cheng, 2018; Romdhane et al., 2022). Porosity and permeability estimations play a vital role in optimizing fluid flow in geothermal reservoirs (Eggertsson et al., 2020), while impermeable caps are essential for the effectiveness of carbon storage reservoirs (Fang et al., 2017). Thus, accurate mapping of crude oil within a drill core becomes imperative for a range of applications beyond traditional oil exploration.

1.1.3. Classification of Crude Oil

Accurate classification of crude oil, which is essential for effective extraction and production, holds significant importance for various stakeholders in the oil sector, including traders, refiners, regulators, and environmental agencies. Through precise classification, stakeholders can better understand the characteristics and properties of different crude oil types, allowing for tailored approaches to their handling and processing. This classification is rooted in a thorough assessment of crude oil's physical properties, molecular structure, and the proportions of hydrocarbons it contains (Selley & Sonnenberg, 2022). Traditionally, this process has been labour-intensive and costly, involving the use of complex equipment and hazardous substances, which pose both logistical and safety challenges (Kharrat et al., 2007).

However, advancements in spectroscopy have revolutionized the classification process, offering numerous advantages over traditional methods. Spectroscopic techniques provide rapid, cost-effective, and non-destructive means of analysing crude oil samples. Moreover, they significantly reduce the labour requirements and enable the processing of a large number of samples with ease, enhancing efficiency and productivity in classification procedures (Pabón & Filho, 2019). By leveraging spectroscopy, stakeholders can accelerate decision-making processes, optimize resource allocation, and mitigate risks associated with crude oil handling and processing.

When categorizing crude oil based on its molecular composition and structure, it is typically classified into aliphatics, aromatics, and hetero-compound groups containing elements such as oxygen, nitrogen, and sulphur. Each of these compounds plays a crucial role in determining the characteristics and properties of the crude oil. For instance, oxygen-containing compounds, including ketones, esters, phenols, and carboxylic acids, can significantly influence the stability, reactivity, and volatility of crude oil (Hsu & Robinson, 2019; Irina Smirnova, 1995; Tissot & Welte, 1984). Similarly, nitrogen compounds, such as amines and amides, contribute to the overall composition and behaviour of crude oil.

One of the most critical considerations in crude oil classification is its sulphur content, which has significant implications for its quality and usability. Crude oil with high sulphur content is commonly referred to as 'sour oil,' while those with low sulphur content are known as 'sweet oil' (Selley & Sonnenberg, 2022). The distinction between sour and sweet crude oils is essential, as sulphur compounds can lead to corrosion and environmental harm during processing and utilization. Sweet crude oil is preferred in the industry due to its reduced corrosiveness and environmental impact, making it easier and safer to handle and process (Groisman, 2014). Therefore, the accurate detection and classification of functional groups within crude oil are essential for informing decisions related to extraction, transportation, storage, and refining processes, ensuring efficiency, safety, and environmental responsibility across the oil sector.

1.1.4. Spectral Properties of Crude Oil

Building on the classification of crude oil, understanding its spectral properties is crucial for non-destructive analysis. Absorption features in the infrared spectrum, arising from hydrocarbons, primarily stem from the vibrational bonds between carbon and hydrogen atoms (Cloutis, 1989; Lyder et al., 2010; Speta et al., 2013). The fundamental vibrations of these bonds are predominantly observed in the thermal infrared (TIR) range, spanning from 2.5 μm to 15 μm (4000 cm^{-1} to 667 cm^{-1}), with overtones and combination tones extending into the visible near-infrared (VNIR), short-wave infrared (SWIR), and TIR range from 0.5 μm to 6.67 μm (20000 cm^{-1} to 1500 cm^{-1}) (Lammoglia & Filho, 2011).

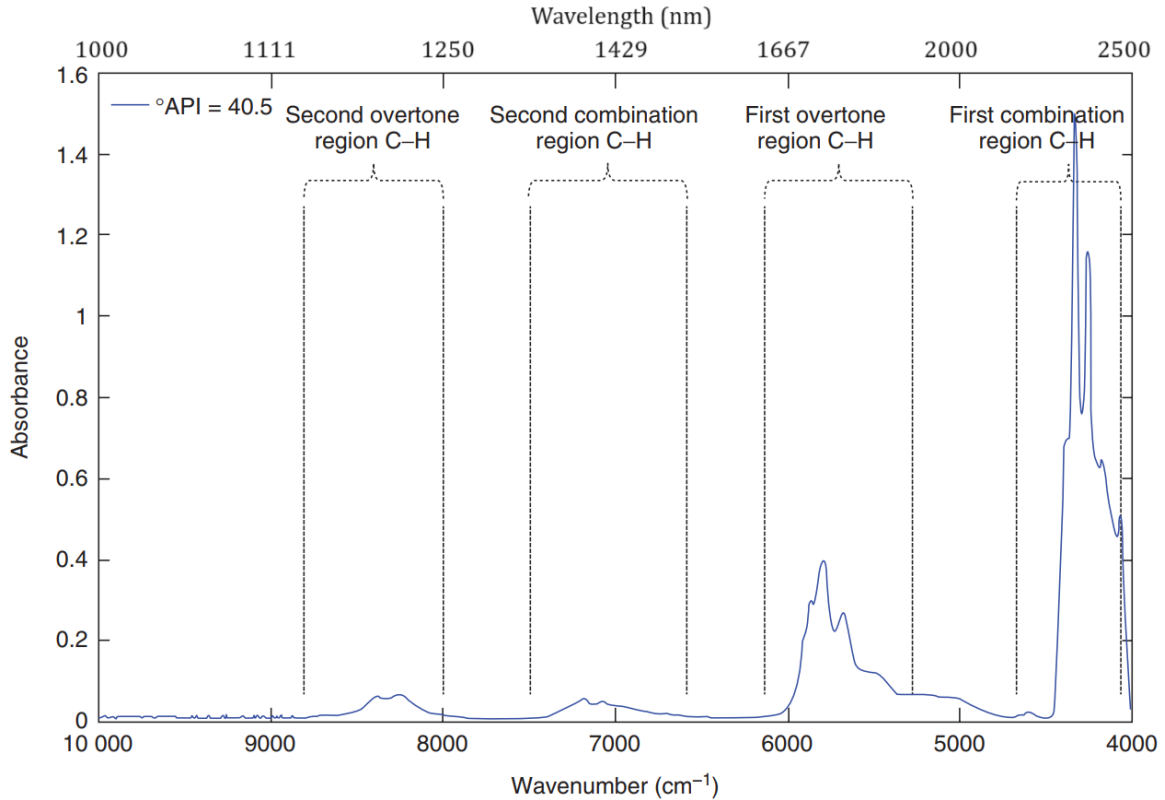


Figure 1.1 Absorption spectrum of light crude oil, highlighting the absorption regions of the C-H bond overtones and combination tones in the SWIR range (Source: Alves & Poppi, 2015).

Figure 1.1 illustrates the absorption spectrum of light crude oil, emphasizing the absorption regions of the C-H bond overtones and combination tones in the SWIR range (Alves & Poppi, 2015). The first overtones manifest between 1.7 μm and 1.8 μm (5555 cm^{-1} and 5882 cm^{-1}), the second overtones between 1.15 μm and 1.21 μm (8264 cm^{-1} and 8696 cm^{-1}), and the third overtones between 0.88 μm and 0.915 μm (10929 cm^{-1} and 11364 cm^{-1}). Additionally, combination tones are discerned between 2.2 μm and 2.5 μm (4000 cm^{-1} and 4545 cm^{-1}), as well as between 1.3 μm and 1.5 μm (6666 cm^{-1} and 7690 cm^{-1}). In the VNIR range, the π (Pi) electronic bonding between atoms causes absorption (Asadzadeh & Filho, 2017). As the number of rings and the complexity of molecules in the oil increase, as seen in heavy oils, this absorption feature becomes broader and the minimum shifts towards longer wavelengths. This broadening and shifting are indicative of the increasing molecular complexity and the presence of larger hydrocarbon structures.

Table 1.1 provides details on the fundamental vibrations, first overtones, and second overtones of the vibrational bonds of molecules present in crude oil and its associated functional groups. The fundamental vibrations were taken from Asemani & Rabbani (2020), Kiefer & Corsetti (2018) and Smith (1998), while the first and second overtones were calculated from the fundamental vibration ranges. The ranges highlighted in blue correspond to TIR spectra, those in yellow to SWIR spectra, and those in green to VNIR spectra. Data on absorption spectra from these studies offer insights into the wavelengths at which absorption features occur and the vibrational bonds responsible for these features. Asemani & Rabbani (2020) utilized this information to relate the absorption features of pure crude oil with its functional group in the TIR range. However, the functional groups of oil in drill cores have yet to be examined, which can be influenced by the absorption features of other minerals, posing a major challenge.

Table 1.1 Fundamental vibrations, first overtones, and second overtones of the vibrational bonds of molecules present in crude oil and its associated functional groups. The ranges in blue correspond to TIR spectra, those in yellow to SWIR spectra, and the ranges in green to VNIR spectra (Modified from: Asemani & Rabbani, 2020; Kiefer & Corsetti, 2017; Smith, 1998).

Vibrational Bonds	Functional Groups	Fundamental Vibrations (nm)	First Overtone (nm)	Second Overtones (nm)
O-H stretching	Alcohol, Phenols and Carboxylic Acid	2941 to 3030	1471 to 1515	735 to 758
N-H stretching	Amides	3101	1551	775
C-H stretching	Aromatics	3226 to 3333	1613 to 1667	807 to 883
C-H stretching	Aliphatics	3333 to 3636	1667 to 1818	883 to 909
C=O stretching	Carboxylic Acids, Esters, Ketones	5556 to 6250	2778 to 3125	1389 to 1563
C=C stretching	Aromatics	6250 to 6667	3125 to 3334	1563 to 1667
CH ₃ bending, CH ₂ scissors	Aliphatics	6667 to 7143	3334 to 3572	1667 to 1786
O-H stretching	Phenols	7326	3663	1832
C-N stretching	Secondary Amides	7692 to 8333	3846 to 4167	1923 to 2083
C-C-O asymmetric stretch	Esters, Alcohols	8333 to 9091	4167 to 4546	2083 to 2273
S=O stretching	Sulphur Oxide Group	9346 to 9709	4673 to 4855	2337 to 2427
C-H out-of-plane bending	Aromatics	11111 to 14286	5556 to 7143	2778 to 3572
C-C bending	Aromatics	14493	7247	3623

The spectral properties of crude oil also depend on its thickness. Lammoglia & Filho (2011) and R. D. M. Scafutto & Filho (2016) demonstrate that as the thickness or concentration of oil increases in a medium, the reflectance value decreases, and the depths of the absorption features increase. This indicates that the concentration of oil can significantly influence its spectral characteristics, thereby affecting the accuracy of methods used in oil exploration and production.

Another important property of crude oil is fluorescence. When illuminated with a UV source, the aromatic and hetero-compound fraction of the crude oil causes fluorescence in the VNIR range (Hagemann & Hollerbach, 1986). This property can help detect oil in seawater as oil spills (Hou et al., 2022) and in drill cores and cuttings (Jiaqi, 2018). The fluorescence spectra depend on the wavelength of the UV source, the concentration of oil and the type of oil. Ryder (2005) and Steffens et al. (2011) demonstrated that as the wavelength of the UV source shifts towards longer wavelengths, the peak of the fluorescence spectra also shifts towards longer wavelengths. Peng et al. (2013) and Steffens et al. (2011) also showed that as the concentration of oil increases, the intensity of the fluorescence spectra decreases. Finally, Hagemann & Hollerbach (1986) and Jiaqi (2018) showed that the fluorescence spectra also depend on the type of the oil, with biodegraded or heavy oils showing a brown fluorescence, light oils showing a green to yellow fluorescence and very light oils or condensates showing a blue fluorescence.

1.1.5. Crude Oil Reservoirs in the Netherlands

In the process of petroleum accumulation, crude oil becomes concentrated and confined within conventional reservoir rocks, which primarily include sandstones comprising silicate minerals like quartz and feldspar, as well as carbonate rocks like limestones consisting of calcite and dolomite (Ali, 2017; Tissot & Welte, 1984). Halite, commonly found in rock salt and salt domes, acts as an effective seal and cap rock, preventing the upward migration of oil and gas. Additionally, clay minerals such as kaolinites, muscovites, illites, and iron oxides, typically present in shales, play crucial roles as seals and cap rocks, further confining the hydrocarbons within the reservoir (Ali, 2017; Tissot & Welte, 1984). Consequently, a diverse array of minerals is encountered in crude oil-bearing drill cores, reflecting the complex geological processes involved in their formation.

In the Netherlands, crude oil reservoirs are distributed across various geological basins, both on-shore and off-shore. These basins include the Southern Permian Basin, Broad Fourteens Basin, West Netherlands Basin, Dutch Central Graben, and Terschelling Basin (Bouw & Lutgert, 2012; den Hartog Jager, 1996; Geluk, 2000; Mijnlief, 2020; Verweij et al., 2003; Verweij & Simmelink, 2002). Within these basins, Type-II and Type-III kerogen are predominant and are associated with oil-gas and gas formations, respectively (de Jager & Geluk, 2007). Lithologies found in these basins primarily consist of sandstones, limestones, shales, and carbonates, with occasional occurrences of chalk, mudstones, marl, anhydrite, and halite. Consequently, the mineral composition of oil-bearing lithologies in the Netherlands is characterized by the prevalence of quartz, feldspar, calcite, and dolomite, along with illite, muscovite, kaolinite, pyrite, and evaporite minerals (Mijnlief, 2020; Verweij & Simmelink, 2002). Figure 1.2 illustrates the distribution of oil and gas fields in the Netherlands, with the black circle indicating the area from where the drill cores used in this study were obtained, located within the Broad Fourteens Basin (Verweij, 2003).

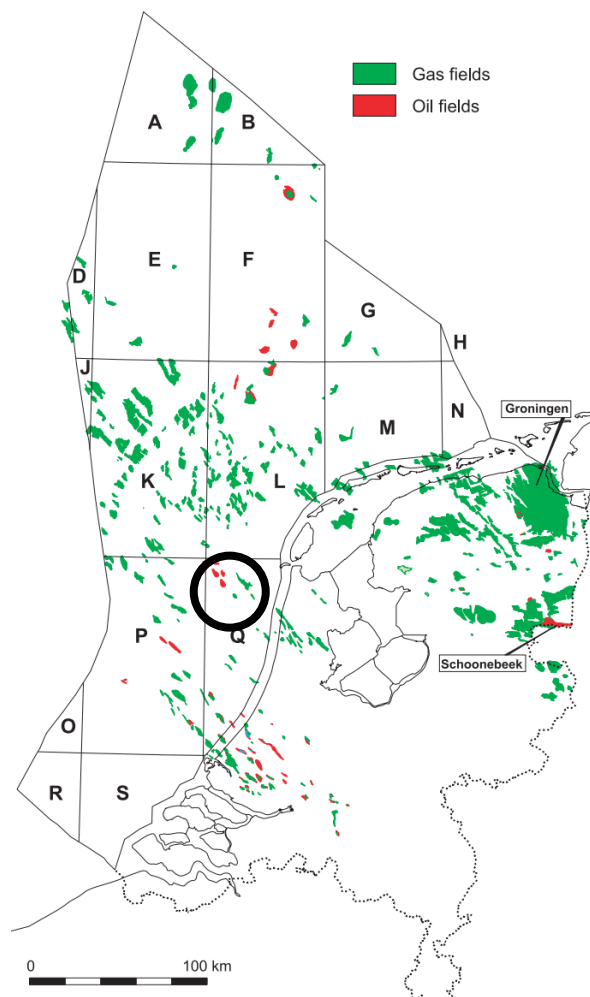


Figure 1.2 Distribution of oil and gas fields in the Netherlands. The black circle marks the area from where the drill core used in this study has been obtained, which lies in the Broad Fourteens Basin (Source: de Jager & Geluk, 2007)

1.2. Research Gap

Hyperspectral scans have played a crucial role in understanding the spectral characteristics of minerals. They allow researchers to delve deep into the composition of rocks and sediments by analysing their unique absorption features across various wavelengths. Iron-bearing minerals, such as goethite, hematite, jarosite, and siderite, are known to exhibit distinctive absorption features in the VNIR region (Sherman, 1985). Similarly, carbonate minerals like calcites and dolomites, as well as clay minerals such as illites,

muscovites, and kaolinites, showcase characteristic absorption features in the SWIR range (Clark et al., 1990; Hunt & Ashley, 1979), while non-hydroxylated silicate minerals like feldspars and quartz exhibit absorption features in the TIR range (Hecker et al., 2010, 2019). These features arise from molecular vibrations within the crystal lattice structure of the minerals and aid in the detection and characterization of these minerals in geological samples.

Furthermore, automated workflows have been developed to streamline the process of mineral mapping in drill cores. These workflows leverage hyperspectral imaging data to detect and classify minerals based on their spectral signatures accurately. By automating this process, researchers can expedite the analysis of large datasets, enabling more efficient geological exploration and resource assessment (Huntington et al., 2006; Schodlok et al., 2016).

In addition to mineral mapping, hyperspectral imaging has been applied to study oil sand drill cores, particularly in regions like Alberta, Canada, known for their bituminous oils (i.e., oil with an API° of 6 to 10). Studies have focused on identifying spectral absorption features of bitumen, quantifying Total Bitumen Content (TBC), and detecting sedimentary and biogenic features within drill cores (Lyder et al., 2010; Rivard et al., 2010; Shchepetkina et al., 2017; Speta, 2016; Speta et al., 2013, 2015, 2016, 2018). The oil sands in this region are comprised of quartz, feldspar, clays, bitumen, and water. They are uncemented, well-sorted, and of medium to fine grain size, held together by highly viscous bitumen. The oil sands belong to the Lower Cretaceous Mannville Group, indicating a fluvial to estuarine to marginal marine environment of deposition.

Speta (2016) and Speta et al. (2016) used Spectral Angle Mapper (SAM) on SWIR and LWIR hyperspectral imagery to map oil sand cores from the McMurray Formation into five classes: oil sand, barren sand, siltstone, mudstone, and siderite. In the SWIR region, these studies primarily focus on bitumen absorption features at 1.7 μm and 2.3 μm , clay mineral absorption features at 1.4 μm and 2.2 μm , water absorption features at 1.9 μm , and siderite features at 1.0-1.2 μm and 2.53 μm . In these studies, the oil is present along with sand, which is not spectrally active in the SWIR range. Moreover, the oil sand endmember spectra used in this process did not have any overlapping features with the endmember spectra of other classes. Thus, the oil sands in the drill core could be correctly mapped. This methodology is effective for simple, uncemented oil sands where the major constituent is quartz, along with clays and siderites.

However, while these methodologies have proven effective in mapping oil sands in regions like Alberta, they may face challenges when applied to hydrocarbon reservoirs in other locations, such as the Netherlands. The reservoirs in the Netherlands often contain lighter oils and a diverse range of minerals (Verweij, 2003), including evaporites like gypsum with absorption features in 1.7 μm and carbonates like calcites and dolomites, with absorption features in 2.3 μm . Understanding how the spectral features of oil overlap with minerals across different wavelength ranges remains a critical research question. Additionally, delineating optimal wavelength ranges and identifying suitable methods for mapping oil within mixtures involving these minerals in a drill core remains a challenge.

1.3. Research Problem

This research aims to address this gap by investigating the absorption features present in crude oil across the VNIR, SWIR, and TIR ranges. By analysing the spectral signatures of oil and typical drill core minerals, the study seeks to develop a prototype workflow for mapping oil and minerals in drill cores from Dutch hydrocarbon reservoirs, which consist of relatively lighter oils than the oil found in the Alberta region. Furthermore, the research also explores the possibility of detecting functional groups present in crude oil by analysing mixed spectra of oil and minerals from the drill core.

1.4. Research Objectives

Main Objective

This research aims to measure and characterise the spectral properties of crude oil in the VNIR, SWIR and TIR range, integrate this into a mapping workflow and further apply this workflow to detect, map, and classify crude oil and minerals using the hyperspectral images of drill cores from the Dutch region.

Sub-Objective 1: To determine the spectra of the heavy, light and very light oil and explain the differences in absorption features in terms of the thickness of oil and functional groups present in these three oil samples.

RQ1: What are the absorption features of the three oil samples in the VNIR, SWIR and TIR range?

RQ2: How do these absorption features differ for heavy, light, and very light oils?

RQ3: What functional groups contribute to the observed differences in the absorption features of heavy, light, and very light oils?

RQ4: How do the spectra of the oil change with respect to its thickness?

Sub-Objective 2: To analyse the absorption features of the oil and the minerals present in a drill core from quartz-rich sandstone reservoir rock that contains clays, evaporites and carbonate minerals.

RQ5: How do the absorption features in the spectra of the oil and minerals differ?

RQ6: How do these spectra interfere, and what are the non-overlapping wavelength ranges that can be identified?

Sub-Objective 3: To develop a prototype workflow for mapping the oil and typical minerals present in a drill core.

RQ7: Which wavelength ranges and mapping methods can be used to form the workflow that can help differentiate and map oil and typical minerals present within a drill core?

Sub-Objective 4: To implement the prototype workflow on the hyperspectral images of sample drill cores and further classify the oil in the drill cores based on the functional groups present.

RQ8: What is the location and relative concentration of the oil found in the drill core?

RQ9: Can the mix spectra of crude oil and typical minerals present in the drill core be used to determine the functional groups present in the oil?

2. DATASETS AND METHODOLOGY

2.1. Datasets

This section describes the datasets that were used in this study. The first set of data used were the crude oil samples provided by PanTerra Geoconsultants B.V. through the contacts of Deep Atlas. The second dataset was two drill cores from the Geological Survey of the Netherlands (GDN) Core House in Zeist.

2.1.1. Crude Oil Samples

This study analysed three distinct oil samples: heavy oil, light oil, and very light oil (condensate), each characterized by different density values, which affect their viscosity and overall behaviour (Figure 2.1).

- **Heavy Oil (H.Oil):** The heavy oil sample has a density of 0.9786 g/cm^3 at 15°C and an $^\circ\text{API}$ gravity of 12.6. This type of oil is characterised by its thick consistency, dark colour, and high viscosity. Handling this oil requires more effort due to its resistance to flow, typically needing tools like a spoon rather than a pipette.
- **Light Oil (L.Oil):** The light oil sample has a density of 0.8505 g/cm^3 and an $^\circ\text{API}$ gravity of 34.1. This oil is less dense and more fluid than heavy oil. It is dark brown and flows more readily, making it easier to handle with a pipette.
- **Very Light Oil (V.Oil):** The very light oil sample, or condensate, has a density of 0.7449 g/cm^3 and an $^\circ\text{API}$ gravity of 57.2. This oil is transparent and exhibits very low viscosity, behaving much like a volatile liquid that flows easily and can be handled effortlessly with a pipette.

These three samples represent a wide spectrum of oil types, each showcasing unique physical properties that underscore their diverse chemical compositions. The spectra of these three oil samples were recorded and analysed across VNIR, SWIR, and TIR ranges, along with UV fluorescence, to discern their distinct absorption features, reflectance, and fluorescence properties.



Figure 2.1 The three oil samples that were used in this study.

2.1.2. Drill Cores

In addition to the crude oil samples, this study utilised two oil-bearing drill cores differentiated based on the type of oil they contain and their mineral composition. The first drill core (DC1) contains transparent oil, while the second drill core (DC2) contains dark-coloured oil. These drill cores provide a valuable context for understanding the interaction between crude oil and the minerals they contain.

Drill Core 1 (DC1)

The first drill core was obtained from Well Q4-10, specifically from an interval between 2668 meters and 2671 meters depth (Figure 2.2). This section is part of the Lower Volpriehausen Sandstone Member (Munsterman et al., 2012). According to the wellsite geological report by Robbemond et al. (2002), this core comprises greyish-red to very dusky-red sandstone. The sandstone is characterized as hard and friable with calcareous cement, exhibiting moderate to good visual porosity. The quartz grains within the sandstone are fine to medium-grained, rounded, and display moderate to well sorting. These grains are transparent to translucent, colourless, and occasionally show milky white and orange hues.

The Lower Volpriehausen Sandstone Member, a part of the Main Buntsandstein Subgroup, is significant in the context of hydrocarbon reservoirs of the Lower Triassic epoch in the southern North Sea area (Kortekaas et al., 2018). This member, along with the Detfurth Sandstone Member, constitutes primary reservoir rocks, predominantly comprising quartz, feldspars, and other clay minerals such as kaolinites, muscovites, and illites (Olivarius et al., 2017).



Figure 2.2 Photograph of Drill Core 1

Drill Core 2 (DC2)

The second drill core was obtained from Well Q01-Helm-A01, spanning an interval from 1247 meters to 1250 meters depth (Figure 2.3), which is part of the Helder Member (Munsterman et al., 2012). According to the well completion report by Ayyad & Parmigiano (1983), this core consists of off-white to light greyish-brown sandstone, which is poorly sorted with no visible cement. The quartz grains in the sandstone are fine to medium-grained and are subangular to subrounded. This drill core has a porosity of 22%, and the middle part contains oil with a 17.4°API (Sebborn, 1982).

The Helder Member belongs to the Vlieland Sandstone Formation of the Lower Cretaceous epoch within the Rijnland Group (Kortekaas et al., 2018).



Figure 2.3 Photograph of Drill Core 2.

Both drill cores originate from members of the Broad Fourteens Basin, known for rich, marine Type-II kerogen source rocks. These source rocks, with an intermediate hydrogen-to-carbon (H/C) by oxygen-to-carbon (O/C) ratio, are both oil and gas-prone (de Jager & Geluk, 2007). The oil in the first drill core is lighter (high °API gravity) and present in a deeper formation. In contrast, the oil in the second drill core, found at relatively shallower depths, has a low °API gravity due to biodegradation (Connan, 1984; Palmer, 1993; Verweij, 2003).

2.2. Methodology

This section details the methodology employed in this study, which is divided into two main parts: the analysis of oil samples and the analysis of drill cores. The three oil samples served as the training data to determine their absorption features and compare them to that of the minerals present in the drill core. This understanding was then applied to the drill core to detect, map and classify the oil and minerals. Various instruments and software were used to record and process the data of the oil samples and the drill cores. Table 2.1 gives the name of the instruments used and their wavelength range.

Table 2.1 Instruments used and their wavelength range.

Instrument	Wavelength Range
Spectral Evolution SR-6500	0.35 μm to 2.50 μm
Specim Camera VNIR	0.38 μm to 1.00 μm
Specim Camera SWIR	1.00 μm to 2.50 μm
Bruker Vertex 70 FTIR Spectrometer	2.50 μm to 15.0 μm

A UV light source of 3 watts and peak emittance at 365 nm was used for the UV fluorescence spectroscopy. The software used to process the data is as follows:

- Hyperspectral Python (HypPy) (Bakker, 2024)
- ENVI 6.0

2.2.1. Oil Samples

The initial focus was on analysing the three oil samples to comprehensively understand the spectral nature of crude oil. This process began with recording the spectra of the oil in the TIR range to identify absorption features caused by fundamental vibrations. Subsequently, the VNIR-SWIR range was examined to capture overtones and combination tones. By varying the thickness of the oil samples, changes in absorption features were observed and documented. Comparative analysis was conducted between the absorption features of the oil and those of minerals typically present in hydrocarbon-bearing drill cores in the Dutch region to identify non-overlapping ranges. In addition, the UV fluorescence spectra of the oil were recorded in the VNIR range to further characterise the samples. Finally, to simulate the presence of oil within a geological context, the oil samples were soaked in pieces of sandstone and scanned using an imaging spectrometer, providing a realistic representation of their spectral characteristics in drill cores.

TIR Spectroscopy (2.5 μm to 15 μm)

This subsection details the process of recording the TIR spectra of the oil samples to identify fundamental vibrations and absorption features in the infrared range. The Bruker Vertex 70 FTIR spectrometer was used to record spectra, utilizing the Attenuated Total Reflectance (ATR) setup with the Pt-ATR-Diamond accessory (Hecker et al., 2011). Each sample was scanned in the range from 2.5 μm to 15 μm at 2 cm^{-1} resolution and a sample scan time of 512 scans per sample to reduce the noise in the spectra. After each scan, the sample compartment and the arm level of the instrument were cleaned with toluene and a blank scan was taken. The resulting transmission spectra of the three oil samples were analysed for their maximum wavelengths of absorption using the localmaxfit expression in the SpecLib Viewer tool in HypPy.

VNIR-SWIR Point Spectroscopy

This subsection outlines the process of recording the VNIR and SWIR spectra of the oil to identify the overtones and combinations of the fundamental vibrations, thereby creating a comprehensive spectral profile of the oil samples. The Spectral Evolution SR-6500 spectrometer was used to record the spectra of the three oil samples. Figure 2.4 shows the photograph of the setup.

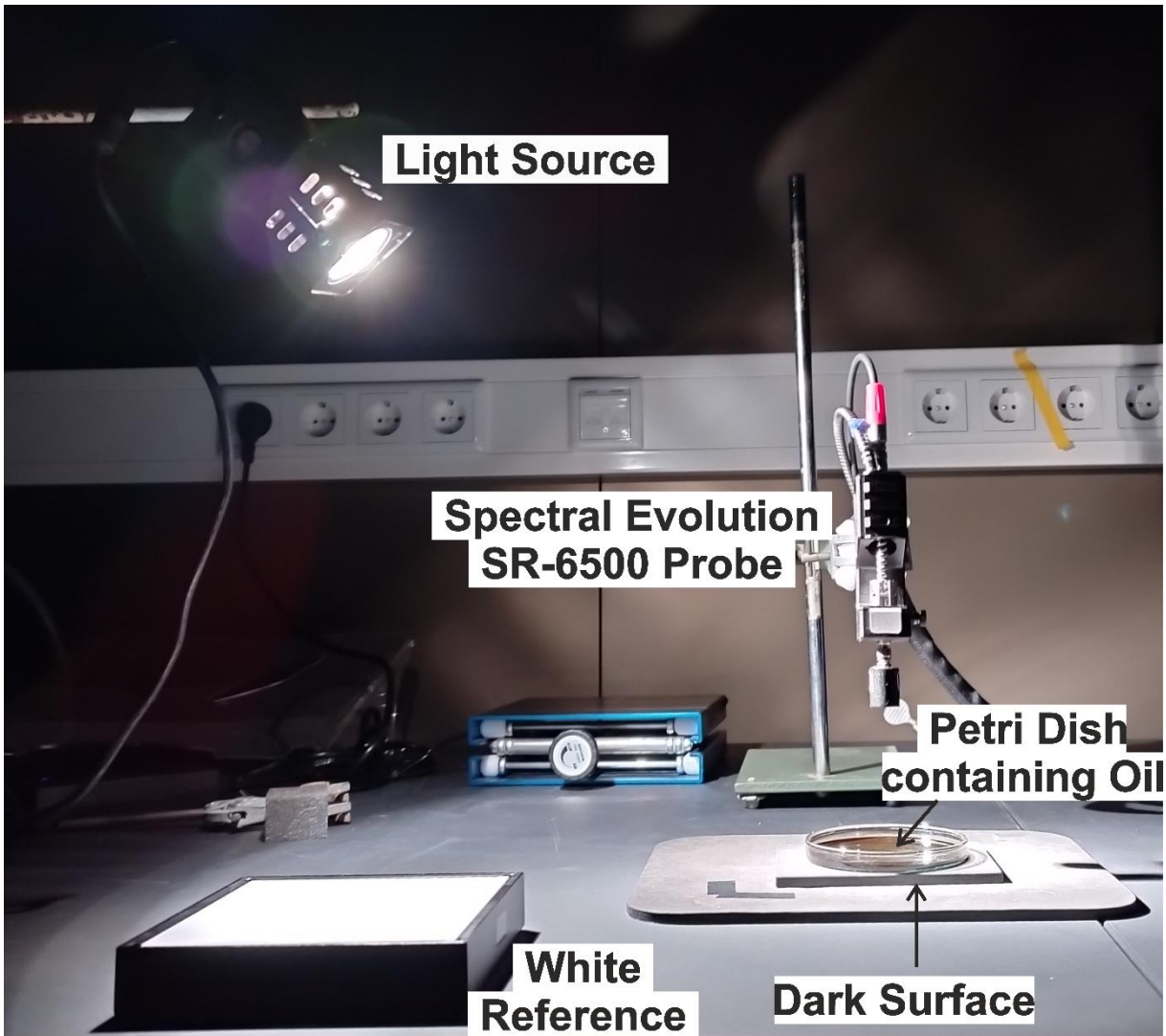
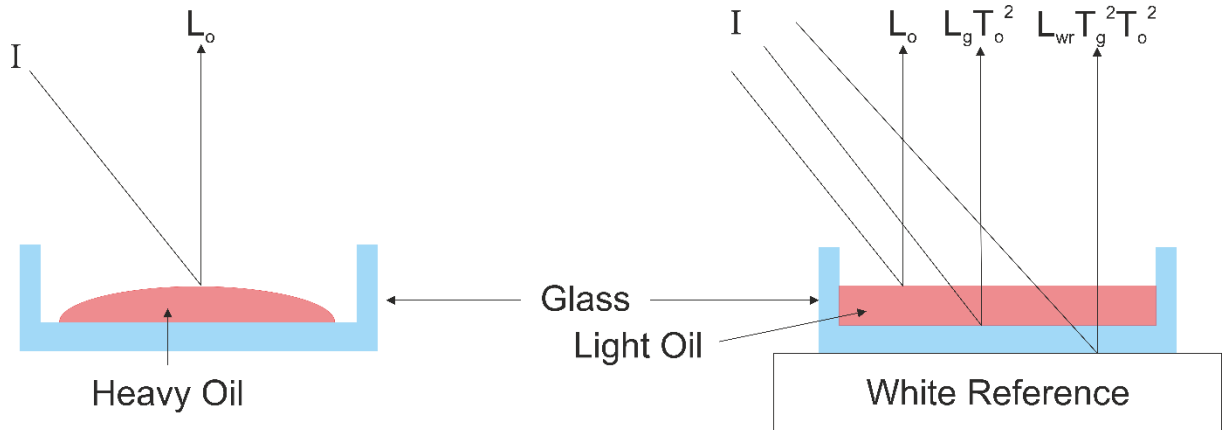


Figure 2.4 Setup of the VNIR-SWIR Point Spectroscopy

To record the spectra of the heavy oil, it was feasible to spread the viscous oil on a petri dish using a spoon, allowing for the recording of its reflectance spectra due to its thick consistency. However, this method was not applicable to very light and light oils. These oils were instead placed on a petri dish using a pipette and positioned on a white reference surface for spectrum recording. Due to their liquid and transparent nature, the produced spectra were a combination of reflectance and transmittance. Additionally, when using a petri dish, the recorded spectra included the spectrum of the glass.

To correct for this, the reflectance spectra of the oil first needed to be subtracted from the recorded spectra. The resulting spectra were then divided by the transmittance and reflectance spectra of the glass to obtain the true transmittance spectra of the oil. However, this result was the square of the transmission spectra of the oil. Figure 2.5 provides a diagrammatic representation of this process.



$$\begin{aligned} \frac{\text{Reflected Light}}{\text{Incident Light}} &= \frac{L_o + L_g T_o^2 + L_{wr} T_g^2 T_o^2}{L_{wr}} \\ &= R_o + R_g T_o^2 + T_g^2 T_o^2 \\ &= R_o + T_o^2 (R_g + T_g^2) \end{aligned}$$

Figure 2.5 Diagrammatic representation of the light ray recorded by the spectrometer after interacting with the oil, glass and white reference. Here I- incident ray, L- reflected ray, T- transmittance and R- reflectance, o- oil, g- glass and wr- white reference.

The reflectance spectra of the oil were recorded by placing the petri dish on a dark surface with very low reflectance, ensuring that only the reflectance spectra of the oil were captured. Upon analysing the reflected spectra, it was observed that the reflected spectra had a very low value and were thus omitted when calculating the transmittance spectra of the oil. Figure 2.6 shows the spectra of the petri dish on the white reference and a dark surface, along with the uncorrected spectra of the oil.

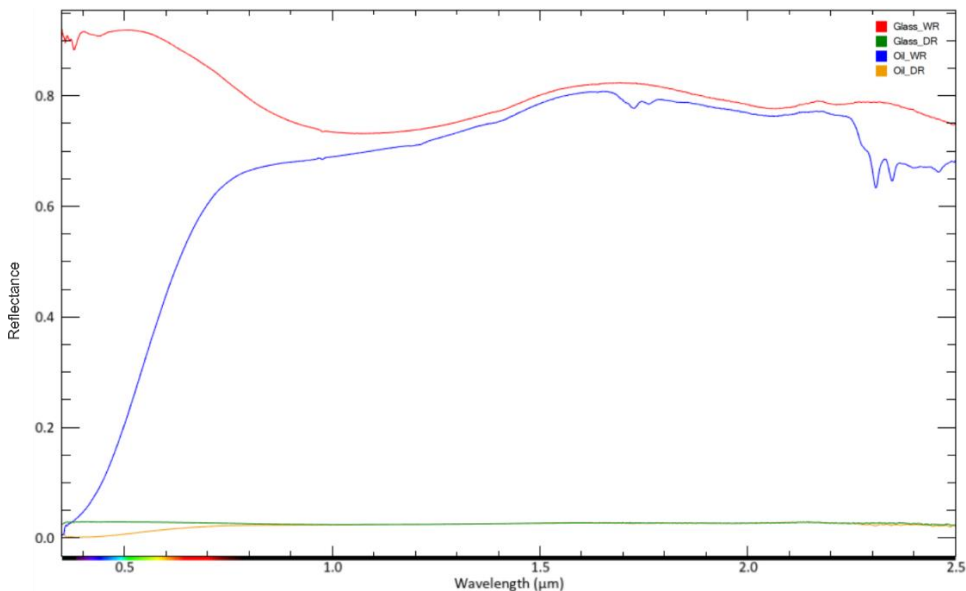


Figure 2.6 Spectra of the glass (petri dish) and oil recorded over a white reference (WR) and dark surface (DR)

Subsequently, the absorption features of the three oil samples were analysed for their minimum wavelength of absorption using the `localminfit` expression in the `SpecLib Viewer` tool in `HypPy`. Additionally, band ratios and mean reflectance values for the three oils were computed using `HypPy`. The mean reflectance value is the sum of reflectance values divided by the total number of wavelength values.

To gain deeper insights into spectral changes with varying oil thickness, recordings were made at incremental oil volumes ranging from 0.25 ml to 6.00 ml in the petri dish. The resulting spectra were then analysed to ascertain the depth of the deepest features, employing the `dpeaks` expression on the shoulders of the feature within the `SpecLib Viewer` tool in `HypPy`.

For the comparison between the absorption features of the oil and minerals, most of the mineral spectra were taken from the USGS Spectral Library Version 7 (Kokaly et al., 2017), except for Anhydrite which was taken from ECOSTRESS Spectral Library Version 1 (Baldrige et al., 2009; Meerdink et al., 2019) because of the lack of absorption features in the Anhydrite spectra from the USGS spectral library. The minimum wavelengths of the absorption features in these spectra were also analysed using the `localminfit` expression in the `SpecLib Viewer` tool in `HypPy`. The spectra of these minerals were also analysed for their spectral similarity to each other using a Spectral Angle Matrix. The names of the minerals used for the comparison between the absorption features of the oil and minerals are given below:

- Illite_GDS4_Marblehead_ASDNGb
- Muscovite_GDS116_Tanzania_ASDNGa
- Kaolinite_KGa-1_(wxl)_ASDNGb
- Chlorite_HS179.4B_ASDFRb
- Gypsum_HS333.3B_(Selenite)_ASDNGa
- Anhydrite CaSO 4 [sulfate-none-coarse-so01a]
- Dolomite_HS102.4B_ASDNGb
- Calcite_WS272_ASDNGa
- Halite_HS433.4B_ASDFRa
- Quartz_HS32.3B_ASDFRc

These minerals were chosen because their spectra were recorded using ASD FieldSpec 3 (ASDFR) and ASD FieldSpec 4 (ASDNG) spectrometers, which have a resampled resolution identical to that of the Spectral Evolution SR-6500 used in this study. Anhydrite was an exception and recorded with a Perkin-Elmer VNIR-SWIR spectrometer. These spectra are of coarse grain minerals, which exhibit deep absorption features that facilitate the identification of distinct absorption wavelengths.

UV Fluorescence Spectroscopy

This subsection details the process of recording the UV fluorescence spectra of the oil samples in the VNIR range to analyse how the fluorescence spectra varied between the three oil samples. To capture these fluorescence spectra, the oil samples were soaked in a piece of Fontainebleau sandstone and exposed to a UV light source of 3 watts and peak emittance at 365 nm, with minor emittance in the blue wavelengths which is visible to the naked eye. The resulting fluorescence spectra were then captured using the Spectral Evolution SR-6500 instrument as it records in the range from 0.35 μm to 2.5 μm . Before recording, the reference spectrum was recorded by illuminating a white reference panel with the UV light source. Additionally, spectra of the unsoaked sandstone illuminated with UV light were acquired to serve as a reference point for comparison. The sandstone piece had dimensions of 2.5 cm by 2 cm by 1cm and a porosity of 12% (C. Hecker, personal communication), ensuring consistent conditions for the fluorescence measurements. Figure 2.7 shows the setup used to record the fluorescence spectra.

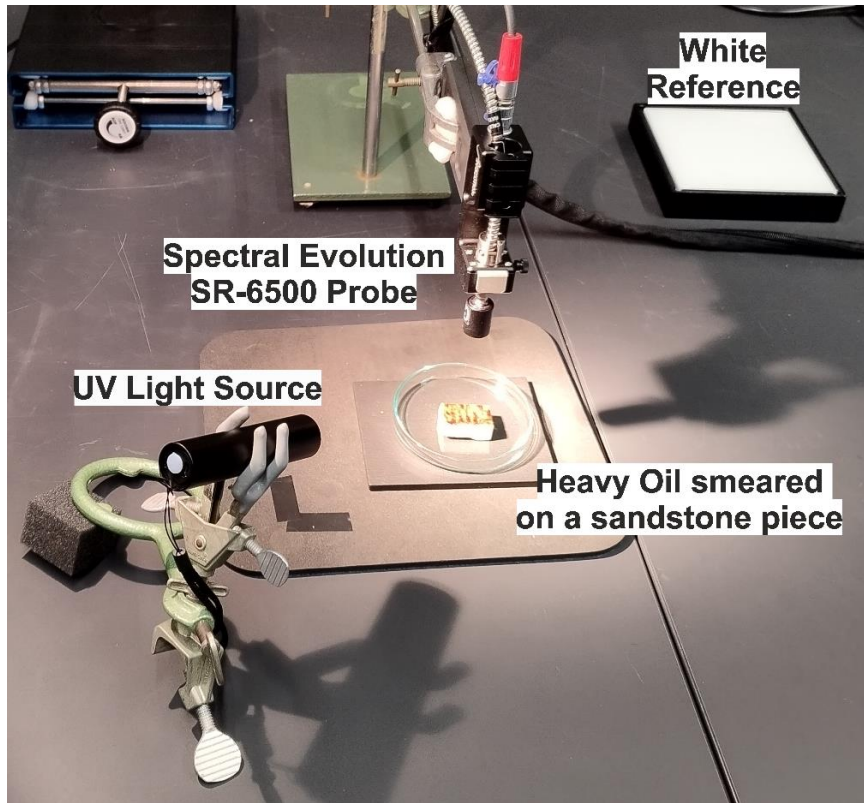


Figure 2.7 Setup used to record the fluorescence spectra.

VNIR-SWIR Imaging Spectroscopy

Finally, to simulate the presence of oil within a drill core, the oil samples were soaked in pieces of Fontainebleau sandstone and scanned using Specim cameras operating in the VNIR and SWIR ranges to provide a realistic representation of their spectral characteristics in drill cores. To analyse variations in spectral signatures resulting from different oil saturations, varying volumes of very light and light oil were introduced into the sandstone using a pipette, beginning with increments of 0.25 ml, 0.50 ml, and 1.00 ml. Conversely, due to its thick consistency, the heavy oil was smeared directly onto the surface of the sandstone. Figure 2.8 shows the setup used in this process. This systematic approach facilitated the examination of how different oil volumes influenced the spectral properties of both the oil and the sandstone substrate. Additionally, efforts were made to minimize the time lapse between oil application and scanning to prevent the evaporation of volatiles present in the oil.

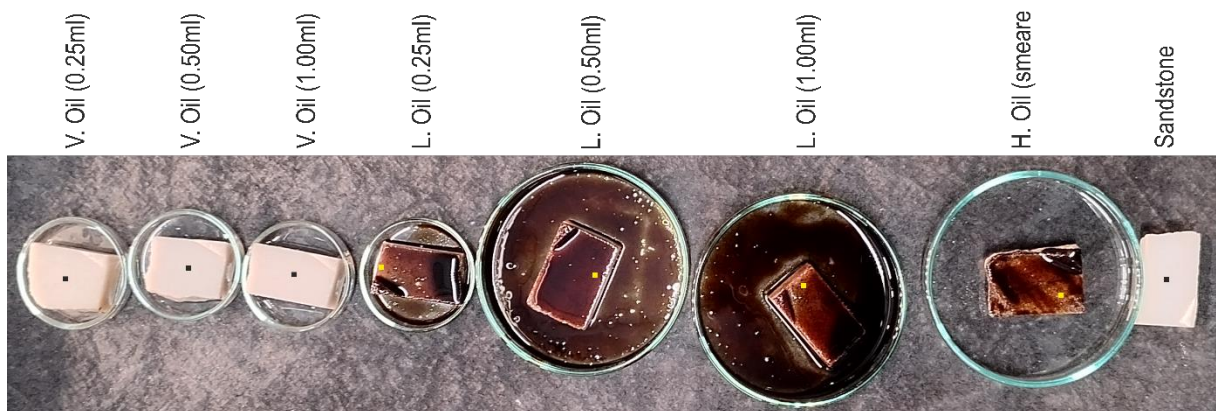


Figure 2.8 Setup of the oil-soaked sandstones and the unsoaked sandstone which were then scanned by the Specim cameras. The black and yellow squares mark the region from which the spectra were taken in section 3.2.3

2.2.2. Drill Core

This section details the analysis conducted on the drill core to detect, map, and classify the oil present within it. Initially, oil detection was performed by illuminating a section of the cores with a UV source and capturing the fluorescence spectra. Following this, to enhance comprehension of the mineralogy of the drill cores, a point spectroscopy analysis was undertaken in the VNIR and SWIR range. Subsequently, the drill core was scanned with an imaging spectrometer, and the obtained scans were analysed using various mapping methods. Lastly, the scratched surface of the drill core underwent analysis using an FTIR spectrometer to provide further insights into its composition and characteristics.

UV Fluorescence Spectroscopy

For oil detection, the drill cores were exposed to UV light of 3 watts, and their spectra were recorded in the VNIR region using the Spectral Evolution SR-6500 with a field of view of around 1.5 cm. The reference spectrum was recorded by exposing a white reference panel to the UV light. Readings of the drill cores under UV light were captured at intervals of every 2 to 4 cm along the length of the core, providing a comprehensive assessment of UV fluorescence across an entire section of the core samples.

VNIR-SWIR Point Spectroscopy

This subsection describes the recording of spectra from the drill cores using the contact probe accessory of the Spectral Evolution SR-6500 instrument, which has a field of view of around 2 cm. A systematic approach was adopted wherein segments of the core measuring less than 10 cm were examined by taking readings at both the top and bottom of the segment. For segments exceeding 10 cm, additional readings were acquired along the length of the segment. This method facilitated the observation of mineral variations within the core and allowed for assessing spectral variations in the oil across different segments.

VNIR-SWIR Imaging Spectroscopy

Both cores were scanned using the Specim cameras in the VNIR and SWIR range to map and classify the oil and minerals within the two drill cores. This imaging procedure resulted in the generation of hyperspectral images for each core. Subsequently, the images underwent several preprocessing steps, including dark and white referencing, y-direction destriping to remove artefacts in the data caused by slight incorrect calibrations of individual camera sensor cells, and cropping spatially to the extent of the drill core and spectrally to remove noisy bands at the starting and ending wavelengths. A spatial binning of 5 was applied to the SWIR images to enhance data quality and manage noise. Similarly, a spatial binning of 5 and a spectral binning of 3 were implemented for the VNIR images using HypPy. This choice of binning values was made to reduce noise. The spatial binning helped to discern the bandings present in the drill cores, which were about 8 to 10 pixels broad. Similarly, the broad absorption features of hematite and oil in the VNIR region were not masked by a spectral binning of 3.

Following preprocessing, the images of the drill core underwent further processing to map the distribution of oil and minerals within the cores and classify the oil based on its concentration. Several mapping techniques were employed for this purpose:

- Band Index

Utilizing the ‘Hydrocarbon Index’ proposed by Kühn et al. (2004) for HyMAP data, the oil distribution within the drill cores was mapped. The Hydrocarbon Index formula is expressed as

$$HI = (\lambda_B - \lambda_A) \frac{R_C - R_A}{\lambda_C - \lambda_A} + R_A - R_B$$

where R_A , R_B and R_C are reflectance values while λ_A , λ_B and λ_C are wavelength values for the absorption feature and its shoulders. For the absorption feature at $1.729 \mu\text{m}$ (HI1.7), as suggested by Kühn et al. (2004), the reflectance values at wavelengths $1.707 \mu\text{m}$, $1.728 \mu\text{m}$, and $1.741 \mu\text{m}$ were used, along with corresponding band numbers. Figure 2.9 explains the relation between the absorption feature minimum B ($1.728 \mu\text{m}$) and the two shoulders at A ($1.707 \mu\text{m}$) and C ($1.741 \mu\text{m}$). Moreover, this study expanded the application to include the oil absorption feature at $2.308 \mu\text{m}$ (HI2.3), incorporating reflectance values at $2.284 \mu\text{m}$, $2.307 \mu\text{m}$ and $2.324 \mu\text{m}$ and their appropriate wavelength values. This process was done using the Band Math tool in HypPy.

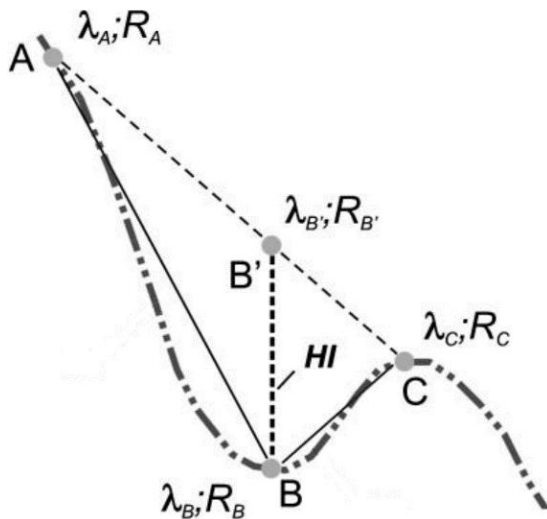


Figure 2.9 Relation between the absorption feature minimum at B and the two shoulders at A and C that is used to generate the Hydrocarbon Index (HI) (modified from Kühn et al. (2004)).

- Spectral Angle Mapper

The Spectral Angle Mapper (SAM) technique quantifies the spectral similarity between a known reference spectrum and an unidentified target spectrum. This is achieved by calculating the angle between the two spectra using dot product multiplication (Asadzadeh & Filho, 2016). In this study, SAM was applied to the drill core dataset to facilitate the mapping of both oil and minerals present within the cores. The minerals were identified from the point spectroscopy analysis on the drill cores, while their endmember spectra were sourced from the USGS library (Kokaly et al., 2017). Utilizing the Spectral Mapper tool in HypPy, rule images for SAM were generated, enabling comprehensive mapping of the oil and mineral distributions within the drill cores.

- Minimum Wavelength Mapper

The Minimum Wavelength Mapper algorithm, a feature of HypPy, was applied to the SWIR images acquired from the drill cores. This algorithm identifies the wavelength positions corresponding to the deepest absorption features within the images, as outlined by Bakker et al. (2011) and van Ruitenbeek et al. (2014). By doing so, it generates wavelength position maps that effectively illustrate the spatial distribution of minerals without necessitating predefined endmembers. The obtained minimum wavelength map was then cross-referenced with values of the deepest absorption features of the oil and minerals in the drill

core samples. This comparative analysis facilitated the mapping of oil and minerals within the drill core, enhancing the understanding of its spatial distribution. Similarly, the depth map helps quantify the relative concentrations of oil within the drill cores.

TIR Spectroscopy (2.5 μm to 15 μm)

Lastly, in order to identify the functional groups present in the oil within the drill cores, both cores underwent a process involving scratching with a steel knife at two distinct locations: one with low oil concentration and another with high oil concentration. The obtained grains were subsequently ground into powder using a mortar, and this powder was subjected to analysis using the Bruker Vertex 70 FTIR-ATR spectrometer. This allowed for the comprehensive examination of functional groups present in the oil samples extracted from the drill cores.

3. RESULTS

The results chapter is divided into two sections; the first is the results of the measurements done on the oil samples, followed by the results of the measurements done on the drill cores.

3.1. Measurements of the Oil Samples

This section presents the measurements taken on the oil samples in the UV, VNIR, SWIR, and TIR ranges. It explores the effects of oil thickness on absorption features and compares the oil and mineral absorption features. Lastly, it presents the imaging spectroscopy measurements of the oils soaked in the sandstone.

3.1.1. TIR Measurements

The results of the Infrared analysis of the oil samples can be seen in Figure 3.1, which shows the very light oil in red, the light oil in green and the heavy oil in blue. All three oil samples exhibit absorption features between 3.3 μm and 3.9 μm , attributed to C-H stretching of Aliphatic bonds (Asemani & Rabbani, 2020). Absorption features between 11.0 μm and 14.5 μm are due to the C-H bending of Aromatics. The region between 5.5 μm and 9.1 μm shows absorption features due to bonds such as C=O, N-H, C=C, O-H, and C-N, associated with hetero-compounds like Carboxylic acids, Esters, Ketones, Amides, Phenols and Alcohols. Additionally, the heavy oil displays broad water absorption features at 2.9 μm and 6.1 μm . Table 3.1 gives a detailed view of the maximum wavelength of the absorption features of the three oil samples and the corresponding functional group that causes the absorption features. Additionally, the heavy oil showed water absorption features at 2.9 μm and 6.1 μm (Scafutto et al., 2021).

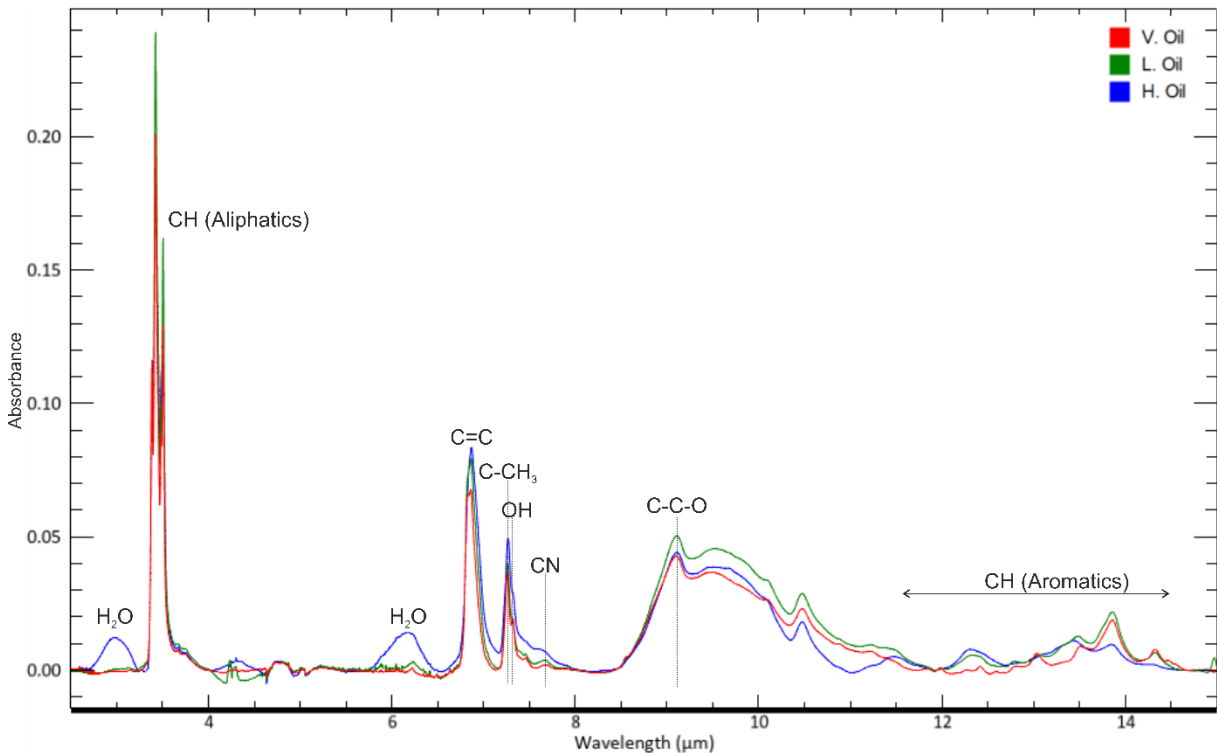


Figure 3.1 TIR spectra of the three oil samples.

Table 3.1 Maximum wavelength of the absorption features of the three oil samples and the corresponding functional group that causes the absorption features in the infrared range.

V.Oil	L.Oil	H.Oil	Reason (Asemani & Rabbani, 2020)
(um)			
-	-	2.982	Water
3.384	3.385	3.390	C-H stretching Aliphatic
3.422	3.423	3.423	
3.452	3.454	3.451	
3.482	3.485	3.483	
3.505	3.505	3.505	
5.737	5.737	5.737	C=O stretching Carboxylic acid and Esters
5.896	5.896	5.900	C=O stretching Carboxylic acid and Esters
5.938	5.938	5.942	C=O stretching Ketones
6.050	6.050	6.053	C=O stretching Amides
-	-	6.100	Water
6.188	6.188	6.188	C=O stretching Ketones
6.345	6.345	6.345	N-H bending Amides and C=C stretching Aromatics
6.811	6.811	-	C=C stretching Aromatics
6.862	6.863	6.869	
6.954	6.954	6.954	
7.113	7.113	7.113	O-H bending Carboxylic Acids and C=C stretching Aromatics
7.252	7.262	7.268	C-C stretching Aliphatic
7.319	7.320	7.324	O-H bending Phenols
7.457	7.459	7.461	C-O-H bending Alcohols
7.676	7.676	7.670	C-N stretching Amide
7.884	7.928	7.900	C-O stretching Carboxylic Acids and C-C-C stretching Ketones
8.163	8.183	8.150	C-C-O stretching Phenols and Esters
8.562	8.562	8.562	C-C-O stretching Alcohols
9.100	9.107	9.109	C-C-O stretching Alcohols and Esters
11.223	11.223	11.223	C-H bending Aromatic
11.377	11.377	11.377	
11.521	11.494	11.507	
11.779	11.792	11.723	
12.165	12.165	12.165	
12.270	12.330	12.315	
13.333	13.333	13.263	
13.514	13.495	13.441	
13.870	13.870	13.870	
14.327	14.327	14.286	

3.1.2. VNIR-SWIR Measurements

The VNIR and SWIR spectra of the three oil samples—very light (red), light (green), and heavy (blue)—are depicted in Figure 3.2. Key absorption features are present around $1.7\ \mu\text{m}$ and $2.3\ \mu\text{m}$, corresponding to the first overtones and combinations of the C-H bonds, respectively (Stuart, 2004). Another major absorption in the VNIR region is caused by the Pi bonds in the oil samples (Asadzadeh & Filho, 2017). While the very light oil shows a high reflectance in this region, which reflects the transparent nature of the oil, the light and heavy oil show a lower reflectance, which reflects the red and black colours of the two oils.

Minor absorption features around $1.2\ \mu\text{m}$ are attributed to the second overtone of the C-H bonds in the oil samples (Stuart, 2004). These absorption features are more prominent in the very light and light oil than in the heavy oil. Additionally, minor absorption features around $1.4\ \mu\text{m}$ are visible in very light and light oils but are masked in heavy oil due to water presence. Similarly, absorption features in the $1.85\ \mu\text{m}$ to $2.2\ \mu\text{m}$ range form a plateau in the very light and light oils but are obscured in the heavy oil due to water absorption.

The mean reflectance values over the VNIR and SWIR range differ significantly among the oils, with the very light oil having a high mean reflectance value of 0.84, the light oil having a mean reflectance value of 0.55 and the heavier oil having a low mean reflectance value of 0.34. Another difference between the three oil samples is the absorption slope due to the Pi bonds: the very light oil lacks this absorption, resulting in no discernible slope, whereas the light and heavy oil exhibit a slope due to this feature. The slope calculated between wavelengths $0.6\ \mu\text{m}$ and $1.1\ \mu\text{m}$ measures $2.28\ \mu\text{m}^{-1}$ for the light oil and $0.54\ \mu\text{m}^{-1}$ for the heavy oil, indicating a steeper slope for the light oil and a gentler slope for the heavy oil. Table 3.2 gives a detailed view of the minimum wavelength of the absorption features of the three oil samples and the corresponding overtones and combinations that cause these absorption bonds.

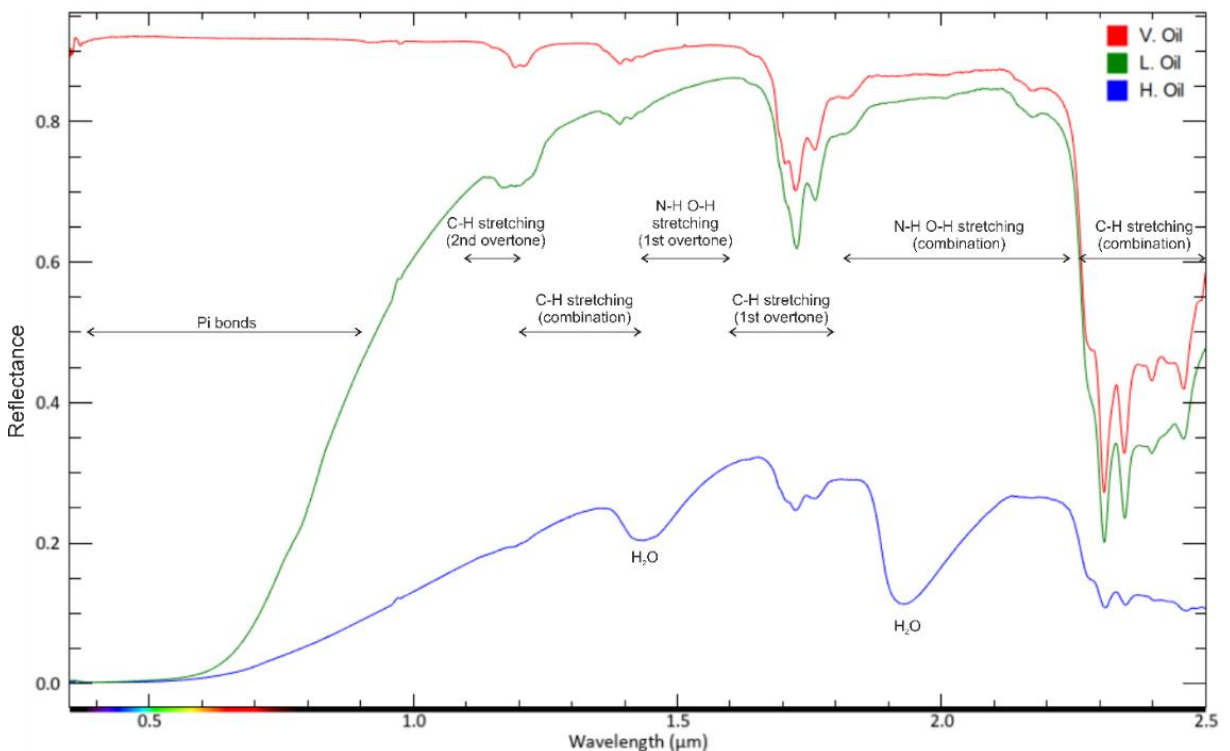


Figure 3.2 VNIR-SWIR spectra of the three oil samples.

Table 3.2 Minimum wavelength of the absorption features of the three oil samples and the corresponding vibrational bonds that cause the absorption features in the SWIR range. c refers to combination, while 1o and 2o refer to the first and second overtone.

V.Oil	L.Oil	H.Oil	Reason	
			(Stuart, 2004)	(Pabón & Filho, 2019)
	(um)			
1.153	1.151	-	C-H stretching 2o	
1.193	1.192	1.193		
1.209	1.208	1.210		C-H Aliphatic
1.362	1.361	1.361	C-H stretching c	
1.392	1.391	1.438		OH stretching
1.412	1.412			C-H Aliphatic
1.432	1.435	1.438	N-H O-H stretching 1o	
1.446	1.446			
1.468	1.465			
1.641	1.640	1.641	C-H stretching 1o	
1.675	1.678	1.679		
1.692	1.693	1.693		
1.704	1.704	1.704		
1.724	1.726	1.723		C-H stretching Aliphatic
1.760	1.761	1.761		C-H stretching Aliphatic
1.796	1.796	1.795		
1.822	1.822	1.825	N-H O-H stretching c	
1.867-2.118	1.867-2.118	1.927		
2.142	2.142	2.147		
2.170	2.169	2.167		C-H stretching Aromatic
2.285	2.285	2.286	C-H stretching c	
2.308	2.308	2.308		C-H stretching Aliphatic
2.346	2.347	2.347		C-H stretching Aliphatic
2.377	2.378	2.377		
2.398	2.398	2.400		
2.426	2.426	2.426		
2.456	2.458	2.455		
2.491	-	-		

3.1.3. Measurements with respect to Thickness of Oil layer

In these measurements, the thickness of the very light and light oils in the petri dish was systematically varied, and their spectra were recorded to examine the impact of increasing oil thickness on spectral characteristics, as depicted in Figure 3.3 and Figure 3.5. The results indicate that as the oil thickness increases, the depth of features also increases, initially affecting longer wavelength features before progressing towards shorter wavelengths. Specifically, absorption features at $1.724\ \mu\text{m}$ and $2.308\ \mu\text{m}$ were selected for analysis as they exhibited the greatest depth in the spectra. Figure 3.4 and Figure 3.6 illustrate the relationship between oil thickness and the depth of these absorption features. It reveals a general trend where increasing oil thickness correlates with greater feature depth. However, there is a notable deviation for the feature at $2.308\ \mu\text{m}$: after initially increasing, the depth begins to decrease due to spectral saturation. This saturation phenomenon becomes evident by observing the reflectance values of other absorption features around this wavelength, as spectra that saturate tend to exhibit low overall reflectance in these regions.

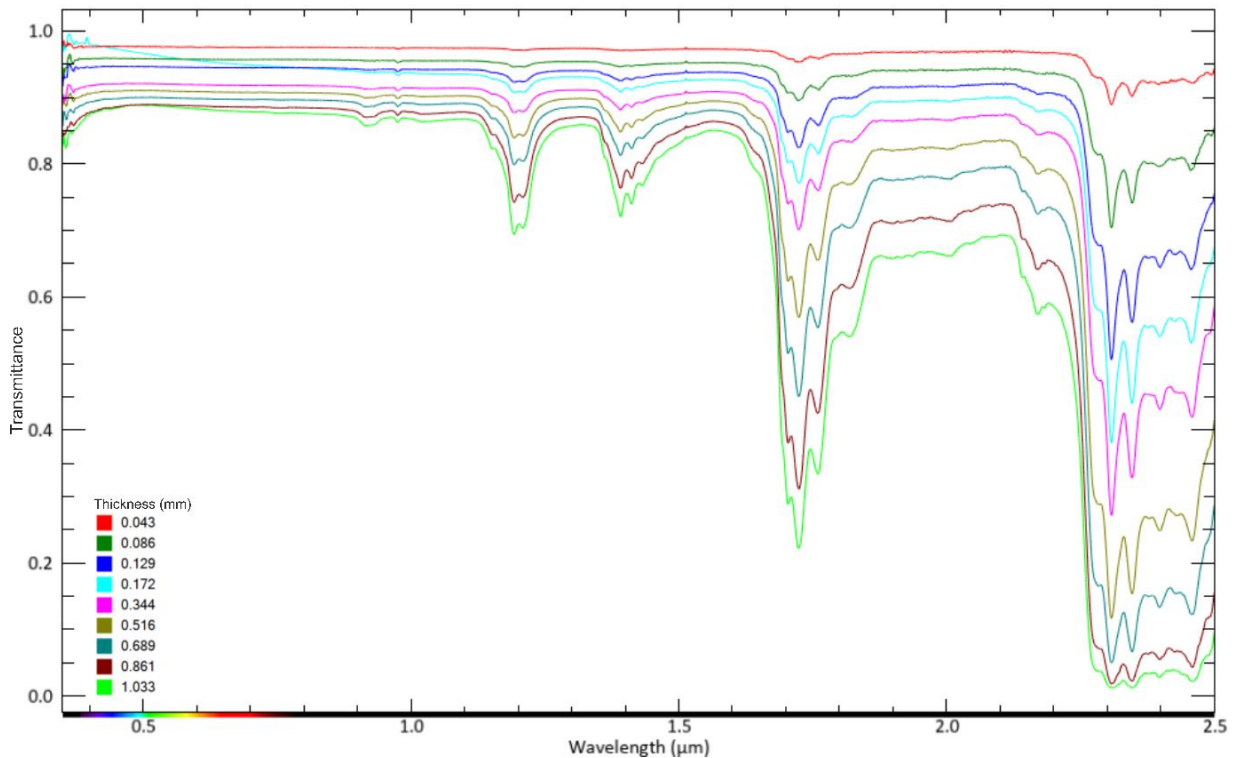


Figure 3.3 Spectra of the very light oil with increasing thickness.

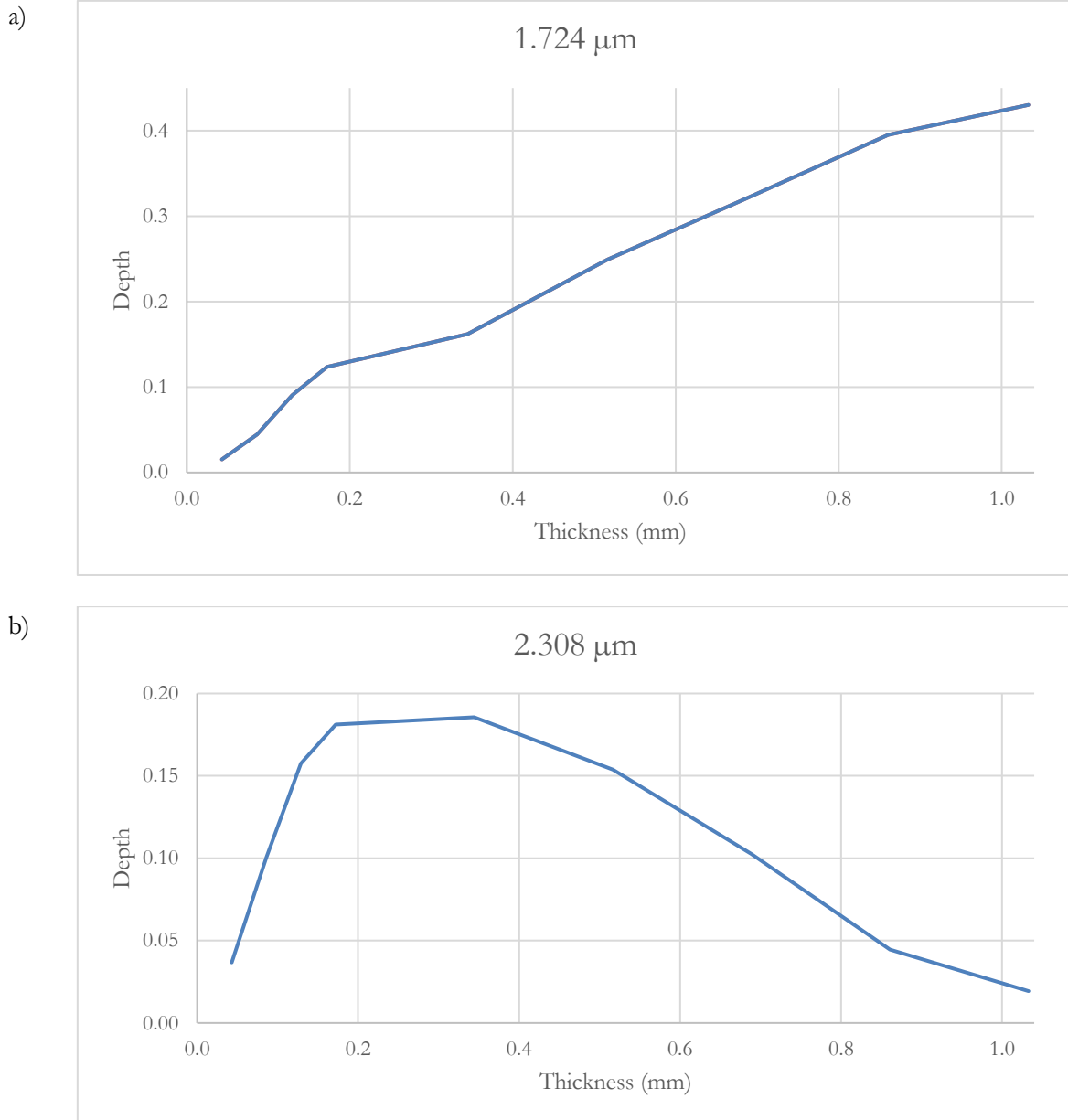


Figure 3.4 Graph showing the thickness vs depth relation of the very light oil at a) 1.724 μm and b) 2.308 μm .

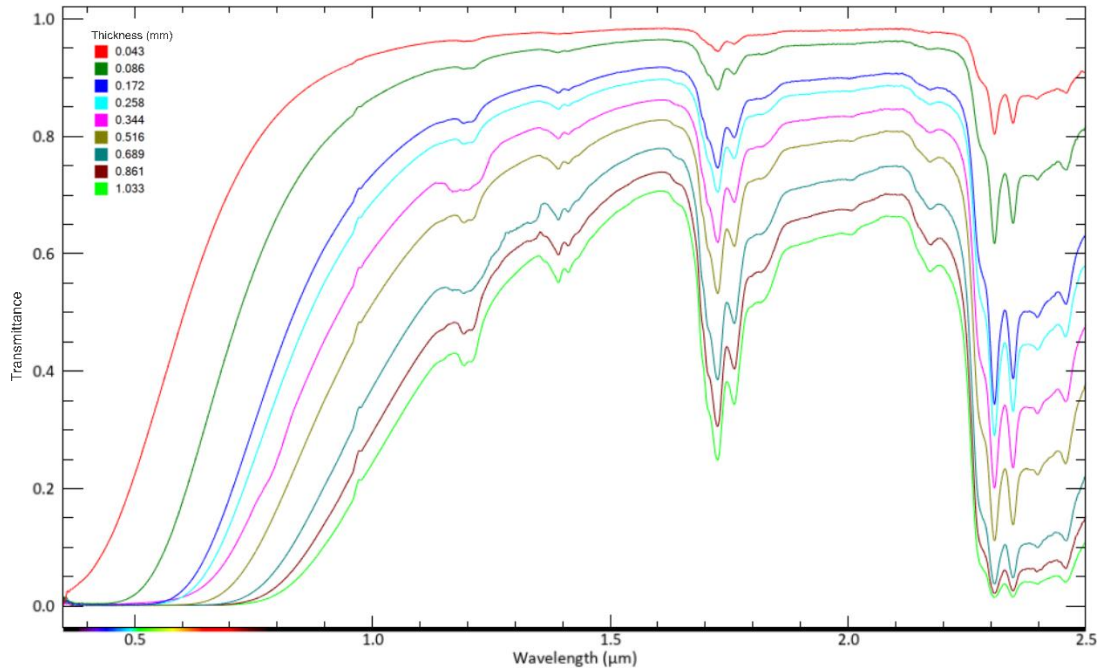


Figure 3.5 Spectra of the light oil with increasing thickness.

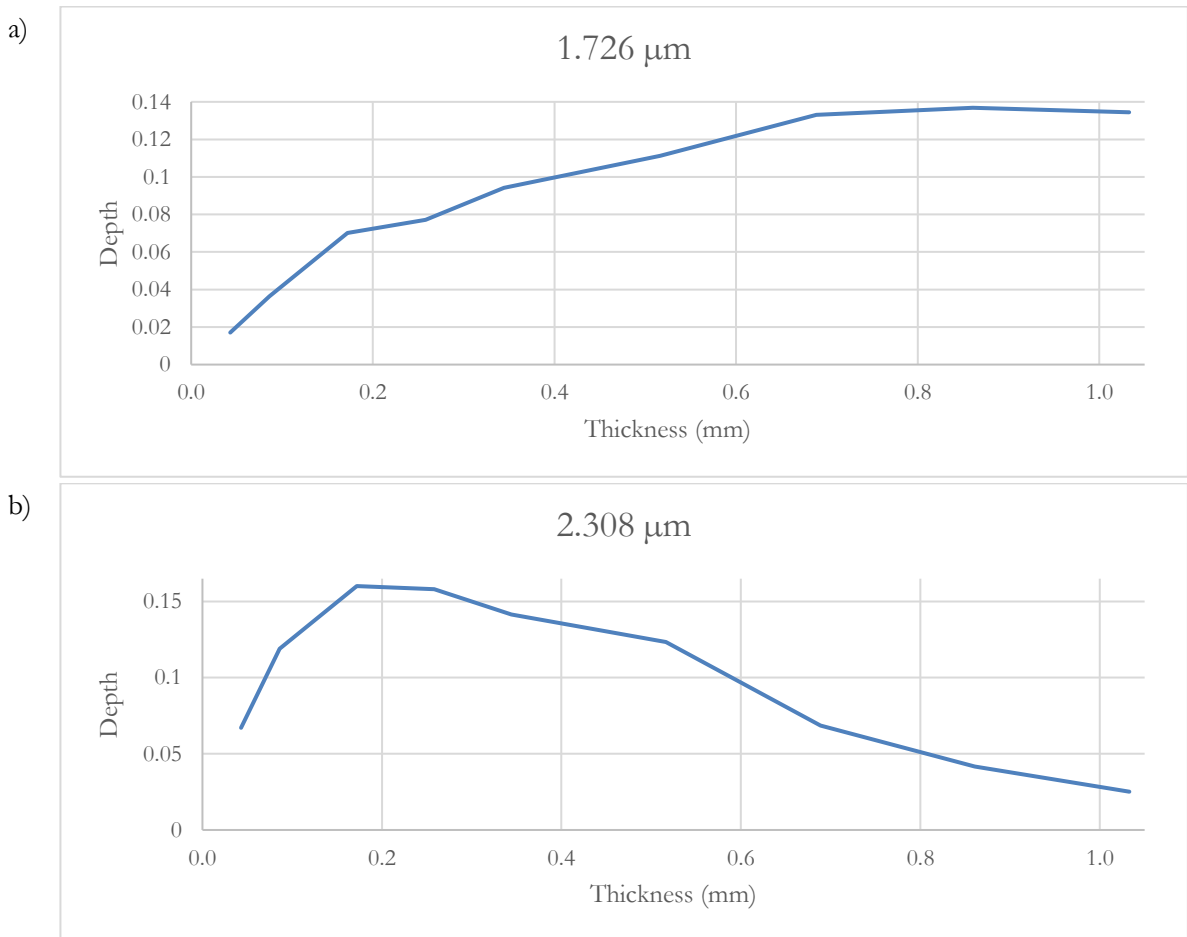


Figure 3.6 Graph showing the thickness vs depth relation of the light oil at a) 1.724 μm and b) 2.308 μm .

3.1.4. Comparing the Spectra of Oil and Minerals

Absorption features of Oil and Minerals

This section provides a detailed comparison of the absorption features of oil with those of minerals commonly found in hydrocarbon-containing drill cores from the Netherlands, specifically focusing on the SWIR range. The following figures show the four ranges examined, with the first four deepest absorption features noted in each range. The starting and ending wavelengths of these ranges were selected based on their alignment with the absorption feature shoulders of the oil and the minerals used in the comparison. The spectra of the minerals and the table of the four deepest absorption features are given in Annex 1.

In the range of 1.1 μm to 1.65 μm (Figure 3.7), the first and second deepest absorption features of the oil at 1.193 μm and 1.209 μm respectively coincide with the fourth deepest feature of gypsum at 1.206 μm . Similarly, the third and fourth deepest features of the oil overlap with the first and second deepest features of illite, muscovite, kaolinite, and chlorite. Moving to the range of 1.65 μm to 1.85 μm (Figure 3.8), there is no overlap of features, although the deepest absorption feature of gypsum (1.749 μm) falls between the first and second deepest absorption features of oil (1.724 μm and 1.761 μm). Further, in the range of 1.85 μm to 2.1 μm (Figure 3.9), the deepest absorption feature of the oil at 2.008 μm closely aligns with the 1.997 μm feature of calcite. In the range of 2.1 μm to 2.5 μm (Figure 3.10), the deepest absorption feature of the oil at 2.308 μm is proximal to the 2.322 μm and 2.326 μm features of dolomite and chlorite, respectively. Moreover, the second deepest oil feature at 2.347 μm coincides with the 2.345 μm and 2.353 μm features of illite and muscovite, respectively. Additionally, the presence of water in the rock can mask the absorption features of oil in the range of 1.1 μm to 1.65 μm and 1.85 μm to 2.1 μm . The optimal ranges to map oil and minerals from this comparison are further discussed in the Discussion chapter.

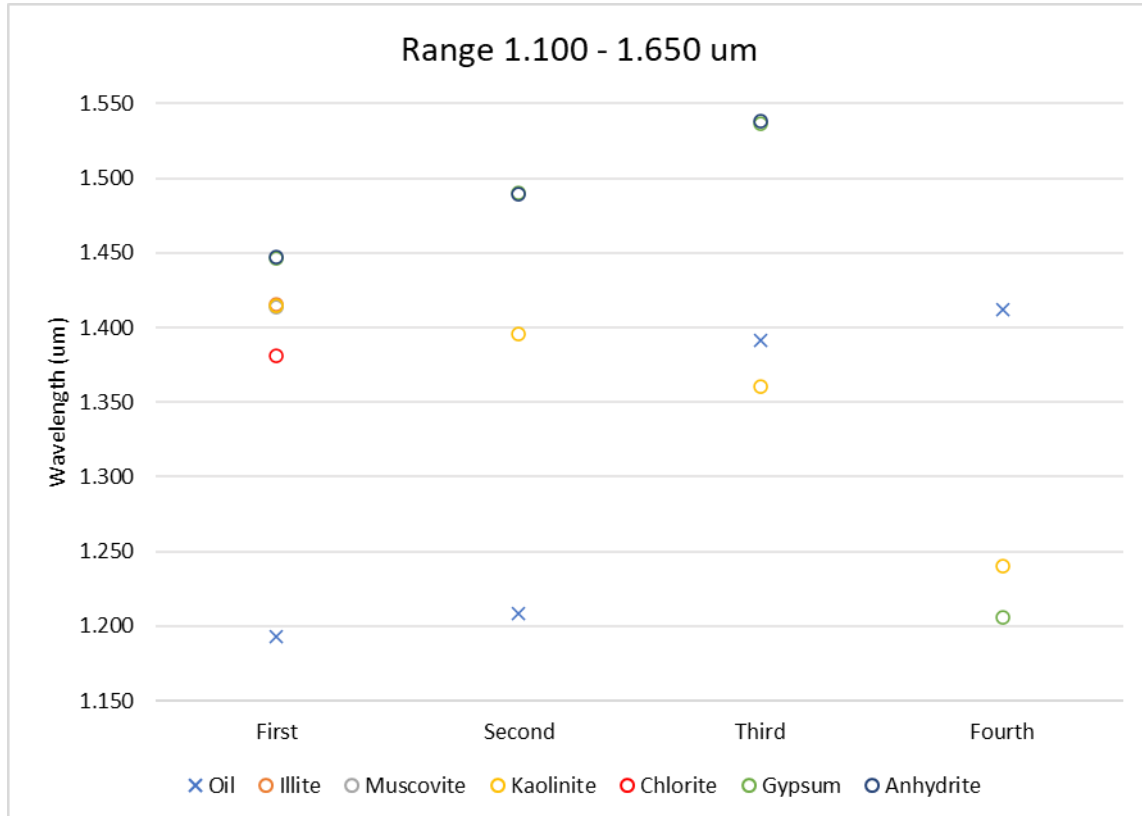


Figure 3.7 Graph showing the interpolated minimum wavelength of the four deepest absorption features in the range of 1.100 μm to 1.650 μm .

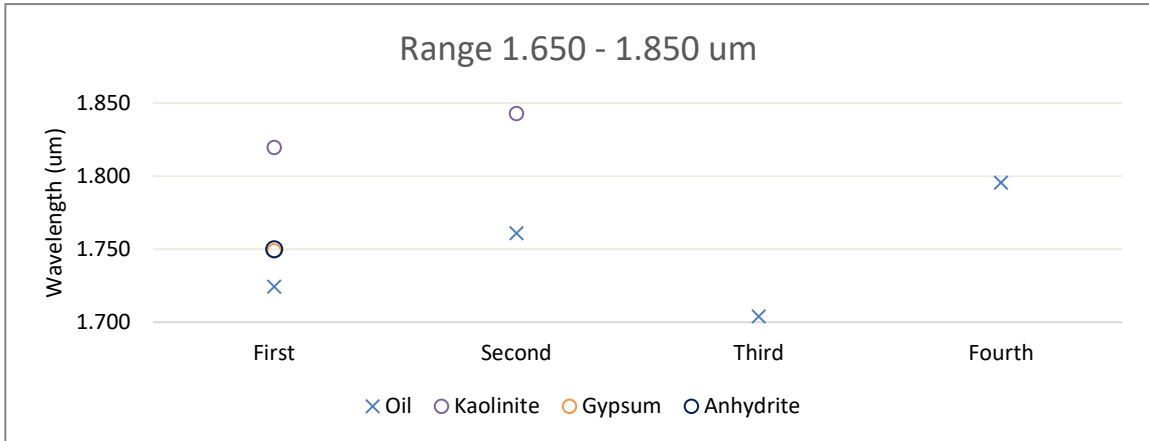


Figure 3.8 Graph showing the interpolated minimum wavelength of the four deepest absorption features in the range of 1.650 μm to 1.850 μm .

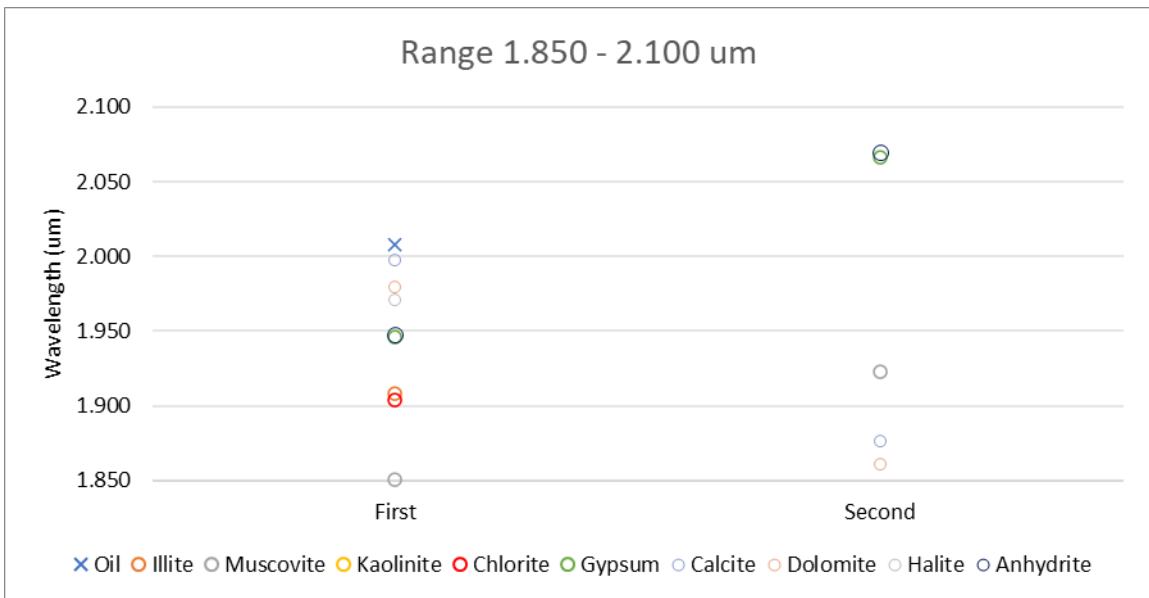


Figure 3.9 Graph showing the interpolated minimum wavelength of the four deepest absorption features in the range of 1.850 μm to 2.100 μm .

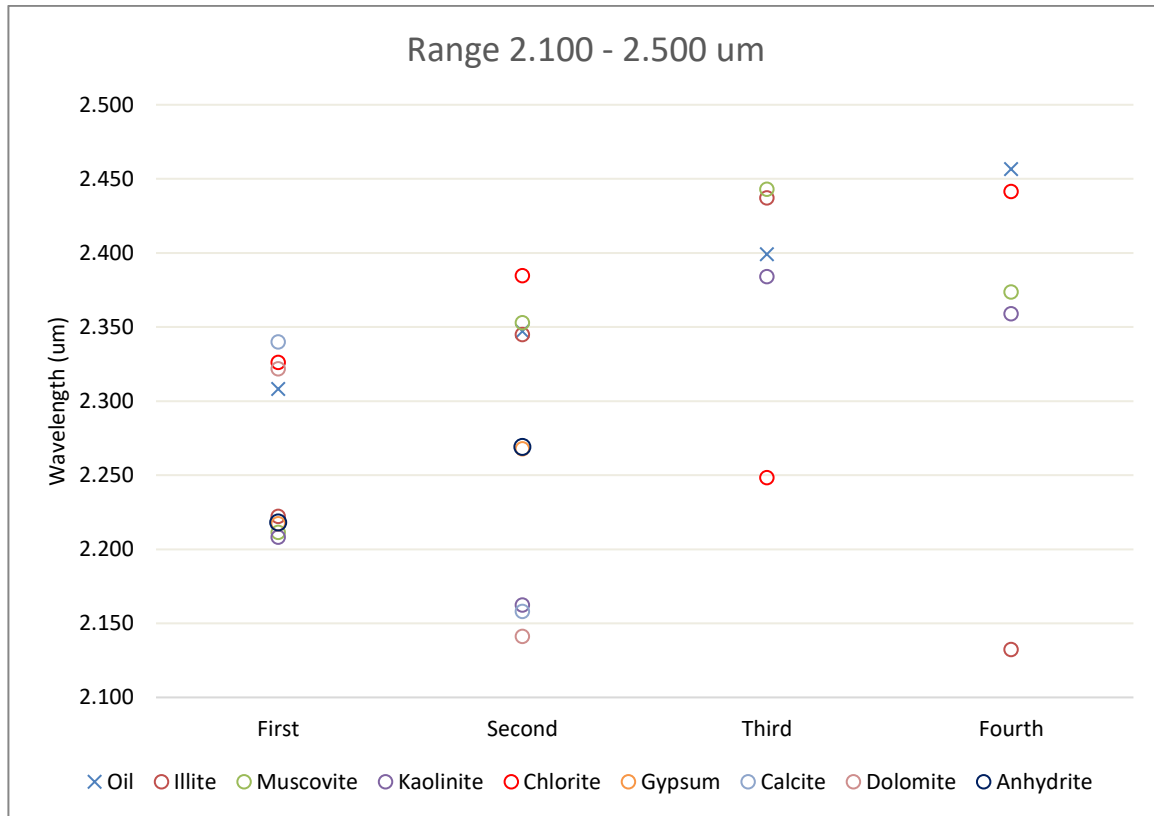


Figure 3.10 Graph showing the interpolated minimum wavelength of the four deepest absorption features in the range of 2.100 μm to 2.500 μm .

Spectral Angle of Oil and Minerals

The spectral angles between the mineral spectra, the light oil (L. Oil) and heavy oil (H. Oil) were also compared across the same four ranges mentioned above: 1.1 μm to 1.65 μm , 1.65 μm to 1.85 μm , 1.85 μm to 2.1 μm , and 2.1 μm to 2.4 μm . A spectral angle matrix was created to assess the similarity of the spectra, where lower values indicate higher similarity. The results are presented in Figure 3.11 to Figure 3.14, and their implications are discussed in the Discussion chapter.

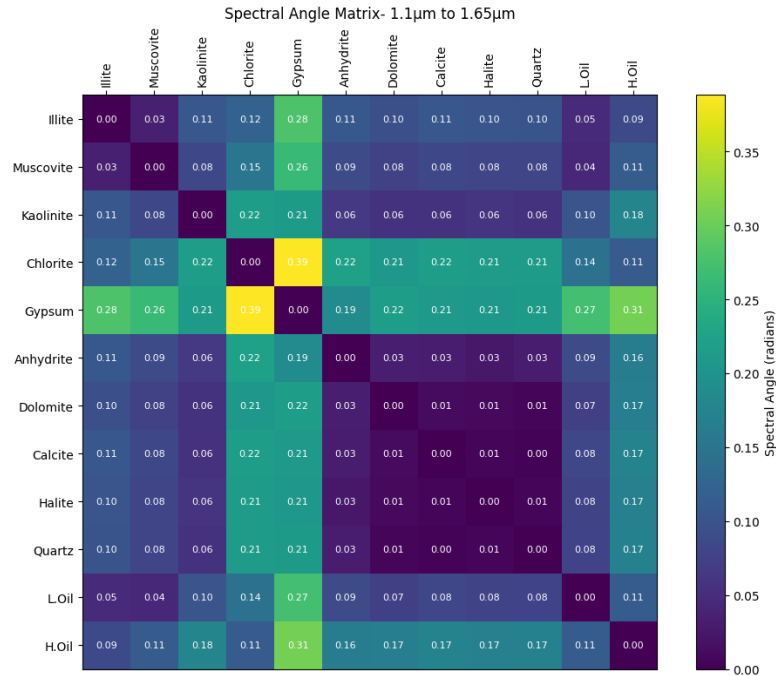


Figure 3.11 Spectral Angle Matrix showing the spectral angle similarity of the minerals and oil in the range of 1.100 μm to 1.650 μm .

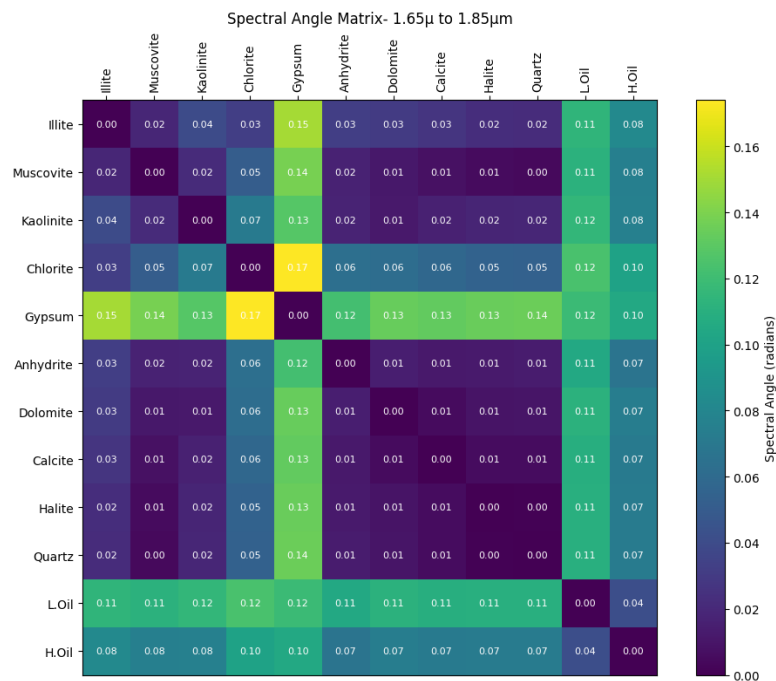


Figure 3.12 Spectral Angle Matrix showing the spectral angle similarity of the minerals and oil in the range of 1.650 μm to 1.850 μm .

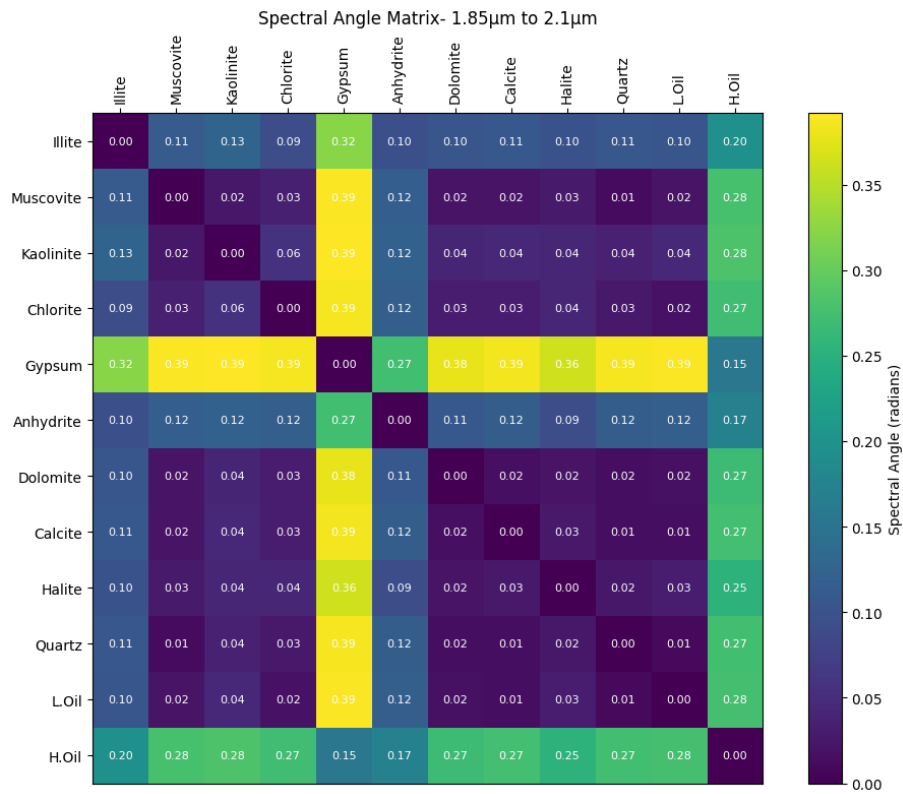


Figure 3.13 Spectral Angle Matrix showing the spectral angle similarity of the minerals and oil in the range of 1.850 µm to 2.100 µm.

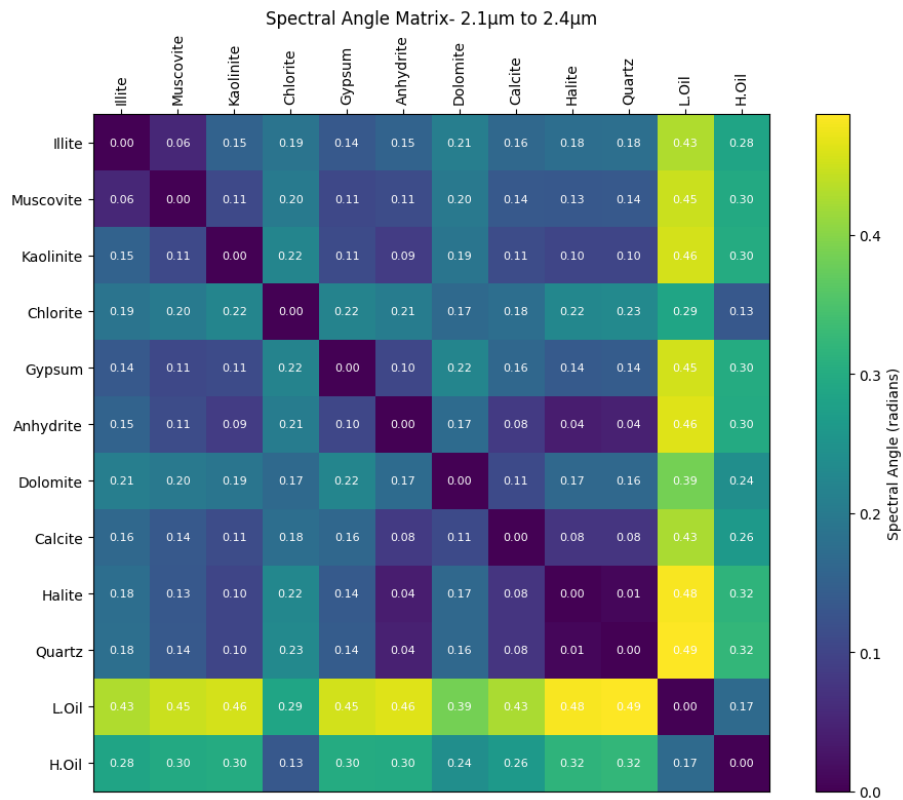


Figure 3.14 Spectral Angle Matrix showing the spectral angle similarity of the minerals and oil in the range of 2.100 µm to 2.400 µm.

3.1.5. UV Fluorescence Measurements

UV measurements were conducted on the three oil samples to investigate differences in their fluorescence spectra. Figure 3.15 presents the fluorescence spectra of sandstone soaked in very light oil (red), light oil (green), heavy oil (blue), and unsoaked sandstone (yellow). The inset graph highlights the fluorescence spectra of unsoaked sandstone and very light oil.

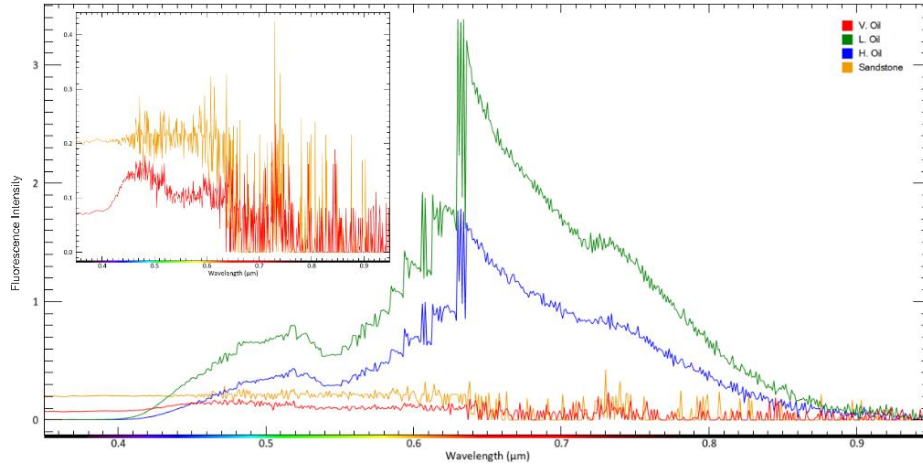


Figure 3.15 Fluorescence spectra of the unsoaked sandstone and the sandstone soaked with the three oil samples, with the inset focusing on the unsoaked sandstone and very light oil.

Figure 3.16 shows a photograph of the representative setup comparing the differences between unsoaked sandstone (S) and sandstone soaked with very light oil (VO), light oil (LO), and heavy oil (HO). The unsoaked sandstone and the sandstone soaked in very light oil exhibit very low fluorescence values and appear black. The very light oil shows a fluorescence peak at around $0.475 \mu\text{m}$. In contrast, the light oil displays higher fluorescence values than the heavy oil, appearing brownish red depending on the oil thickness. The fluorescence spectra for both light and heavy oils show a minor peak at $0.519 \mu\text{m}$ and $0.734 \mu\text{m}$ and a major peak at $0.630 \mu\text{m}$, corresponding to the brownish-red colour observed. The relationship between the three oil samples and their fluorescence spectra will be further discussed in the Discussion chapter.

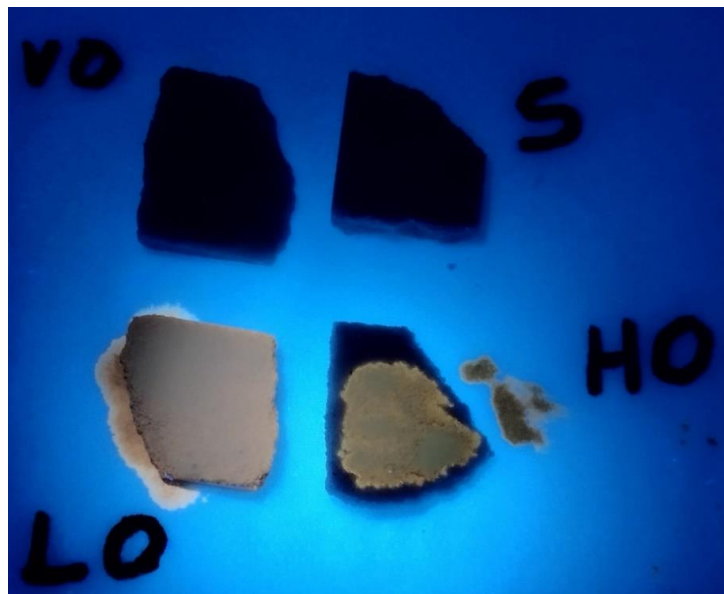


Figure 3.16 Photograph of the unsoaked sandstone (S) along with the sandstone soaked with very light oil (VO), light oil (LO) and heavy oil (HO).

3.1.6. VNIR-SWIR Imaging Measurements

The Specim cameras were used to record the spectra of sandstone samples soaked in oil in the VNIR and SWIR range. Figure 3.17 displays the spectra in the SWIR range, with very light oil in red, light oil in green, heavy oil in blue, and unsoaked sandstone in yellow. The thickness of the spectral line indicates the concentration of oil: the thinnest line represents 0.25 ml, the medium thick line represents 0.5 ml, and the thickest line represents 1.0 ml. The yellow spectrum of the sandstone shows OH features at 1.4 μm and 1.9 μm , along with a clay absorption feature at 2.2 μm . These OH absorption features are also present in the oil spectra, with the very light and light oil having shallower features compared to the deeper features in the heavy oil.

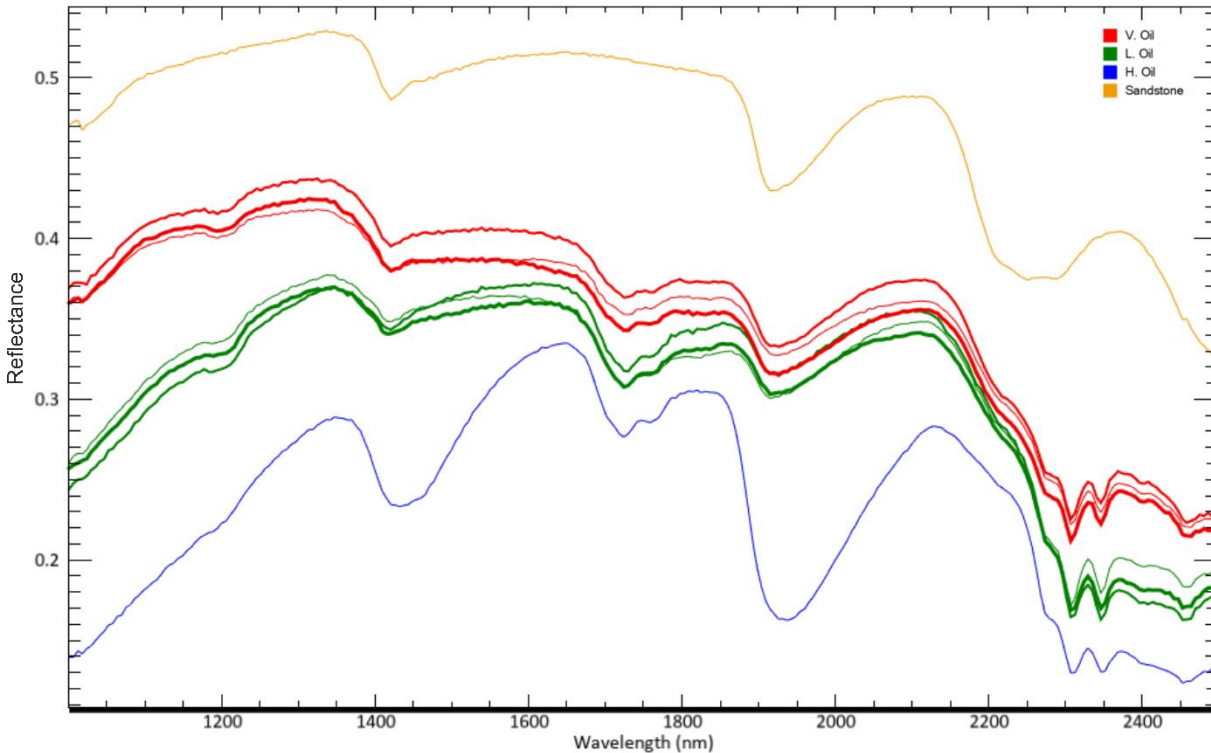


Figure 3.17 Spectra of the oil soaked sandstone recorded by the Specim camera in the SWIR range. The thinnest line represents 0.25 ml, the medium thick line represents 0.5 ml, and the thickest line represents 1.0 ml of oil in the sandstone.

Major absorption features at 1.724 μm , 1.758 μm , 2.308 μm , and 2.348 μm are observed in all three oil samples, with minor oil absorption features around 1.2 μm evident in the very light and light oil. Similar to pure oil samples, the spectra of oil soaked in sandstone show that the very light oil has a higher overall reflectance, followed by the light oil, with the heavy oil having the lowest overall reflectance. No significant differences are observed in the spectra with varying volumes of oil in terms of its absorption features and mean reflectance.

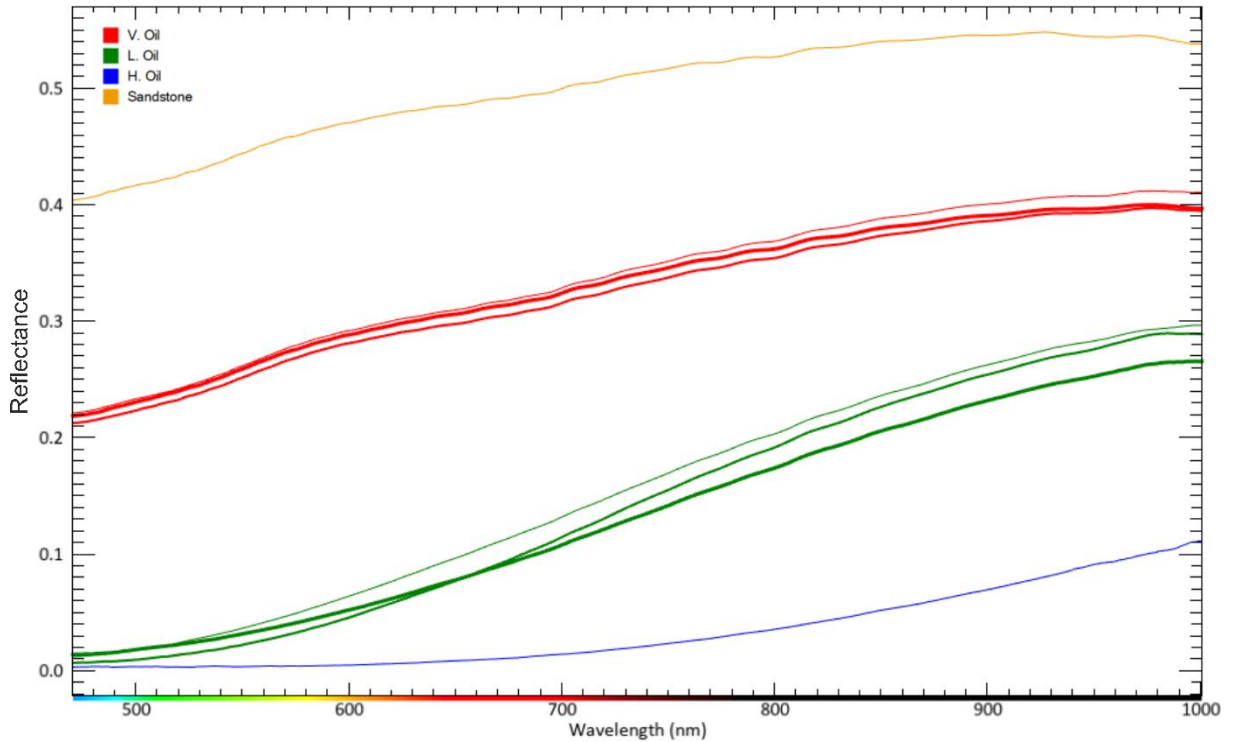


Figure 3.18 Spectra of the oil soaked sandstone recorded by the Specim camera in the VNIR range. The thinnest line represents 0.25 ml, the medium thick line represents 0.5 ml, and the thickest line represents 1.0 ml of oil in the sandstone.

Figure 3.18 shows the spectra in the VNIR region. The spectra of the sandstone in yellow have the highest reflectance, followed by the very light oil in red, the light oil in green, and the heavy oil in blue with the lowest reflectance. The various thicknesses of the spectra represent the volume of oil soaked in the sandstone, with the thinnest line representing 0.25 ml, followed by 0.5 ml, and the thickest line representing 1.00 ml. The dip in the sandstone spectra towards shorter wavelengths is also reflected in the spectra of the very light oil. The absorption due to Pi bonds in this range is also seen in the spectra of the light and heavy oil, with the light oil having a steeper slope compared to the gentler slope of the heavy oil. Like the spectra in the SWIR range, no major differences are observed in the spectra with varying volumes of oil soaked in the sandstone in terms of its absorption features and mean reflectance.

3.2. Measurements on the Drill Cores

3.2.1. UV Fluorescence Measurements

Measurements on Drill Core 1 show the fluorescence spectra of oil in all readings of the drill core, with variations in fluorescence intensity (Annex 2). The fluorescence spectra display a major peak at around $0.62\ \mu\text{m}$ and minor peaks at $0.5\ \mu\text{m}$ and $0.73\ \mu\text{m}$ (Figure 3.19a). Similarly, UV fluorescence measurements on Drill Core 2 show the fluorescence spectra of oil in all readings of the drill core (Annex 2). The fluorescence spectra exhibit a major peak at around $0.62\ \mu\text{m}$ and minor peaks at $0.51\ \mu\text{m}$ and $0.73\ \mu\text{m}$ (Figure 3.19b). For better clarity, these spectra were smoothed with one level of smoothing in ENVI.

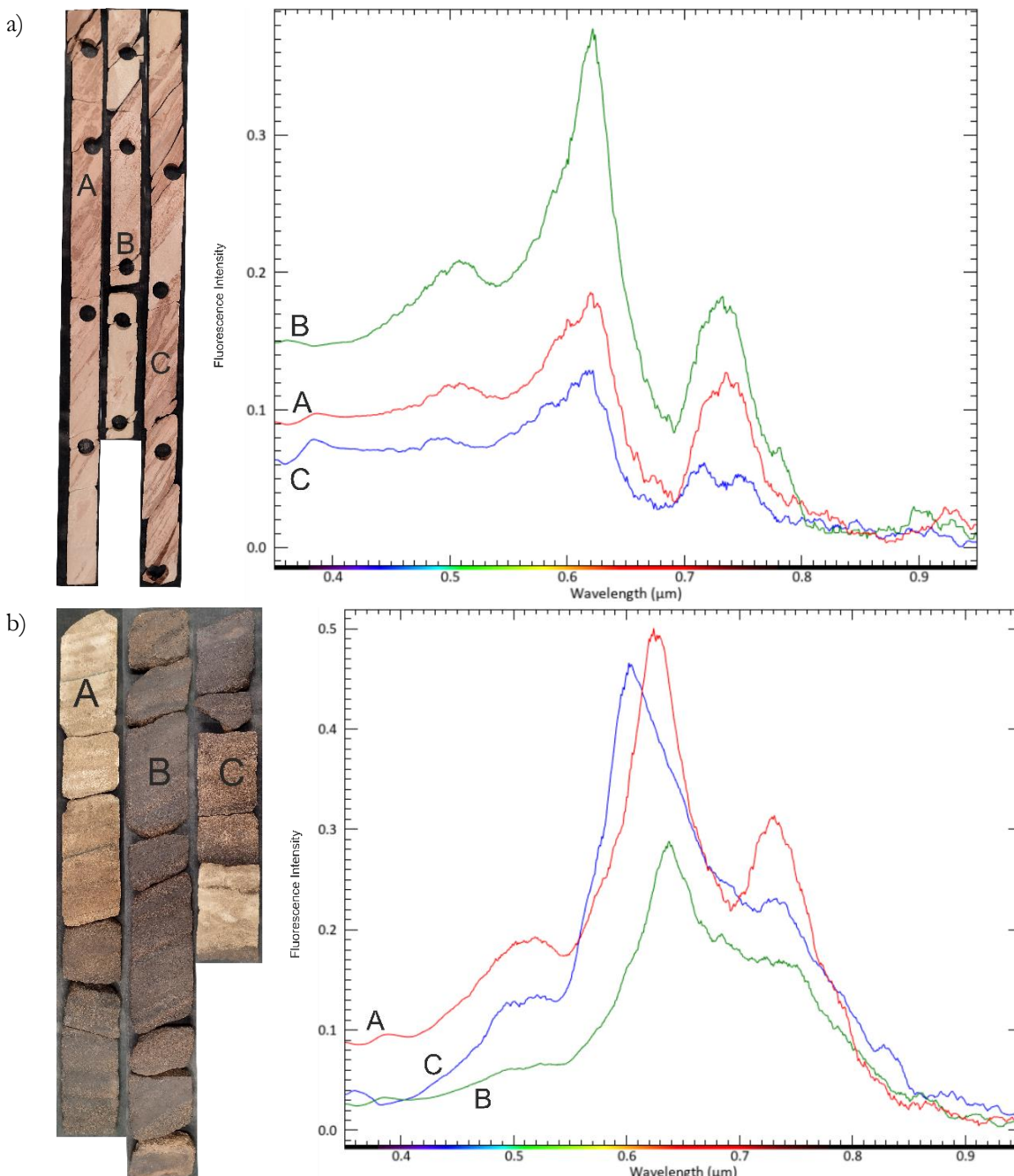


Figure 3.19 Fluorescence Spectra of (a) Drill Core 1 and (b) Drill Core 2.

3.2.2. VNIR-SWIR Point Spectral Measurements

In addition to the mineral composition stated in the literature, a point spectral measurement of the drill core was conducted to identify other minerals (Annex 3). Point spectral measurements of Drill Core 1 using the Spectral Evolution SR-6500 instrument revealed the presence of hematite (0.875 μm broad absorption feature in spectrum D), gypsum (triplet absorption features at 1.45 μm in spectrum B), and kaolinite (2.206 μm feature in spectrum C) (GMEX, 2008), in addition to quartz and calcite, which were stated by Robbmond et al. (2002) (Figure 3.20). Oil absorption features were observed throughout DC1, with the prominent absorption features at 1.7 μm and 2.3 μm . Unlike pure oil, the 2.349 μm absorption feature of oil in the drill core was deeper than the 2.308 μm feature. The probable reasons for this will be covered in the Discussion chapter.

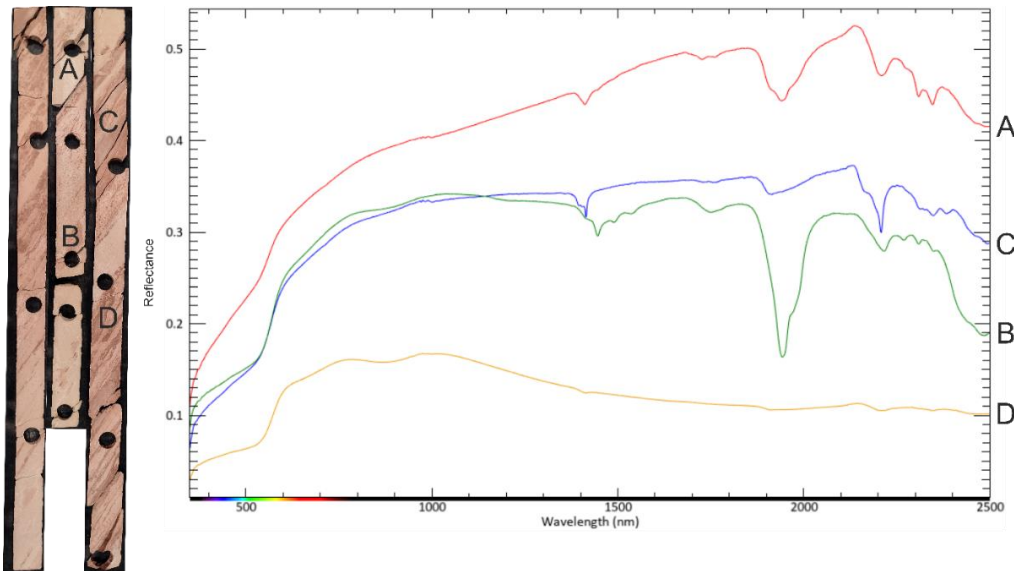


Figure 3.20 Spectra of the oil (A), gypsum (B), kaolinite (C) and hematite (D) present in Drill Core 1 as revealed by point spectral analysis.

Point spectral measurements of Drill Core 2 also show the presence of kaolinite (2.206 μm feature in spectra A and C), in addition to quartz, as reported by Ayyad & Parmigiano (1983) (Figure 3.21). Similar to DC1, oil absorption features were detected throughout DC2. The light-coloured sections of DC2 exhibited relatively higher reflectance values and shallower oil absorption features (A and C), whereas the darker sections showed lower reflectance values and deeper oil absorption features (B).

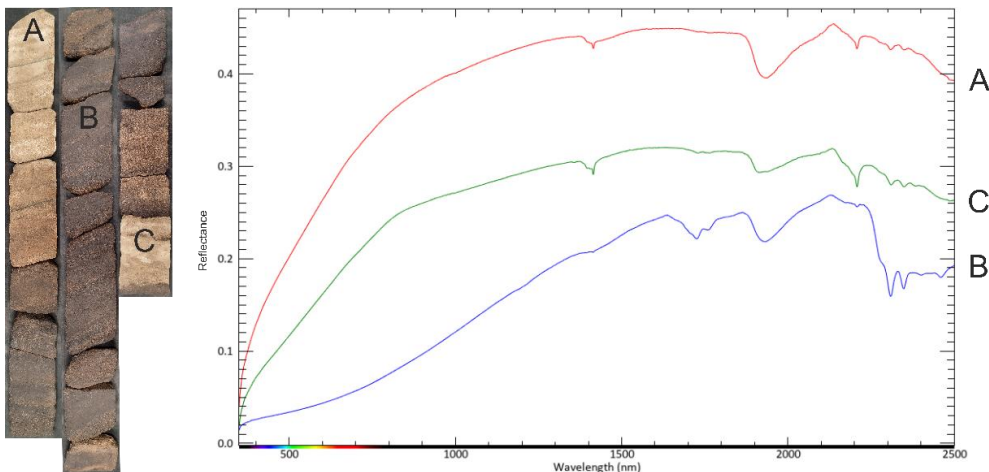


Figure 3.21 Spectra of the oil (B) and kaolinite (A and C) present in Drill Core 2 as revealed by point spectral analysis.

3.2.3. VNIR-SWIR Imaging Measurements

Drill Core 1 and Drill Core 2 were scanned using the Specim cameras in the VNIR and SWIR regions. Figure 3.22 shows the absorption in the VNIR region of Drill Core 1 from the four regions mentioned in Figure 3.20. The transparent oil in this drill core does not exhibit any absorption in the VNIR range and thus reflects the absorption due to the presence of hematite in the drill core. Figure 3.23 illustrates the absorption in Drill Core 2 in the VNIR range. The spectra from the lighter regions (A and D) show the absorption slope of the sandstone (quartz), while spectra from the darker regions (B and C) show the gentle absorption slope of the heavy oil present in the drill core.

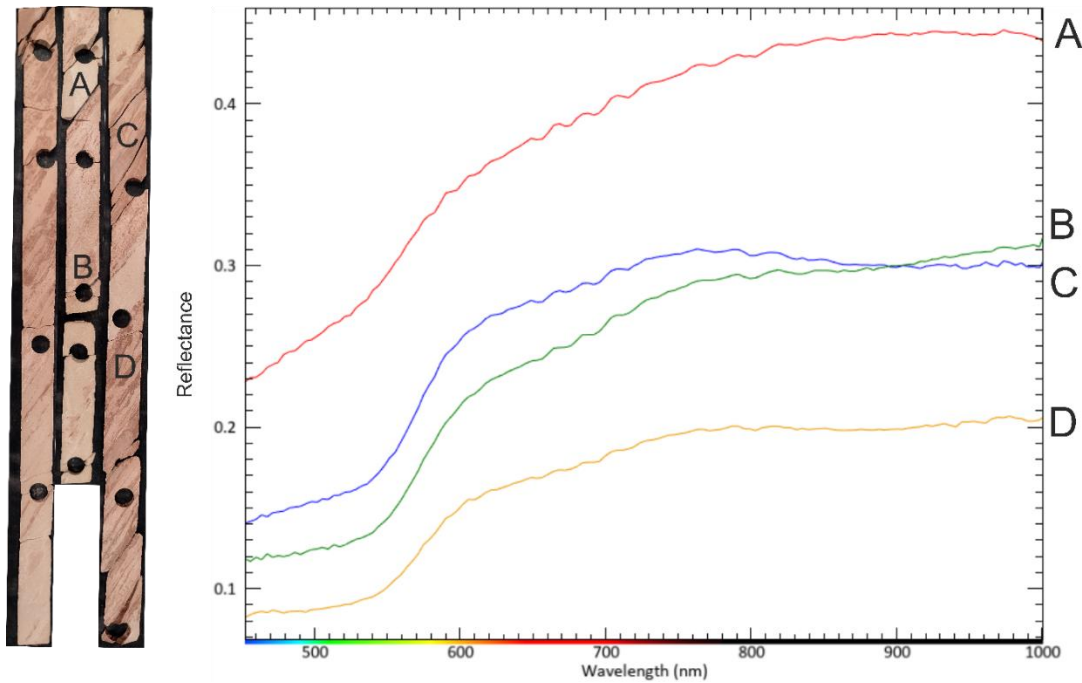


Figure 3.22 VNIR spectra of Drill Core 1 showing the broad absorption features of hematite.

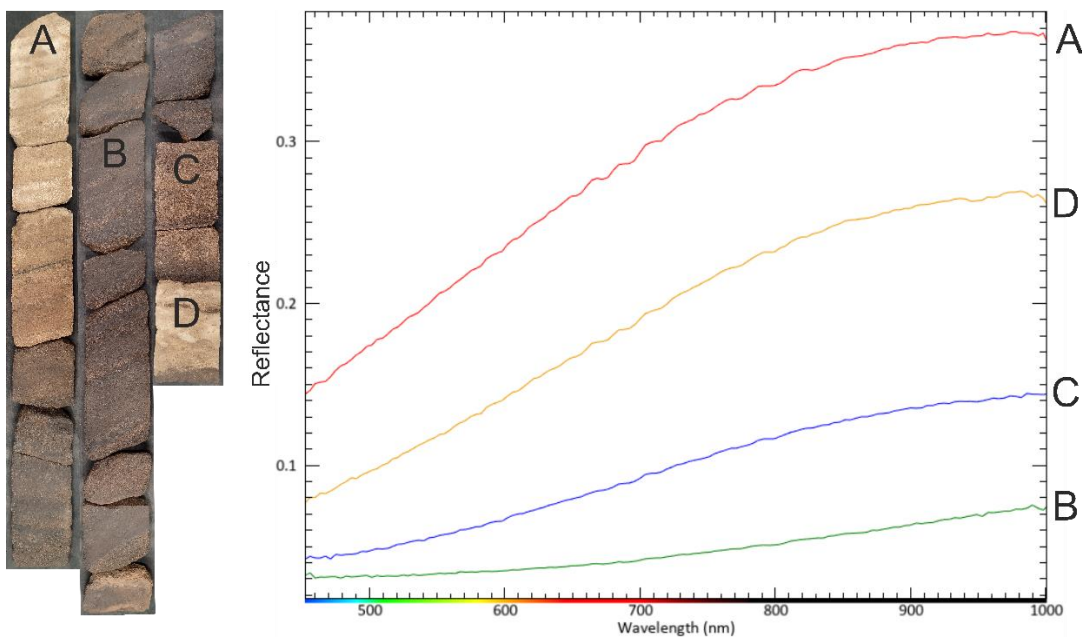


Figure 3.23 VNIR spectra of Drill Core 2 showing the absorption due to quartz (A and D) and oil (B and C).

Figure 3.24 shows the absorption in the SWIR region of Drill Core 1 from the four regions mentioned in Figure 3.20. Spectrum A shows the absorption features of oil at 2.308 μm and 2.349 μm . Spectrum B shows the triplet absorption features of gypsum at 1.449 μm , the deep water absorption feature at 1.95 μm , and the shallow feature at 1.75 μm ; Spectrum C shows the kaolinite absorption feature at 2.206 μm . Lastly, spectrum D is the low reflectance spectra of hematite, as identified in Figure 3.20. Figure 3.25 shows the absorption features of kaolinite at 2.206 μm in spectra A and D. Spectrum D also shows minor oil absorption features at 2.3 μm . Spectrum B and C show the absorption features of oil at 1.7 μm and 2.3 μm , with the 2.3 μm feature having a greater depth than the 2.3 μm feature in spectrum D.

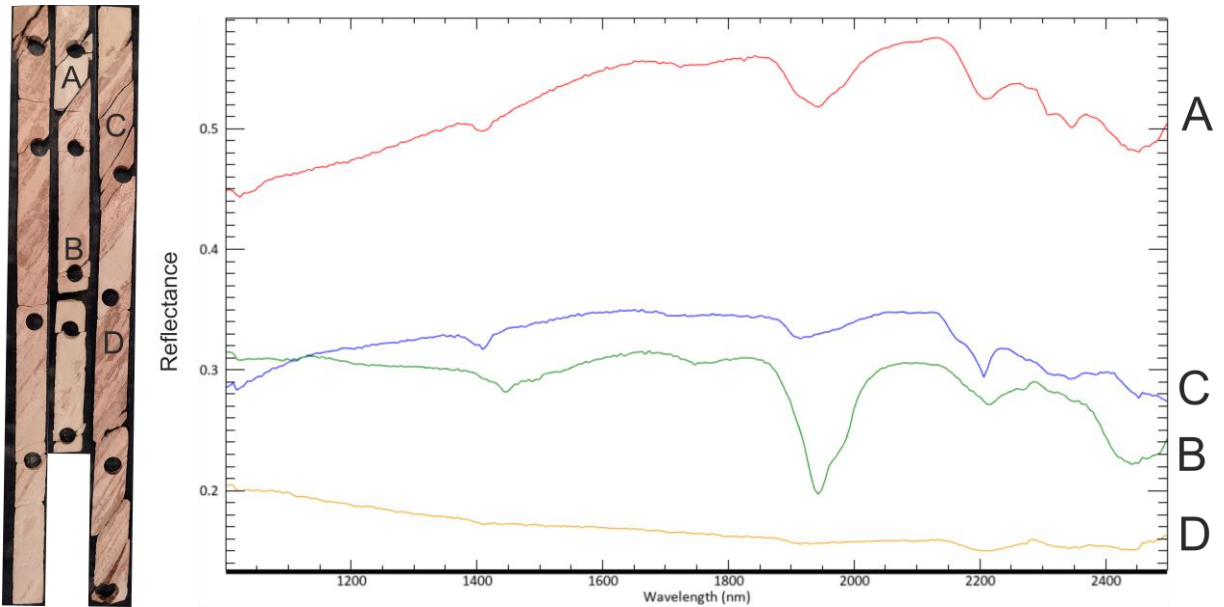


Figure 3.24 SWIR spectra of Drill Core 1 showing the mix spectra of oil (A), gypsum (B), kaolinite (C), and hematite (D)

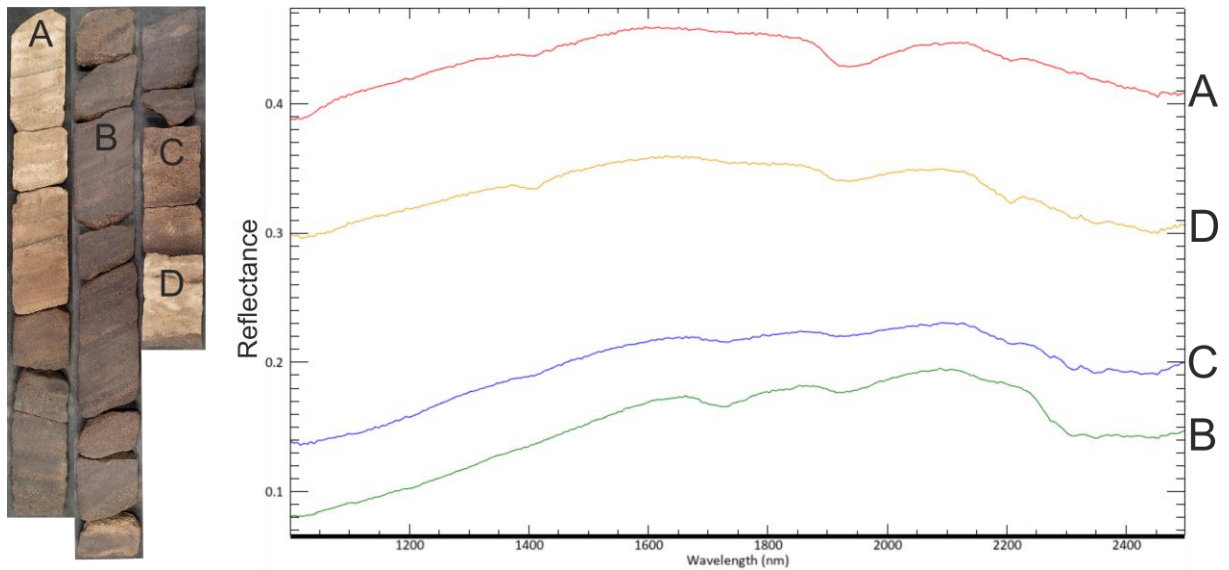


Figure 3.25 SWIR spectra of Drill Core 2 showing the mix spectra of oil (B and C) and kaolinite (A and D).

Section 3.1.4 demonstrated that the major absorption features of the oil, clays, evaporites and carbonate minerals are present in the SWIR region. Consequently, the SWIR Specim camera images of the drill cores were processed to map the spatial distribution of the oil and minerals in the drill core. Hematite, although present in the drill core, was not taken as an endmember because it does not have any diagnostic absorption features in the SWIR range. The results of these mapping processes are presented in this section and will be discussed in the discussion chapter.

Band Index

For the Band Index measurements, the Hydrocarbon Index was applied at two distinct absorption features: 1.7 μm (HI1.7) and 2.3 μm (HI2.3). The results obtained from Drill Core 1 illustrated the presence of oil within the cores, with clearer indications emerging from HI2.3 compared to the HI1.7 index (Figure 3.26). The resulting images varied in brightness, corresponding to the concentration of oil present.

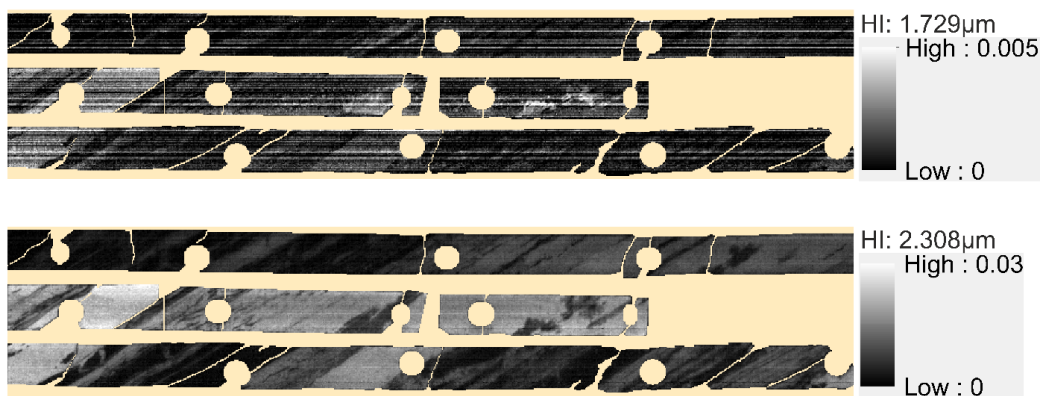


Figure 3.26 Hydrocarbon Index applied to Drill Core 1 at 1.7 μm and 2.3 μm .

Similarly, in the measurements on Drill Core 2, HI2.3 showcased better results, exhibiting reduced noise levels and providing clearer representations of oil concentration when compared to HI1.7 (Figure 3.27).

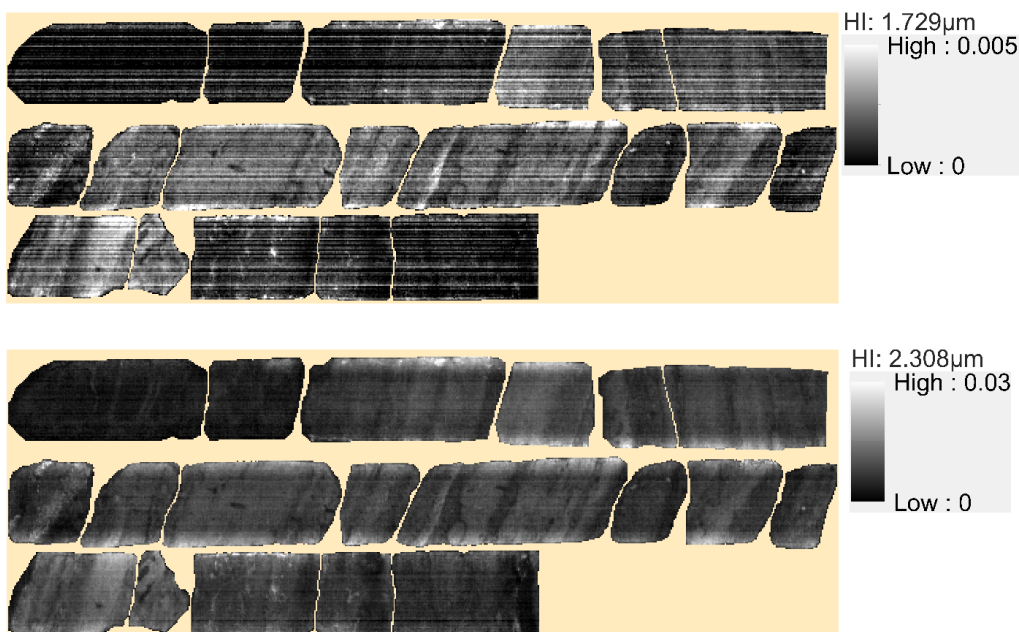


Figure 3.27 Hydrocarbon Index applied to Drill Core 2 at 1.7 μm and 2.3 μm .

Spectral Angle Mapper

The Spectral Angle Mapper algorithm was applied on the drill cores, covering various wavelength ranges from 1.100 μm to 1.650 μm , 1.650 μm to 1.850 μm , 1.850 μm to 2.100 μm , and 2.100 μm to 2.400 μm . Endmember spectra utilized in this process were sourced from the USGS spectral library (Kokaly et al., 2017). Below are the rule images generated from the SAM analysis. These images employ grayscale intensity to represent spectral angle values, where darker shades signify smaller spectral angles, indicating closer matches between pixel and endmember spectra for each pixel.

For Drill Core 1, four endmembers were employed: kaolinite, gypsum, calcite, and oil. In the range of 1.1 μm to 1.65 μm (Figure 3.28), kaolinite and calcite exhibit low spectral angle values dispersed throughout the core, while oil and gypsum display low spectral angle values in specific bands.

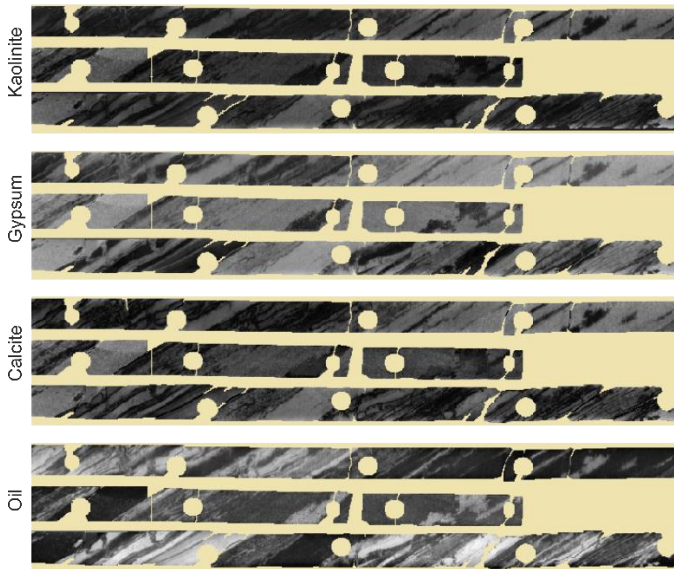


Figure 3.28 SAM rule image of Drill Core 1 in the range of 1.1 μm to 1.65 μm .

Between 1.65 μm and 1.85 μm (Figure 3.29), calcite exhibits low spectral angle values distributed across the core, while gypsum displays low values in isolated patches, and kaolinite appears as bands with low spectral angle values. Oil showcases low spectral angle values primarily in the core's central region, coinciding with the rule image of gypsum.

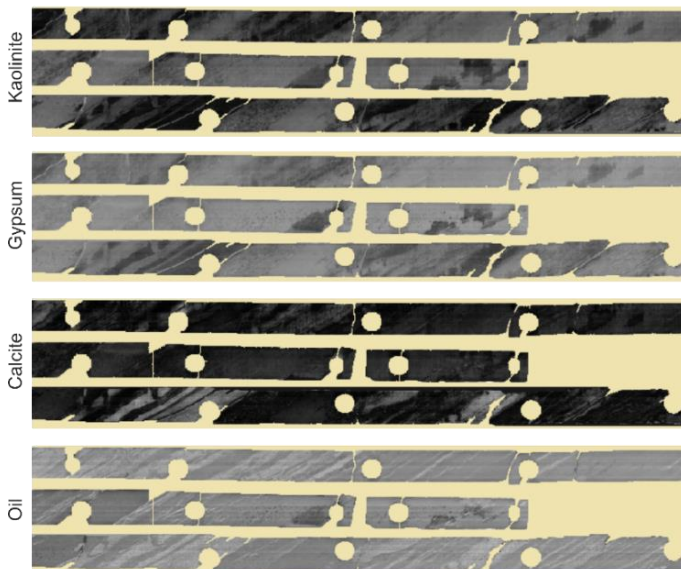


Figure 3.29 SAM rule image of Drill Core 1 in the range of 1.65 μm to 1.85 μm .

Within the 1.85 μm to 2.1 μm range (Figure 3.30), all minerals exhibit generally low spectral angle values throughout the drill core, with the exception of some patches. Notably, gypsum demonstrates low values exclusively within these patches.

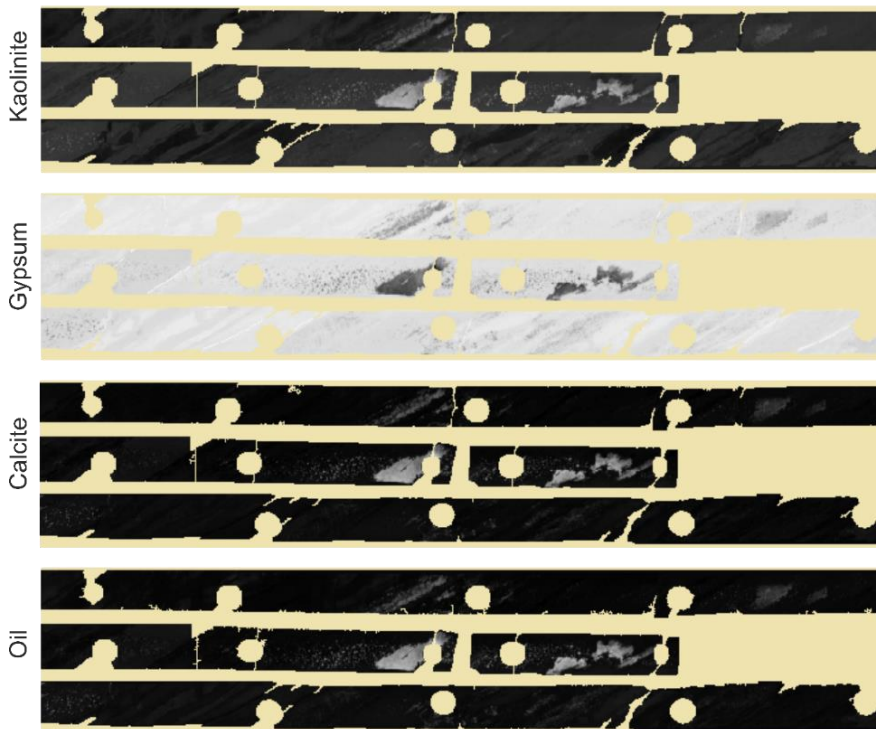


Figure 3.30 SAM rule image of Drill Core 1 in the range of 1.85 μm to 2.1 μm .

From 2.1 μm to 2.4 μm (Figure 3.31), calcite predominantly exhibits low spectral values across the core, with gypsum displaying low values in patches highlighted across other wavelength ranges. Oil and kaolinite, however, consistently show high values throughout the core.

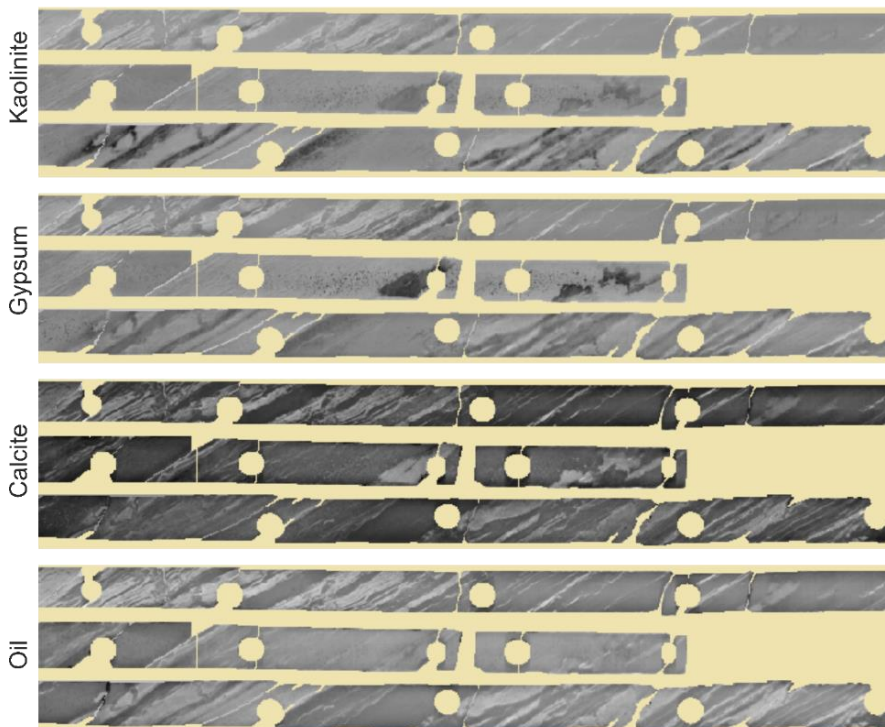


Figure 3.31 SAM rule image of Drill Core 1 in the range of 2.1 μm to 2.4 μm .

For Drill Core 2, two endmembers were utilized: kaolinite and oil. Between 1.1 μm and 1.65 μm (Figure 3.32), kaolinite and oil demonstrate a similar trend in values, with low spectral angle values at the beginning and end of the core and relatively higher values in the middle section.

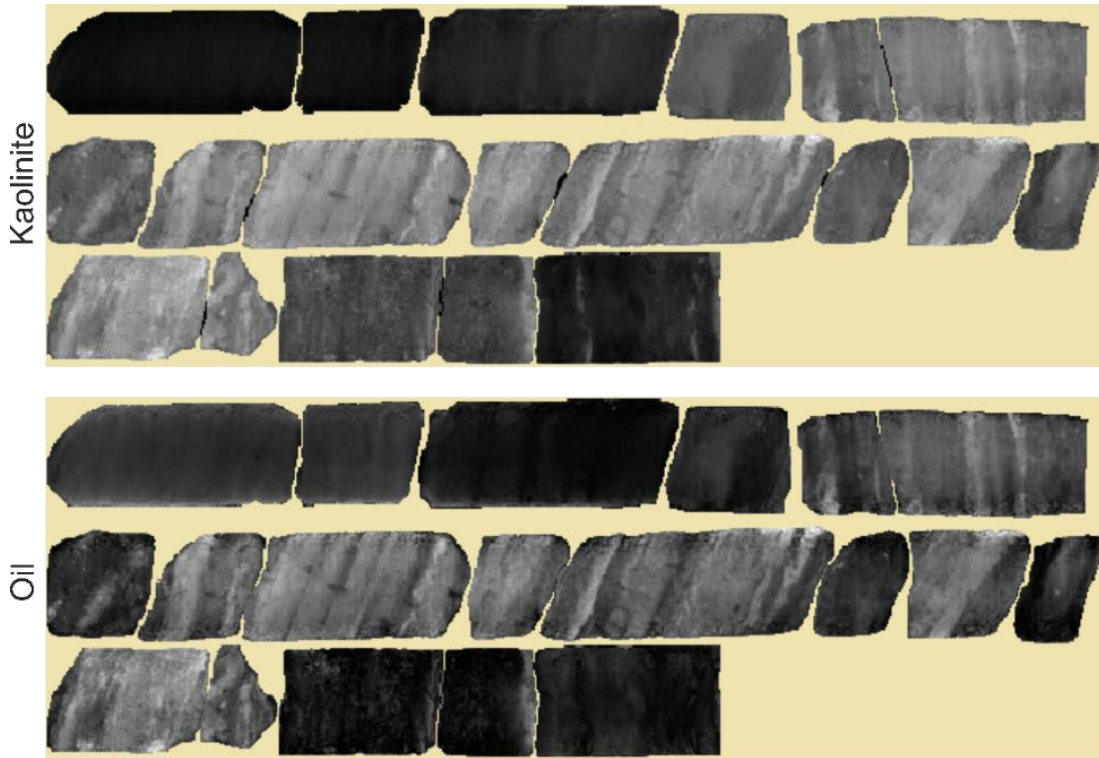


Figure 3.32 SAM rule image of Drill Core 2 in the range of 1.1 μm to 1.65 μm .

In the 1.65 μm to 1.85 μm range (Figure 3.33), kaolinite and oil exhibit opposite trends in spectral angle values, with kaolinite showing low values at the start and end of the core, whereas oil exhibits high values.

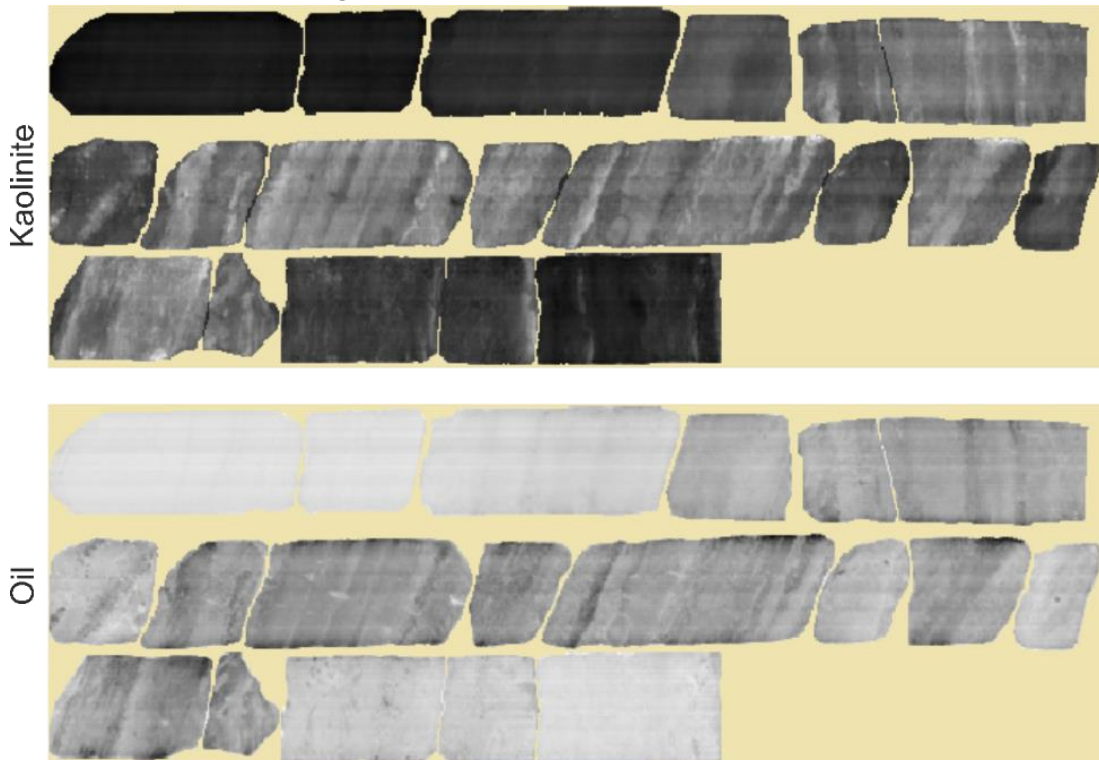


Figure 3.33 SAM rule image of Drill Core 2 in the range of 1.65 μm to 1.85 μm .

Within the 1.85 μm to 2.1 μm range (Figure 3.34), kaolinite and oil display similar trends, with kaolinite consistently exhibiting higher values than oil.

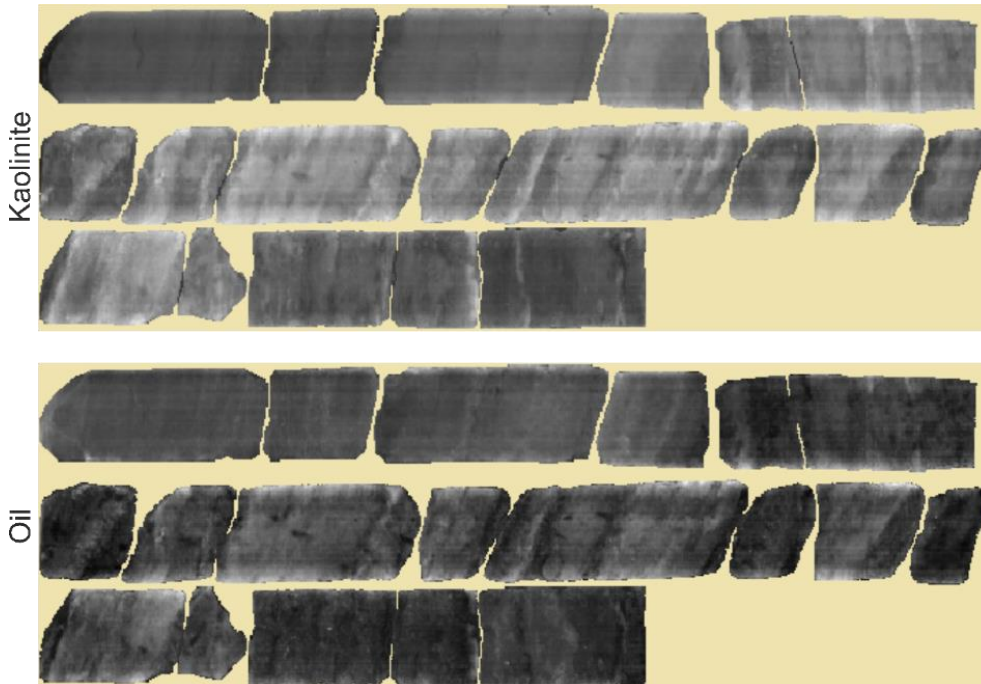


Figure 3.34 SAM rule image of Drill Core 2 in the range of 1.85 μm to 2.1 μm .

From 2.1 μm to 2.4 μm (Figure 3.35), kaolinite shows low values throughout the core, with the lowest values at the beginning and end. In contrast, oil shows high values, with the highest values also present at the beginning and end of the core.

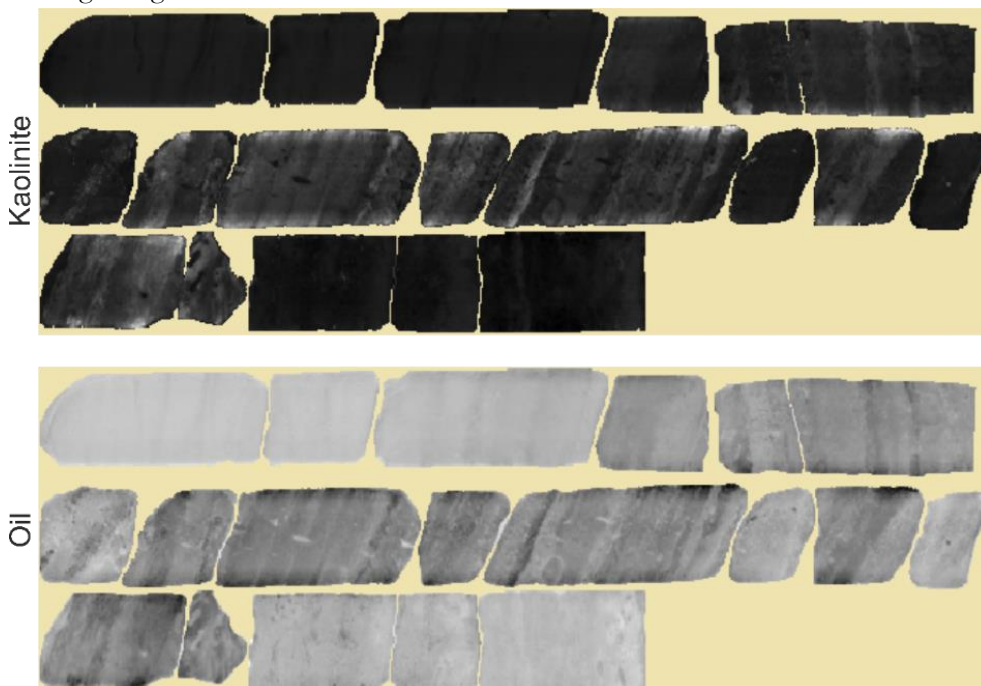


Figure 3.35 SAM rule image of Drill Core 2 in the range of 2.1 μm to 2.4 μm .

Minimum Wavelength Mapper

The Minimum Wavelength Mapper algorithm was employed on the drill cores across several wavelength ranges: 1.100 μm to 1.650 μm , 1.650 μm to 1.850 μm , 1.850 μm to 2.100 μm and 2.100 μm to 2.400 μm . Additionally, the 2.100 μm to 2.400 μm range was further broken down into 2.185 μm to 2.225 μm and 2.300 μm to 2.360 μm to focus on the clay and oil absorption features, respectively. The results of this process are given below. The minimum wavelength values corresponding to the colours were taken from the interpolated wavelength band of the deepest feature.

In the range of 1.1 μm to 1.65 μm , Drill Core 1 displayed absorption features, highlighted by various colours such as green (A), yellow (C), and orange (B), corresponding to specific minimum wavelengths of 1.3 μm , 1.409 μm , and 1.448 μm respectively (Figure 3.36).

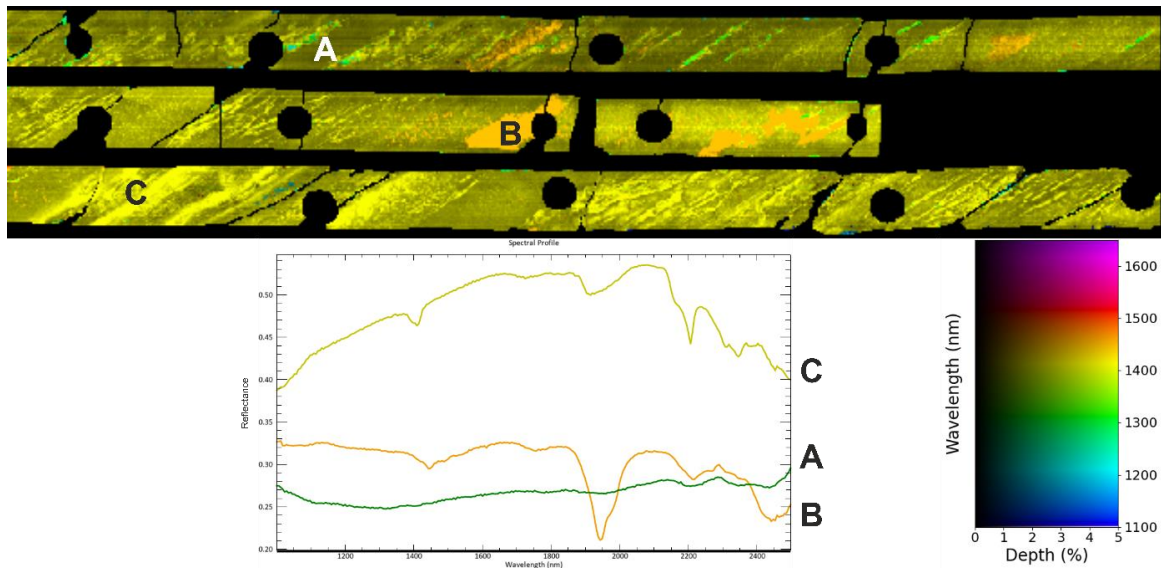


Figure 3.36 Minimum wavelength map of Drill Core 1 in the range 1.1 μm to 1.65 μm .

Moving to the range of 1.65 μm to 1.85 μm , Drill Core 1 exhibited absorption features represented by dark green (A) and yellowish-green (B) colours, indicating wavelengths around 1.723 μm and 1.748 μm respectively (Figure 3.37).

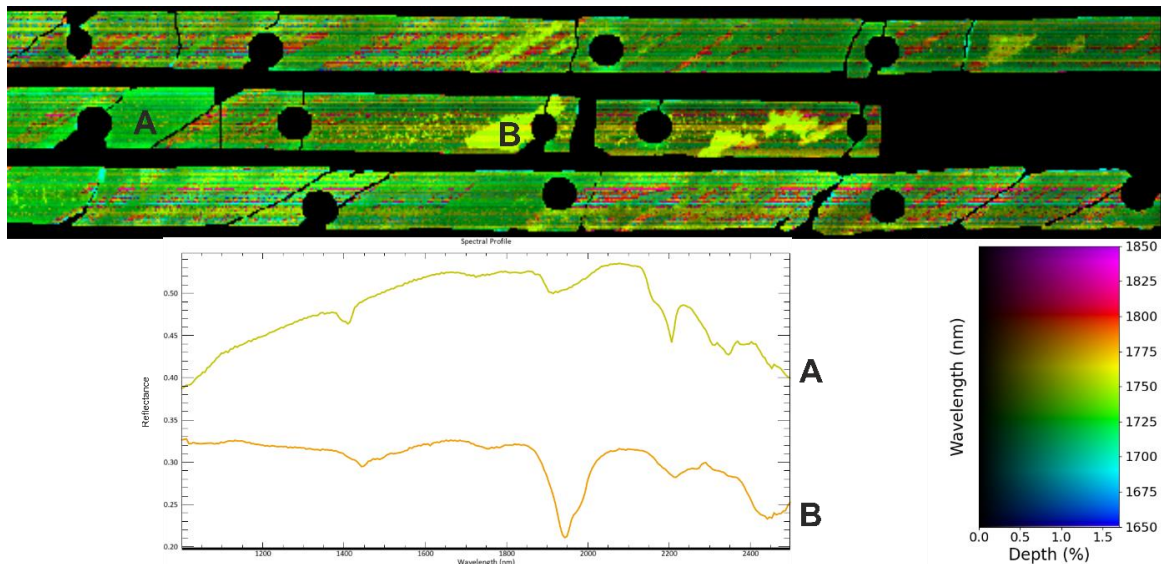


Figure 3.37 Minimum wavelength map of Drill Core 1 in the range 1.65 μm to 1.85 μm .

Further analysis in the range of 1.85 μm to 2.1 μm revealed absorption features reflected in blueish-green (A) and bright green (B) colours, corresponding to wavelengths around 1.914 μm and 1.947 μm respectively (Figure 3.38).

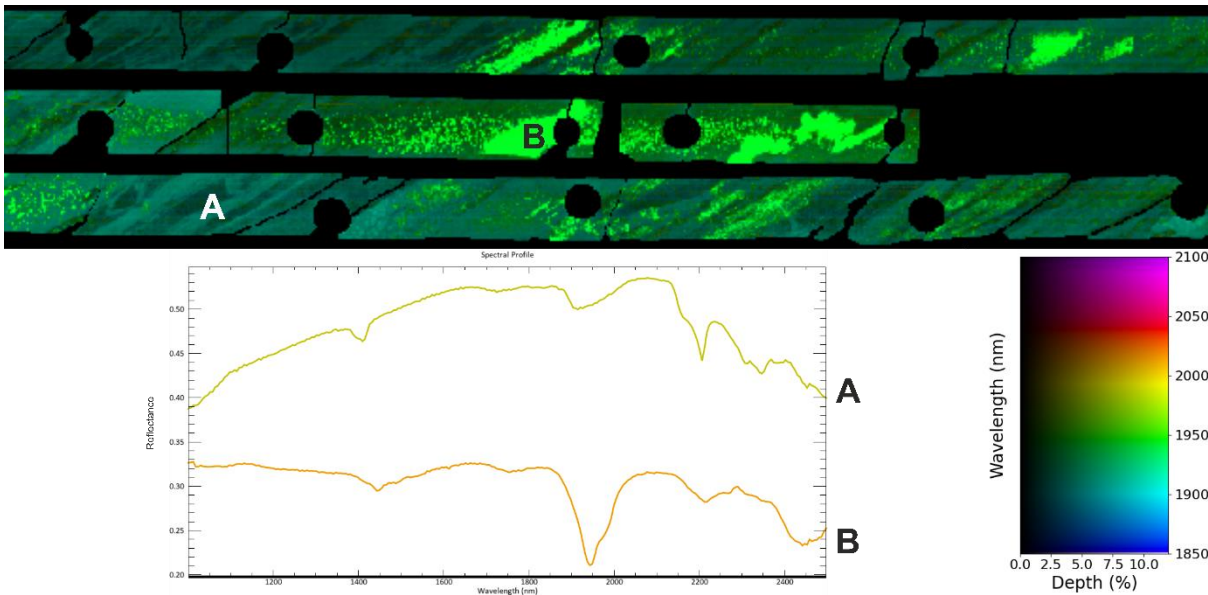


Figure 3.38 Minimum wavelength map of Drill Core 1 in the range 1.85 μm to 2.1 μm .

Expanding the analysis to the range of 2.1 μm to 2.4 μm , Drill Core 1 displayed absorption features denoted by green (D), yellow-green (C), orange (A), and pink (B) colours, associated with wavelengths such as 2.206 μm , 2.215 μm , 2.307 μm , and 2.344 μm respectively (Figure 3.39).

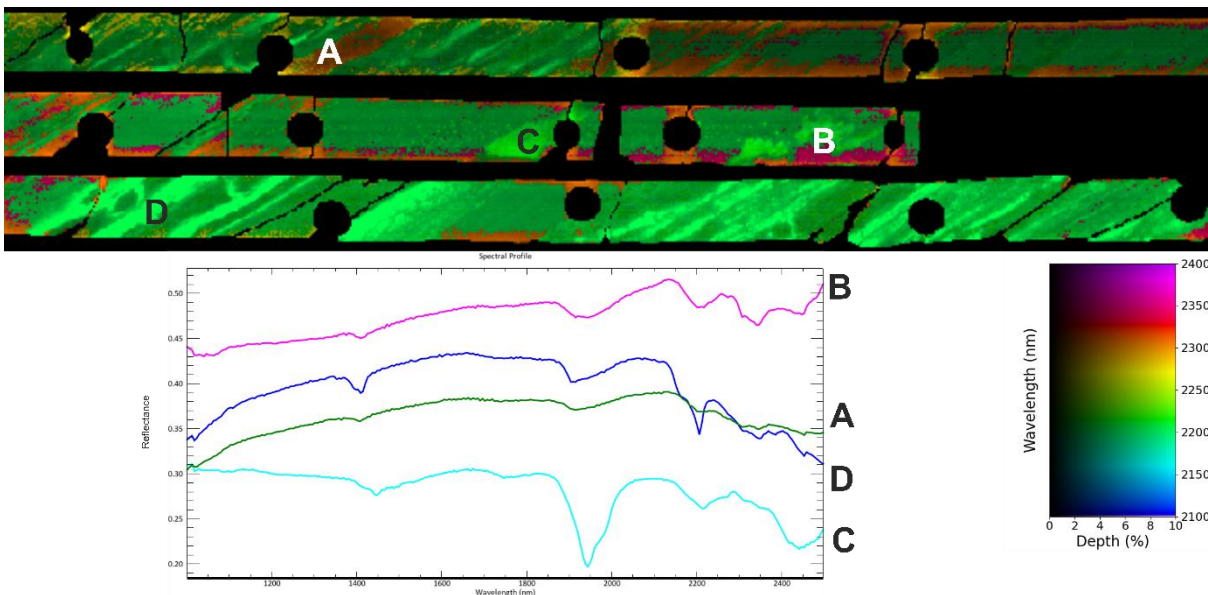


Figure 3.39 Minimum wavelength map of Drill Core 1 in the range 2.1 μm to 2.4 μm .

Further subdivisions within the range of 2.1 μm to 2.4 μm provided more detailed insights as this range focuses on the clay absorption features. For instance, within the range of 2.185 μm to 2.225 μm , distinctive absorption features were observed, represented by yellowish-green (B) and red (A) colours, indicating wavelengths around 2.206 μm and 2.215 μm respectively (Figure 3.40).

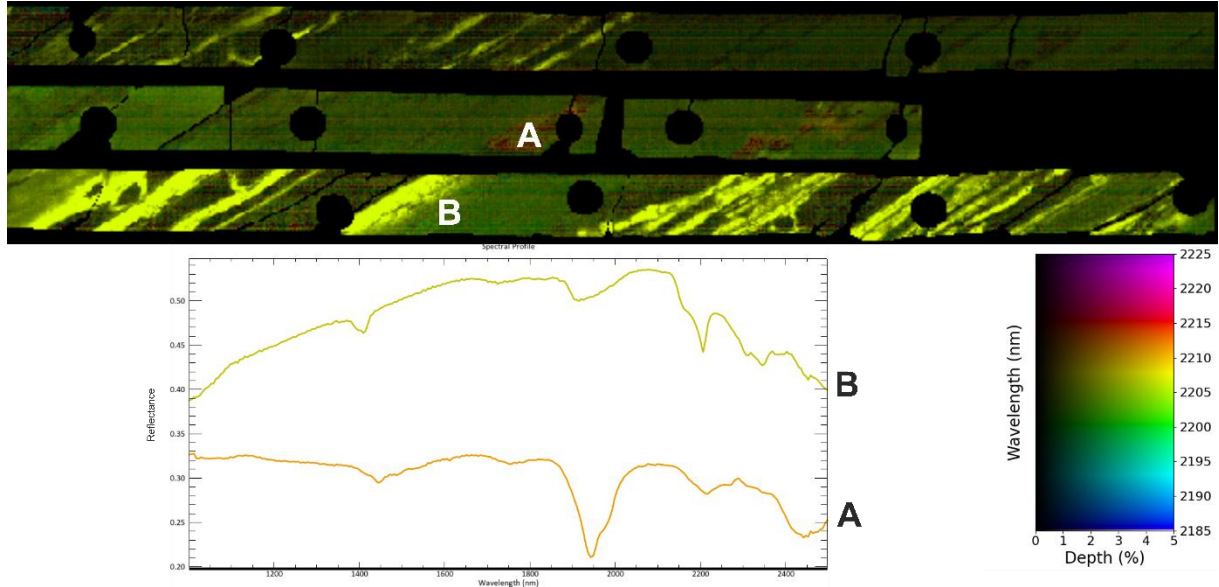


Figure 3.40 Minimum wavelength map of Drill Core 1 in the range 2.185 μm to 2.225 μm .

Lastly, in the range of 2.3 μm to 2.36 μm , two distinctive absorption features were observed, represented by dark blue (B) colour corresponding to a 2.308 μm feature and red (A) colour corresponding to a 2.344 μm feature (Figure 3.41).

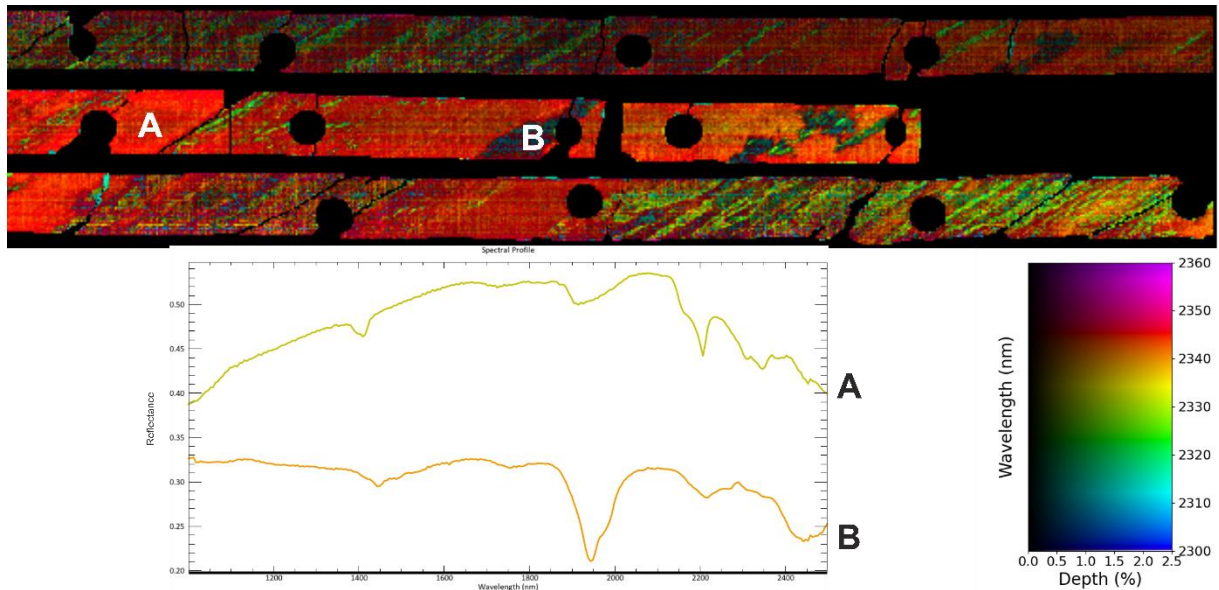


Figure 3.41 Minimum wavelength map of Drill Core 1 in the range 2.3 μm to 2.36 μm .

Similarly, for Drill Core 2, absorption features across these wavelength ranges were also analysed, revealing distinctive colours corresponding to the minimum wavelengths of the deepest features in that range.

In the range of 1.1 μm to 1.65 μm , the resulting image displayed two notable features: a blue (B) colour denoting features from 1.108 μm to 1.215 μm and a yellow (A) colour indicating a specific feature at 1.410 μm (Figure 3.42).

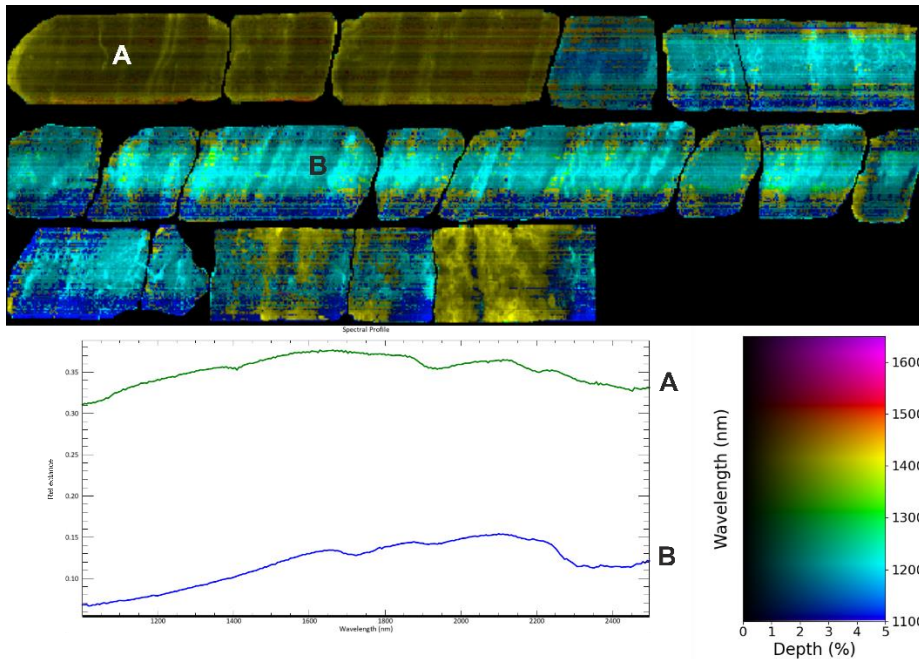


Figure 3.42 Minimum wavelength map of Drill Core 2 in the range 1.1 μm to 1.65 μm .

Analysis within the 1.65 μm to 1.85 μm range revealed the presence of two distinct absorption features, with a dark green (A) colour highlighting features from 1.691 μm to 1.746 μm and a green (B) colour corresponding to a feature at 1.725 μm (Figure 3.43).

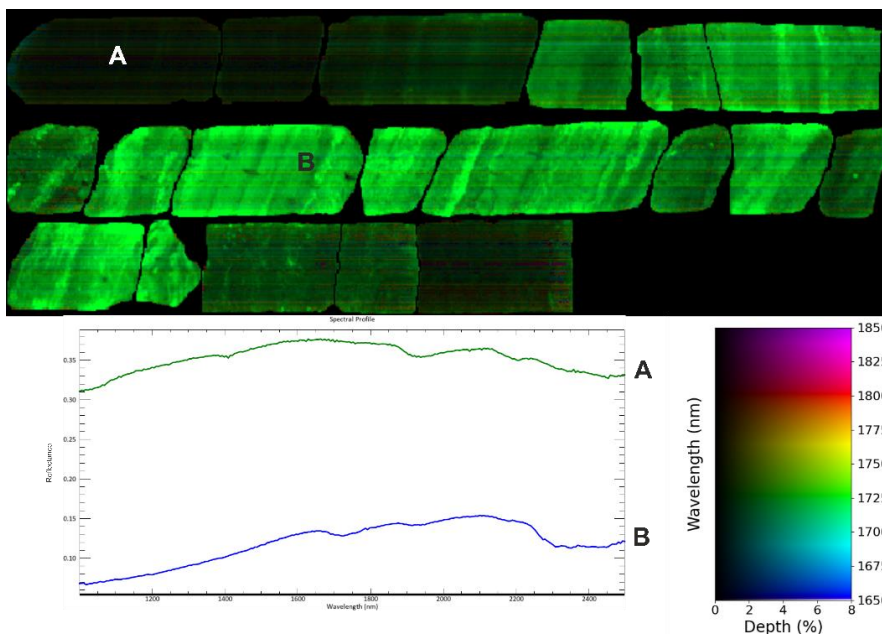


Figure 3.43 Minimum wavelength map of Drill Core 2 in the range 1.65 μm to 1.85 μm .

Additionally, an absorption feature in the 1.85 μm to 2.1 μm range was observed, represented by a blueish-green (A) colour spanning from 1.904 μm to 1.947 μm (Figure 3.44).

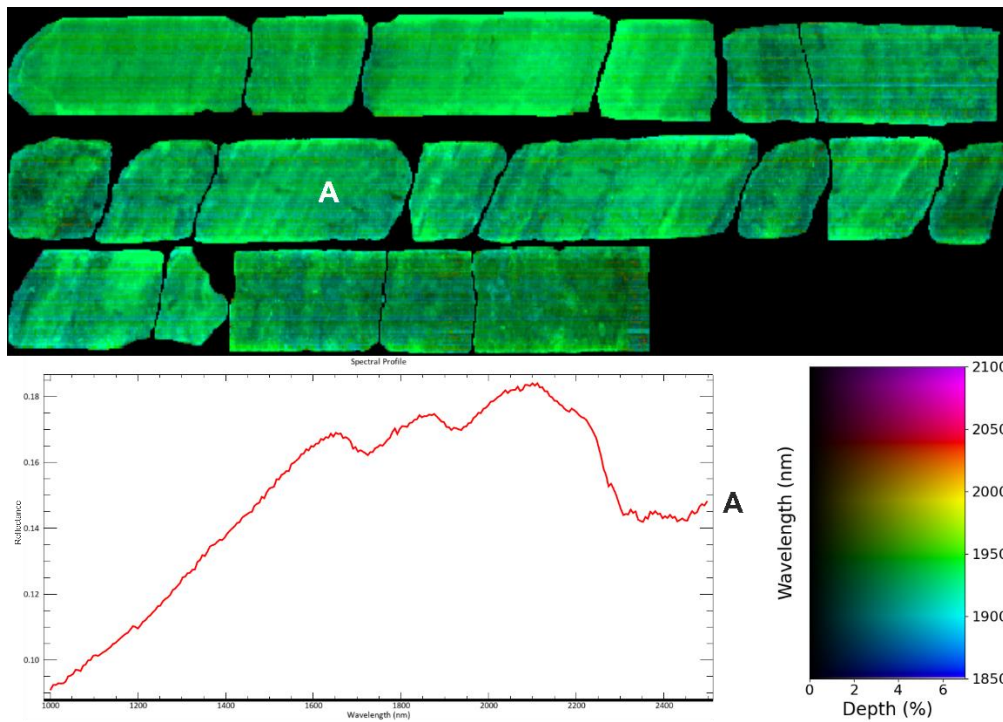


Figure 3.44 Minimum wavelength map of Drill Core 2 in the range 1.85 μm to 2.1 μm .

Moving to the 2.1 μm to 2.4 μm range, the analysis unveiled two distinctive absorption features: a dark green (B) colour indicating a feature at 2.206 μm and an orange (A) colour corresponding to a distinct feature at 2.307 μm (Figure 3.45).

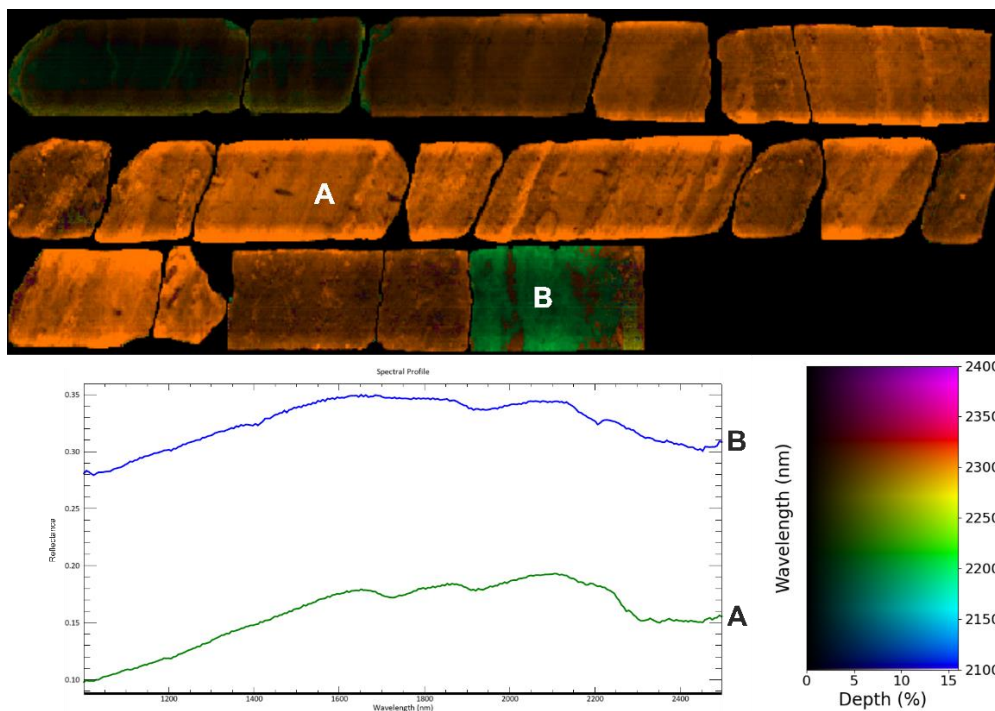


Figure 3.45 Minimum wavelength map of Drill Core 2 in the range 2.1 μm to 2.4 μm .

Further examination within the narrower range of 2.185 μm to 2.225 μm revealed a distinctive absorption feature denoted by a yellow (A) colour, corresponding to a specific feature at 2.206 μm (Figure 3.46).

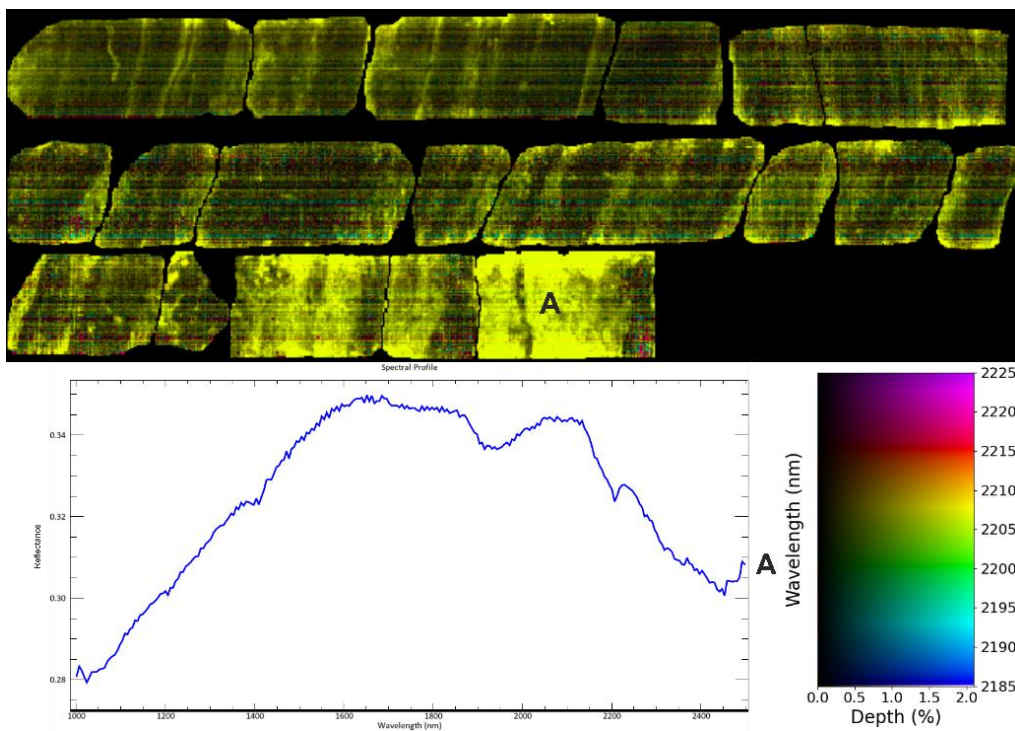


Figure 3.46 Minimum wavelength map of Drill Core 2 in the range 2.185 μm to 2.225 μm .

Lastly, analysis in the range of 2.3 μm to 2.36 μm showed two distinctive absorption features, with a blue (A) colour indicating a feature at 2.309 μm and a red (B) colour corresponding to a distinct feature at 2.347 μm (Figure 3.47).

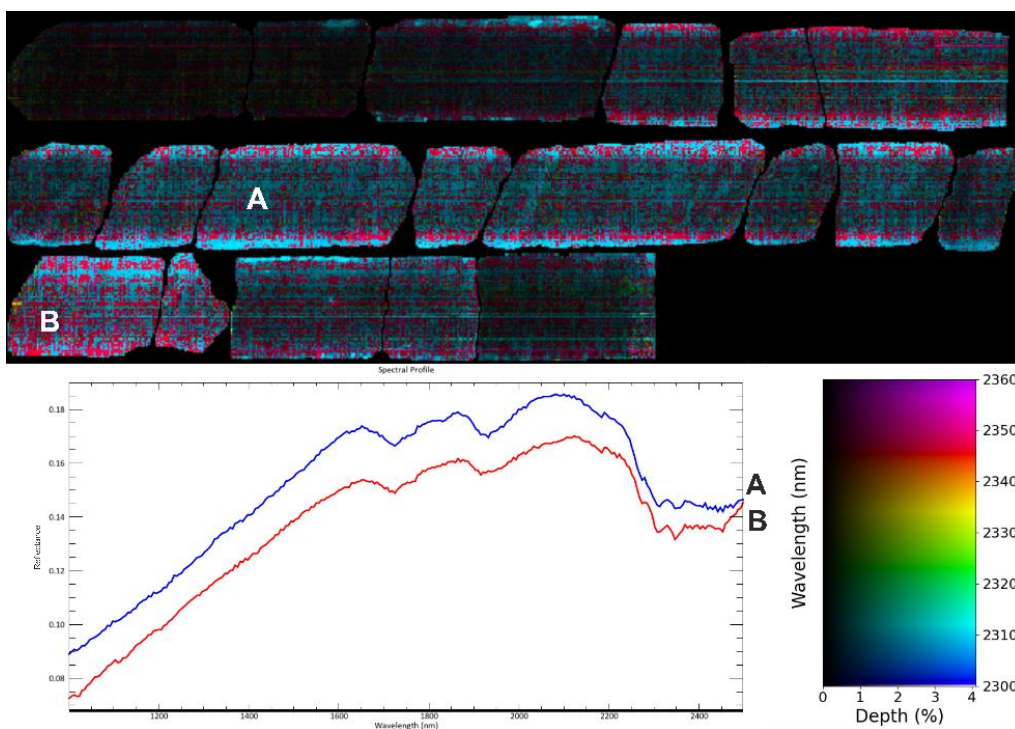


Figure 3.47 Minimum wavelength map of Drill Core 2 in the range 2.3 μm to 2.36 μm .

3.2.4. TIR Measurements

TIR measurements were conducted on powdered samples from the drill core from sections with low and high oil concentrations. The objective was to identify the functional groups present in the oil of the drill core. The measurements of Drill Core 1 revealed absorption spectra characteristic of quartz (Hecker et al., 2010), along with minor absorption features corresponding to oil around 3.45 μm (Asemani & Rabbani, 2020)(Figure 3.48). Notably, no other distinctive absorption features of oil were observed in this sample. Similarly, the TIR spectra of Drill Core 2 displayed absorption patterns indicative of quartz alongside minor absorption features associated with oil around 3.45 μm (Figure 3.49).

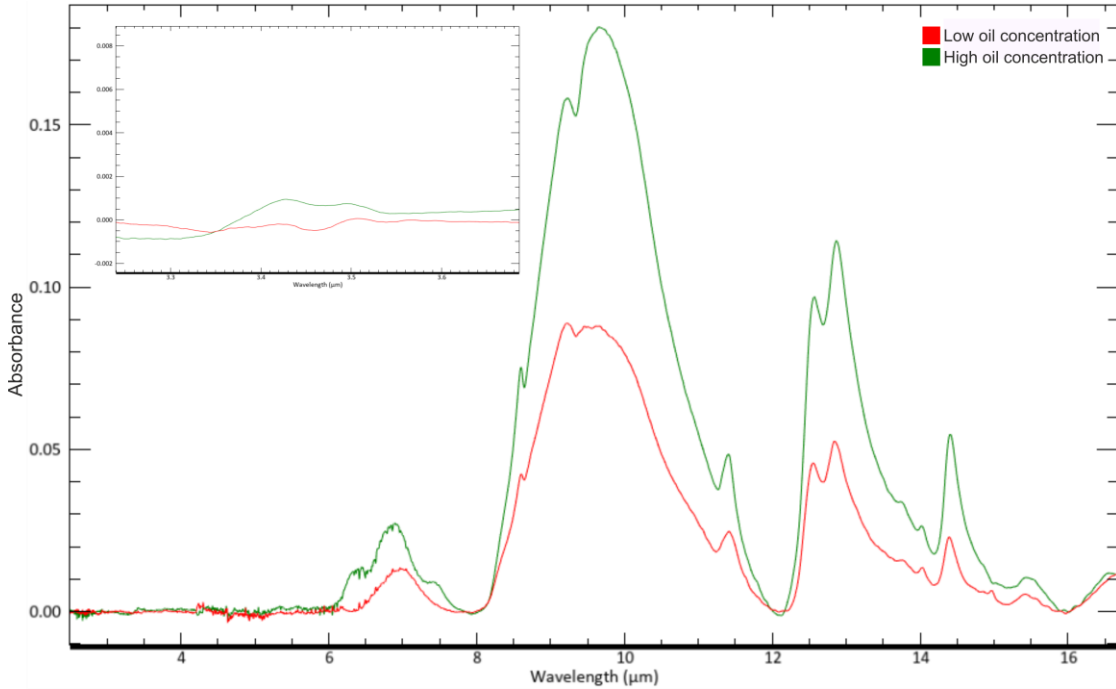


Figure 3.48 TIR spectra of the powdered samples from Drill Core 1.

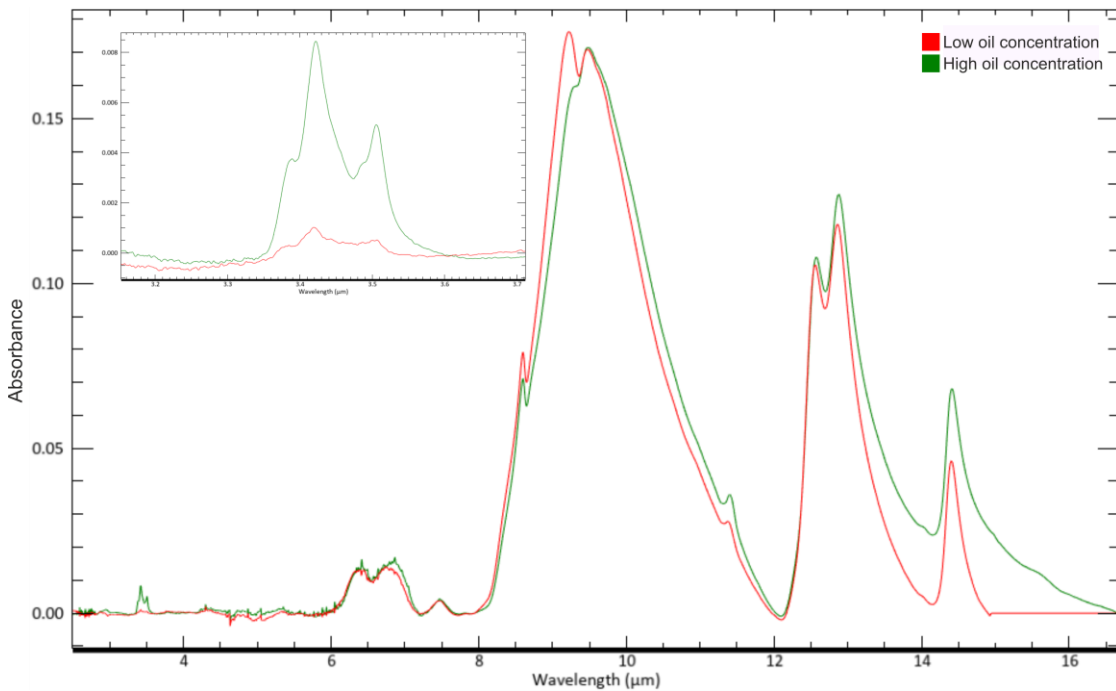


Figure 3.49 TIR spectra of the powdered samples from Drill Core 2.

4. DISCUSSION

This chapter discusses the results presented in Chapter 3 and is organised into seven sections. Section 4.1 discusses the results of the methods used to characterise the three oil samples used in this study and highlights the similarities and differences between them. Section 4.2 examines the effect of increasing oil thickness on the spectra of the oil and its implications for oil concentration and the absorption features observed in the spectra of oil from a drill core. Section 4.3 compares the spectra and absorption features of the oil and minerals typically found in a hydrocarbon bearing drill core from the Dutch region, identifying the optimal wavelength ranges and absorption features for mapping oil and minerals in drill cores. Section 4.4 discusses the results of the methods used to further understand the composition of the two hydrocarbon bearing drill cores used in this study. Section 4.5 discusses the results of the mapping techniques employed to map the oil and minerals in the two drill cores. Section 4.6 further compares the outcomes of the mapping techniques, emphasizing their efficiencies and limitations. Finally, Section 4.7 presents a prototype workflow for detecting the presence of oil in drill cores, mapping the oil and minerals present in the drill core and further classifying the oil in the drill core based on its concentration and functional groups.

4.1. Characterization of the Oil Samples

This study used three oil samples: heavy oil, light oil and very light oil. The three oil samples were characterised by analysing their spectra in the TIR, SWIR and VNIR ranges, along with their UV fluorescence spectra. In the TIR range, absorption features of oil are due to fundamental vibrations are primarily associated with stretching and bending modes of the molecular bonds (Stuart, 2004). The analysis of the oil samples in the TIR range reveals various functional groups responsible for these absorption features, as seen in section 3.1.1. The spectra of the oil samples indicate the presence of aliphatics and aromatics, along with other functional groups such as carboxylic acids, esters, ketones, amides, alcohols, and phenols. This consistent presence of functional groups across all three oil samples suggests that there is no significant difference among the samples concerning the types of functional groups present. Further distinctions can be made based on the complexity of the molecules present—how light or heavy the molecules are in the functional groups. However, this level of detail is not discernible from the spectra of the oil samples seen in Figure 3.1. For instance, while aliphatics and aromatics can be identified in the spectra of the three oil samples, distinguishing between long-chain hydrocarbons (heavy molecules) and short-chain hydrocarbons (light molecules) is not possible solely based on spectral data. All three oils show absorption features due to the type of bonds in the molecule and not on the complexity of the molecule.

The combinations and overtones of the fundamental vibrations cause absorption features in the SWIR and VNIR ranges. In the SWIR range, the absorption features due to the combinations and overtones of the aliphatics and aromatics are distinct in the spectra, as seen in section 3.1.2. These features are primarily attributed to the C-H bonds within these compounds. However, the absorption features due to other functional groups are not as distinct. These features are either present as minor absorption features around 1.4 μm or they form a plateau around 1.9 μm . Additionally, the presence of water in the oil or the drill core can easily mask these features. Similarly, the absorption features of O-H bonds in minerals can overshadow these minor features. This masking effect is evident in the spectra of heavy oil, where the broad absorption feature of water present in the oil overlaps with the distinct absorption features of the oil (Figure 3.2). This overlap complicates the identification of specific functional groups within the heavy oil samples. Similarly, in the spectra of the oil-soaked sandstone, the water absorption feature can obscure the underlying oil absorption features (Figure 3.17).

The very light and light oils exhibit distinct absorption features in the SWIR range attributed to bonds involving C-H, N-H, and O-H, as documented in Table 3.2. Due to the similarities in their absorption features due to these functional groups, distinguishing between very light oil and light oil based on these features alone is not feasible, as illustrated in Figure 3.2. In contrast, heavy oil predominantly shows absorption features from C-H bonds but also demonstrates significant absorption related to water. The presence of distinct water absorption features sets heavy oil apart from both very light and light oils in spectral analysis. Overall, while all three oils exhibit common C-H absorption features, differentiation among them in the SWIR range is primarily based on their mean reflectance/transmittance values, with the very light oil having the highest mean transmittance value, light oil with intermediate transmittance value, and the heavy oil having the lowest reflectance value (Section 3.1.2).

In the SWIR spectra acquired from the oil samples immersed in sandstone and examined using Specim cameras, as shown in Section 3.1.6, the discernible absorption features observed across all three oil samples primarily originate from the combination, first overtones and second overtones of C-H bonds at wavelengths of 2.3 μm , 1.7 μm , and 1.2 μm , respectively. However, while these features are clear, those associated with other functional groups found in pure oil samples are obscured by the broad absorption characteristic of water, as seen in Figure 3.17. Consequently, the functional groups associated with hetero-compounds cannot be detected in an oil-bearing drill core, as these features are masked due to the absorption features of water or OH bonds present in the drill core minerals. Regarding the variation observed in the spectra of the very light and light oils concerning the oil concentration in the sandstone, no significant differences are noted in the absorption features due to functional groups or in the mean reflectance values. This is probably because in a sandstone piece of 2.5 cm by 2 cm by 1 cm with 12% porosity, the oil amount of 0.25 ml was sufficient to saturate the sandstone, while higher quantities of 0.5 ml and 1.0 ml led to overflow into the petri dish containing these samples.

The major differences among the three oil samples are in the VNIR range due to the absorption caused by the Pi bonds (Section 3.1.2). The very light oil, regardless of its thickness, lacks absorption in the VNIR region due to its transparent nature, as seen in Figure 3.3. Conversely, the light oil exhibits a steep slope in the VNIR range, which persists even as the oil thickness increases (Figure 3.5). In contrast, the heavy oil presents a gentler slope (Figure 3.2). These patterns are also evident in the Specim camera VNIR image of the oil-soaked sandstone (Section 3.1.6). While the very light oil is transparent in the VNIR range, the spectra exhibit a sloped appearance compared to pure oil samples, attributed to the absorption of the sandstone (quartz) in which the oil was immersed (Figure 3.18).

The UV fluorescence property of oil aids in its detection, as oil exhibits fluorescence under UV light, providing a non-destructive method for quickly detecting the presence of oil. (Section 3.1.5). In Figure 3.15, the fluorescence spectra graph of the three oil samples shows that the very light oil displays low fluorescence values, with its peak fluorescence occurring at wavelengths around 0.45 μm , as noted by Jiaqi (2018). Both the light and heavy oils show high fluorescence values with peak fluorescence around the same wavelength, which differs from findings by Hagemann & Hollerbach (1986) and Jiaqi (2018), where light oils typically show peak fluorescence at around 0.5 μm and heavy oils at around 0.6 μm . Additionally, there is a variation in the fluorescence intensity peaks between the light and heavy oils. This intensity difference is likely due to the variation in oil concentration, as mentioned by Peng et al. (2013) and Steffens et al. (2011), who attribute the decreasing fluorescence intensity with increasing oil concentration to the increase in scattering and absorption of the fluorescence spectra by the oil. The light oil, soaked into the sandstone, forms a low concentration at the surface, resulting in higher fluorescence intensity compared to the heavy oil, which was smeared on the surface of the sandstone.

4.2. Influence of the Oil Layer Thickness

Section 3.1.3 shows the effect of increasing oil thickness on the spectra of the oil. As the thickness of the oil increases, there is a corresponding decrease in the mean transmittance value of the oil (Figure 3.3 and Figure 3.5), accompanied by an increase in the depth of the absorption features (Figure 3.4 and Figure 3.6). This relationship between feature depth and oil thickness allows for estimating the relative concentration of oil in the drill core. Spectra from regions with shallower oil absorption features suggest lower oil concentrations compared to spectra from regions with deeper oil absorption features, which imply higher oil concentrations in that region. However, a limitation of this estimation arises from the saturation of the absorption feature at 2.308 μm with further increases in oil thickness, resulting in a decrease in the depth of this absorption feature (Figure 3.4b and Figure 3.6b). The depth of the absorption feature is calculated with respect to the shoulders of the feature. As the oil concentration increases, both the transmittance value of the shoulders and the absorption minima decreases, with the rate of decrease for the absorption minima being higher than that of the shoulders. However, after saturation of the absorption minima, the rate of decrease for the shoulders is more than that of the absorption minima and, therefore, shows a decrease in the depth of the feature.

Additionally, a trend is noted where the increase in feature depth with increasing oil thickness primarily affects longer wavelength features before progressing towards shorter wavelengths. This is because longer wavelengths exhibit absorption features due to combination bands and first overtones, which are stronger and more pronounced. In contrast, shorter wavelengths show absorption features from second and third overtones, as well as combination bands, which are inherently weaker. Therefore, in regions of a drill core with low oil concentrations, the 2.308 μm feature tends to be more prominent than the 1.723 μm feature. Consequently, mapping techniques focused on the 2.308 μm feature are less noisy due to its higher prominence compared to techniques focused on the 1.723 μm feature. This estimation holds when the 2.308 μm feature is not saturated.

Furthermore, this estimation assumes that these features do not overlap with absorption features from other minerals. Conditions that overlap with the absorption features of other minerals are discussed in the next section (Section 4.3).

4.3. Comparing the Spectra of Oil and Minerals

In Section 3.1.4, the comparison of absorption features between oil and the minerals typically found in hydrocarbon bearing drill cores from the Dutch region reveals specific spectral ranges suitable for distinguishing between the oil and minerals. Such as, in the ranges from 1.1 μm to 1.65 μm and from 1.85 μm to 2.1 μm (Figure 3.7 and Figure 3.9), the absorption features of oil either overlap or closely align with mineral absorption features, making these ranges less suitable for precise oil mapping. However, within the range of 1.6 μm to 1.8 μm , the first, third and fourth deepest features of oil at 1.724 μm , 1.704 μm and 1.796 μm , respectively, exhibit no overlaps with minerals, except for the second deepest feature at 1.761 μm , which has a close overlap with gypsum and anhydrite features at 1.750 μm . Similarly, in the range from 2.1 μm to 2.4 μm , the first, third and fourth deepest features of oil at 2.308 μm , 2.399 μm , and 2.457 μm , respectively, do not overlap with minerals, except for the second deepest feature at 2.347 μm , which overlaps with illite, muscovite and calcite absorption features at 2.345 μm , 2.353 μm and 2.340 μm respectively. Thus, the deepest oil features within the ranges from 1.65 μm to 1.85 μm and from 2.1 μm to 2.4 μm are particularly suitable for mapping oil within a drill core. This finding is also seen in the Spectral Angle Matrices (Figure 3.11 to Figure 3.14), where the same ranges exhibit high spectral angle values between oil and minerals. Therefore, these ranges, from 1.65 μm to 1.85 μm and from 2.1 μm to 2.4 μm , are optimal for oil mapping, also using methods that rely on spectral angle differences.

Additionally, clays such as illite, muscovite and kaolinite can be differentiated from oil in the 2.1 μm to 2.4 μm range by highlighting the 2.2 μm feature due to AlOH (GMEX, 2008). Chlorite shows diagnostic absorption features in this range as well, with the first, second and fourth deepest features of chlorite at 2.326 μm , 2.385 μm and 2.441 μm , respectively, aligning closely with the second, third and fourth deepest features of oil at 2.347 μm , 2.399 μm and 2.457 μm , respectively. The third deepest feature of chlorite at 2.248 μm due to FeOH does not show any overlap with oil absorption features, making it an optimal feature for differentiating it from oil. Gypsum and anhydrite show absorption features in all four ranges; however, their diagnostic triplet absorption feature in the 1.1 μm to 1.65 μm at around 1.446 μm , 1.490 μm and 1.536 μm , along with the deep absorption feature in the 1.85 μm to 2.1 μm at around 1.946 μm , can be used to differentiate them from oil in the drill core. This distinction is also observed in the spectral angle matrix, where the ranges of 1.1 μm to 1.65 μm and 1.85 μm to 2.1 μm show high spectral angle values for gypsum. In the SWIR range, calcite and dolomite have diagnostic absorption features in the range of 2.1 μm to 2.4 μm . However, the 2.340 μm feature of calcite and 2.322 μm feature of dolomite aligns closely with the second deepest feature of oil at 2.347 μm , making differentiation difficult. Lastly, quartz and halite neither have distinct absorption features in the SWIR range nor do they exhibit 100% reflectance and, therefore, mask or diminish the already minor features of oil.

To summarise, the comparative analysis highlights specific spectral ranges that are optimal for distinguishing oil from minerals in hydrocarbon-bearing drill cores from the Dutch region. The ranges from 1.65 μm to 1.85 μm and from 2.1 μm to 2.4 μm can be used for oil mapping due to minimal overlap with mineral absorption features, supported by high spectral angle values. Minerals such as gypsum, anhydrite, dolomite and chlorite can be differentiated using their unique absorption features despite some overlaps with oil. However, halite and quartz, lacking diagnostic features in the SWIR range, may still obscure the minor oil absorption features. Overall, these findings enhance the precision of hydrocarbon exploration by identifying optimal spectral ranges and features for accurate oil mapping in drill cores.

4.4. Composition of the Drill Cores

This study utilized two drill cores with varying types of oil and mineral compositions. Drill Core 1 is a hydrocarbon bearing sandstone with calcareous cement containing transparent oil (Robbemond et al., 2002). Drill Core 2 is from a quartz-rich sandstone reservoir rock containing heavy oil (Ayyad & Parmigiano, 1983). To further understand the mineral composition of the two drill cores, point spectral measurements in the VNIR and SWIR range were conducted (Section 3.2.2). These measurements reveal the presence of kaolinite, gypsum, and hematite in Drill Core 1 (Figure 3.20). Most spectra from Drill Core 1 show the absorption features of oil, except for a few spectra where hematite dominates (Spectra D in Figure 3.20). Major absorption features of oil noted are at 1.7 μm and 2.3 μm , attributed to the C-H bonds of aliphatics and aromatics. The 2.349 μm feature is deeper than the 2.308 μm feature, likely due to the absorption feature of calcite at 2.340 μm , as this drill core contains calcareous cement. The minor features of oil at 1.4 μm and 1.9 μm are masked by the OH absorption feature of gypsum and kaolinite or by the broad absorption feature of water in the drill core. The point spectral measurements of Drill Core 2 show the absorption features of kaolinite (Figure 3.21). These measurements also show the oil absorption features of varying depth, particularly at 1.7 μm and 2.3 μm . The broad absorption feature of water in the drill core masks out minor absorption features of oil at 1.9 μm . Consequently, in both the drill cores, the absorption features due to the hetero-compounds present in the oil could not be detected from the spectra of the oil within the drill core.

To further detect the presence of oil in the drill cores, the UV fluorescence spectra were recorded (Section 3.2.1). The results from Drill Core 1 show the fluorescence spectra of oil in all the measurements. The transparent oil present in the drill core produces a fluorescence peak at around 0.62 μm (Figure 3.19a),

which is close to the fluorescence peak of the light and heavy oil samples at 0.63 μm (Figure 3.15). This is different from the trend outlined by Hagemann & Hollerbach (1986) and Jiaqi (2018), where fluorescence peaks of very light oils are around 0.4 μm to 0.45 μm , as also observed in the very light oil used in this study (Section 3.1.5). This dissimilarity is likely due to the loss of volatiles from the oil in the drill core over time, resulting in a shift of the peak fluorescence intensity towards longer wavelengths. The measurements on Drill Core 2 also showed the fluorescence spectra of oil in the light sections as well as the dark sections of the drill core (Figure 3.19b). The peak intensity of the fluorescence spectra is around 0.62 μm , which is close to the peak fluorescence intensity of the heavy oil in Figure 3.15. Thus, through the UV fluorescence measurements, oil was detected throughout both Drill Core 1 and Drill Core 2.

The analysis of the VNIR and SWIR imagery of the drill cores shows the spectra of the oil and minerals contained in the two drill cores. Drill Core 1, which contains transparent oil, shows the absorption features of hematite in the VNIR spectra from the drill core (Figure 3.22). On the other hand, Drill Core 2 contains heavy oil and shows absorption due to quartz in the lighter parts (spectra A and D in Figure 3.23), while the darker parts that contain the heavy oil show the gentle absorption slope of the heavy oil (spectra Band C in Figure 3.23). Figure 3.24 shows the absorption in the SWIR region of Drill Core 1, containing minerals like kaolinite and gypsum, while Figure 3.25 shows the spectra of kaolinite. The spectra of the oil and minerals from the two drill cores obtained using the Specim cameras show a lower contrast as compared to those obtained using the point spectral measurements in Section 3.2.2

TIR measurements of powdered drill core samples revealed the presence of C-H absorption features of aliphatics at 3.4 μm , as seen in Figure 3.48 and Figure 3.49. However, these absorption features at 3.4 μm were minor, and no additional oil absorption features were detected. Thus, the other functional groups present in the oil from the two drill cores could not be detected using this method.

In conclusion, the study of the two drill cores, containing varying types of oil and mineral compositions, utilized point spectral measurements in the VNIR and SWIR ranges to reveal significant findings. Drill Core 1, a hydrocarbon-bearing sandstone with calcareous cement, showed prominent oil absorption features at 1.7 μm and 2.3 μm . Drill Core 2, a quartz-rich sandstone with heavy oil, also displayed oil absorption features. UV fluorescence measurements further confirmed the presence of oil in both drill cores, with fluorescence peaks aligning closely with those of light and heavy oil samples. TIR measurements identified minor C-H absorption features of aliphatics but failed to detect other functional groups in the oil. Overall, while significant oil absorption features were identified, the masking effects of minerals and water present challenges for complete oil characterization in drill cores.

4.5. Techniques to map the Oil and Minerals in the Drill Core

The SWIR Specim camera images of the two drill cores were processed to map the oil and minerals present in the drill cores. The results of this process are discussed below.

Band Index

The Hydrocarbon Index method evaluates the absorption feature of oil along with its surrounding shoulders, providing insight into the depth of the absorption feature and can serve as an indicator of oil concentration. In this study, the Hydrocarbon Index was applied to two absorption features of oil (Section 3.2.3): the feature around 1.7 μm (HI1.7) as initially suggested by Kühn et al. (2004) and around 2.3 μm (HI2.3) which is another prominent absorption feature of oil as seen in Section 3.1.4.

As discussed in Section 4.2, the depth of oil absorption features affects longer wavelength features first before progressing to shorter wavelengths. Consequently, the 1.7 μm feature is shallower than the 2.3 μm

feature, resulting in higher noise levels when applying the Hydrocarbon Index to the 1.7 μm feature (Figure 3.24 and Figure 3.25). Additionally, as seen in Section 4.3, oil absorption features are affected by their proximity to absorption features of other minerals. This was observed in Drill Core 1, where HI1.7 also produced high values in locations containing gypsum. This is due to the proximity of the oil feature at 1.724 μm to the gypsum feature at 1.749 μm . Conversely, HI2.3 on Drill Core 1 was not affected by the calcareous cement present, as the calcite feature at 2.340 μm did not interfere with the oil feature at 2.308 μm .

Thus, when comparing the results, the HI2.3 exhibited lower noise levels and provided a better spatial distribution of oil than the HI1.7. However, the accuracy of HI2.3 remains untested in the presence of minerals like dolomite and chlorite, which have absorption features at 2.322 μm and 2.326 μm , respectively.

Spectral Angle Mapper

The Spectral Angle Mapper was applied over four spectral ranges (Section 3.2.3), differing from the approach of Speta (2016), who applied SAM over the full range of 1.0 μm to 2.5 μm . This is because oil and minerals have diagnostic absorption features specific to certain wavelength ranges. By applying SAM over these specific ranges, the sensitivity and accuracy of the method can be enhanced. This is evident when comparing the Spectral Angle Matrices in Figure 3.11 - Figure 3.14 to the Spectral Angle Matrix over the full range in Annex 4. A significant improvement is observed in the range of 2.1 μm to 2.4 μm , where higher spectral angle values between oil and minerals are recorded compared to the full range. Limiting SAM to a narrower wavelength range also reduces the computational burden compared to analysing the full spectrum. This can result in faster processing times and more efficient use of computational resources, especially when dealing with large datasets.

In Drill Core 1, four endmembers were used: kaolinite, gypsum, calcite, and oil (as given in Section 3.2.2). Upon comparing the rule image of the oil endmember in the range of 1.1 μm to 1.65 μm (Figure 3.28) with the photograph of Drill Core 1 (Figure 2.2), it was observed that the high spectral angle values of the rule image coincide with the more reddish-brown areas of the drill core, which correspond to the hematite present, as identified by spectrum D in Figure 3.20. This is because the spectra of hematite in this range show a slope towards longer wavelengths, opposite to the shown by the spectra of the oil.

The rule image of oil endmember in the range of 1.65 μm to 1.85 μm (Figure 3.29) shows low spectral angle values in locations where gypsum is present (spectrum B in Figure 3.20). This is due to the proximity of the 1.724 μm oil absorption feature to the 1.749 μm gypsum absorption feature, despite gypsum and oil having high spectral angle values in this range, as seen in Figure 3.12.

The rule image of the oil endmember in the range of 1.85 μm to 2.1 μm (Figure 3.30) shows low spectral angle values throughout the drill core except at locations where gypsum is present (spectrum D in Figure 3.20). This is because the minor absorption features of oil in this range form a plateau, showing high spectral similarity with the broad absorption feature of water in the drill core, unlike the deep absorption feature of gypsum at 1.946 μm . This is also reflected in the rule image of gypsum endmember in this range, which shows low values in areas where gypsum is present. The spectral angle matrix in the range of 1.850 μm to 2.100 μm (Figure 3.13) confirms that gypsum has high spectral angle values with oil and other minerals.

In the range of 2.1 μm to 2.4 μm , the rule image of the oil endmember shows high values which coincide with hematite (Figure 3.31), similar to the results in the range of 1.1 μm to 1.65 μm . The remaining areas

show consistent spectral angle values, even in areas where gypsum is present. This indicates that the range from 2.1 μm to 2.4 μm can be used to map the spatial distribution of oil in a drill core, even in the presence of gypsum. This range also highlights the areas where kaolinite is present, as shown in spectrum C in Figure 3.20. However, the presence of calcite, as mentioned by Robbmond et al. (2002), cannot be confirmed due to the proximity of the 2.340 μm calcite feature to the 2.347 μm oil feature.

In Drill Core 2, two endmembers were used: kaolinite and oil (as given in Section 3.2.2). The lighter regions at the start and end of the drill core, as seen in Figure 2.3, show high spectral angle values, while the darker regions show a lower spectral angle value in rule images of oil in the range of 1.65 μm to 1.85 μm and the range of 2.1 μm to 2.4 μm (Figure 3.33 and Figure 3.35). In these regions, the spectra of the oil endmember show high similarity with the spectra of the drill core. In the other ranges from 1.1 μm to 1.65 μm and from 1.85 μm to 2.1 μm , no particular trend was observed between the light and dark areas (visual appearance of the drill core in Figure 2.3) and the value of the spectral angle (Figure 3.32 and Figure 3.34). Thus, both the ranges from 1.65 μm to 1.85 μm and from 2.1 μm to 2.4 μm provided results for the spatial distribution of the oil in Drill Core 2, as also demonstrated by the spectral angle matrix in Figure 3.12 and Figure 3.14.

Minimum Wavelength Mapper

The Minimum Wavelength Mapper was applied over four ranges, with the last range further subdivided into two smaller ranges, as seen in section 3.2.3. The wavelengths obtained from the minimum wavelength map were then cross-referenced with the minimum wavelengths of the absorption features of the minerals listed in Section 3.1.4 to determine the minerals present.

For Drill Core 1, the minimum wavelength map over the 1.1 μm to 1.65 μm range reveals three colours (Figure 3.36). The green colour at 1.3 μm corresponds to the low reflectance spectra of hematite in the drill core, as indicated by spectrum A. The yellow colour at 1.409 μm corresponds to the OH feature of minerals (kaolinite), as shown by spectrum C. Additionally, the orange colour at 1.448 μm represents the deepest feature of the triplet gypsum feature present in this range.

In the range of 1.65 μm to 1.85 μm (Figure 3.37), the green colour at 1.723 μm represents the oil feature, as identified by spectrum A, while the yellowish-green colour at 1.748 μm represents the gypsum feature, as indicated by spectrum B. This range highlights the spatial distribution of oil and gypsum within the drill core, with distinct colours marking their presence.

In the range of 1.85 μm to 2.1 μm (Figure 3.38), the blueish-green colour at 1.914 μm corresponds to the OH feature of water or minerals (kaolinite) present in the drill core, as indicated by spectrum A. The bright green colour at 1.947 μm corresponds to the gypsum feature, as shown by spectrum B. This range maps the presence of gypsum, which is distinct from the OH features of water or kaolinite.

In the range of 2.1 μm to 2.4 μm (Figure 3.39), the green colour at 2.206 μm corresponds to the AlOH feature of kaolinite, as indicated by spectrum D. The yellow-green colour at 2.215 μm represents the gypsum feature, as shown by spectrum C. The orange and pink colours correspond to the 2.307 μm and 2.342 μm features of oil, respectively, as indicated by spectra A and B. This range shows the spatial distribution of oil, kaolinite, and gypsum within the drill core.

In the subdivided range of 2.185 μm to 2.225 μm (Figure 3.40), focusing on clay absorption features, the bright yellowish-green colour corresponds to the 2.206 μm feature of kaolinite, as indicated by spectrum

B, while the dull red colour corresponds to the 2.215 μm feature of gypsum, as shown by spectrum A. This finer subdivision aids in identifying clay minerals within the drill core.

In the subdivided range of 2.3 μm to 2.36 μm (Figure 3.41), focusing on oil absorption features, the blue and red colours correspond to the 2.308 μm and 2.344 μm features of oil, respectively, as indicated by spectra B and A.

Thus, the ranges of 1.65 μm to 1.85 μm and 2.3 μm to 2.36 μm can be used to map the spatial distribution of oil in the drill core. However, for the range of 1.65 μm to 1.85 μm , in mixed spectra of gypsum and oil, gypsum exhibits deeper absorption features than oil, which are recorded by the minimum wavelength mapper in this range. Gypsum exhibits absorption features in all four ranges. Notably, in the range of 1.85 μm to 2.1 μm , the OH feature of gypsum is deeper than the OH features of water or kaolinite present in the drill core, making this range suitable for mapping gypsum in Drill Core 1. Kaolinite shows a prominent absorption feature at 2.206 μm in the 2.1 μm to 2.4 μm range, which is highlighted in the 2.185 μm to 2.225 μm range.

For Drill Core 2, in the range of 1.1 μm to 1.65 μm (Figure 3.42), blue colours representing wavelengths from 1.108 μm to 1.215 μm correspond to the minimum of the absorption slope seen in spectrum B. The yellow colour at 1.410 μm indicates the OH feature of kaolinite (spectrum A). In the range of 1.65 μm to 1.85 μm (Figure 3.43), the green colour corresponds to the 1.725 μm feature of oil, as seen in spectrum B. In the range of 1.85 μm to 2.1 μm (Figure 3.44), the bluish-green colour, representing wavelengths from 1.904 μm to 1.947 μm , is due to the broad absorption feature of water present in the oil as well as in the drill core. In the range of 2.1 μm to 2.4 μm (Figure 3.45), the green colour signifies the 2.206 μm AIOH feature of kaolinite, as seen in spectrum B, while the orange colour denotes the 2.307 μm feature of oil, as seen in spectrum A. In the subdivided range of 2.185 μm to 2.225 μm (Figure 3.46), the yellow colour marks the 2.206 μm feature of kaolinite. This finer range allows for precise mapping of kaolinite, distinguishing its absorption features from a mixed spectrum of kaolinite and oil. In the subdivided range of 2.3 μm to 2.36 μm (Figure 3.47), the blue and red colours represent the 2.309 μm and 2.347 μm features of oil, respectively. Thus, like in Drill Core 1, the ranges of 1.65 μm to 1.85 μm and 2.3 μm to 2.36 μm can be used to map the spatial distribution of oil in Drill Core 2. Similarly, kaolinite can be mapped in the range of 2.1 μm to 2.4 μm range, with further focus on the 2.185 μm to 2.225 μm range.

In conclusion, this study applied various spectral analysis techniques to the SWIR Specim camera images of the two drill cores to map the spatial distribution of oil and minerals in the drill cores. The HI2.3 exhibited lower noise levels and provided a better spatial distribution of oil than HI1.7. The Spectral Angle Mapper technique mapped the oil and mineral endmembers, with the ranges of 1.65 μm to 1.85 μm and 2.1 μm to 2.4 μm focusing on the mapping of oil. The Minimum Wavelength Mapper was used to map the spatial distribution of oil, gypsum, and kaolinite, particularly highlighting oil features in the 2.3 μm to 2.36 μm range and gypsum features in the 1.85 μm to 2.1 μm range. These findings demonstrate the effectiveness of specific spectral ranges for mapping oil and minerals within drill cores.

4.6. Comparison of Mapping Methods

Comparing the outcomes of the Hydrocarbon Index, Spectral Angle Mapper, and Minimum Wavelength Mapper provides insights into their effectiveness and applicability. Firstly, the Hydrocarbon Index method offers a straightforward approach to identifying the location and relative concentration of oil. The value of the index indicates the depth of the absorption feature and thus relates to the concentration of oil. Since this method only considers three wavelength bands—the two shoulders and the absorption low—it is computationally less demanding compared to the Spectral Angle Mapper or Minimum Wavelength

Mapper, which involves multiple wavelengths. This makes the Hydrocarbon Index method a more accessible option for quick analysis. However, its limitation lies in its specificity to oil, necessitating the use of additional band indices for mapping other minerals present in the drill core.

On the other hand, the Spectral Angle Mapper method effectively maps the spatial distribution of oil and various minerals within the drill core. By using endmember spectra, SAM can differentiate between oil and minerals such as kaolinite, gypsum and calcite. The rule images generated by SAM reflect the concentration of oil. This is because as the concentration of oil increases, the pixels in the image of the drill core become more pronounced in oil absorption features, resulting in lower spectral angle values with the endmember spectra of oil. Despite its effectiveness, SAM has limitations. It is computationally intensive due to its reliance on spectral angle calculations across the entire dataset. Additionally, SAM requires prior knowledge of the spectral endmembers representing different minerals within the drill core, which necessitates a detailed understanding of the composition of the drill core. This requirement can limit applicability in cases where spectral libraries or endmember spectra are not readily available or well-defined.

The Minimum Wavelength Mapper method also proved effective in mapping the spatial distribution of both oil and minerals in the drill cores. By relating the minimum wavelength values over specific ranges, this method was able to distinguish between oil and minerals like kaolinite and gypsum. In both Drill Core 1 and Drill Core 2, the Minimum Wavelength Mapper mapped the spatial distribution of the oil and minerals by identifying distinct absorption features in the specified wavelength ranges. The subdivided ranges, particularly from 2.185 μm to 2.225 μm and 2.3 μm to 2.36 μm , provided finer resolution for mapping kaolinite and oil, respectively. A key advantage of the Minimum Wavelength Mapper is the feature depth band, which provides insights into the relative concentration of oil within each drill core. A high value in the feature depth band indicates a deep feature and, therefore, a high concentration of oil. Additionally, the method uses interpolated wavelengths and depths as compared to the fixed wavelength values used in band indices. Interpolating the spectra helps to find the wavelength where the minimum occurs within a specified range, rather than relying on pre-defined, fixed wavelengths, as the actual wavelengths at which absorption features occur can vary slightly due to factors such as mineral composition and particle size. By measuring depth at interpolated wavelengths, the method accurately captures the interpolated depth of the absorption feature. Thus, this method provides a better understanding of the absorption features of the oil and minerals present in the drill core as it provides information on the wavelength as well as the depth of the feature. Furthermore, the Minimum Wavelength Mapper method simplifies the process by not requiring any endmember input, unlike the Spectral Angle Mapper. This makes it particularly useful for simultaneously mapping the spatial distribution of multiple minerals by correlating the minimum wavelength map it generates with the absorption features of the minerals. However, this method is computationally demanding.

4.7. Implications for the Prototype Workflow

The ultimate goal of this study was to develop a prototype workflow for mapping hyperspectral images of drill cores, enabling the accurate detection and classification of oil and minerals in a range of drill cores with different types of oil and minerals. The effectiveness of different methods, including UV fluorescence analysis, Hydrocarbon Index, Spectral Angle Mapper, and the Minimum Wavelength Mapper, was assessed across two drill cores: Drill Core 1 containing transparent oil along with kaolinite, gypsum, calcite, hematite and quartz, and Drill Core 2 containing heavy oil along with kaolinite and quartz. Figure 4.1 gives the flowchart of the workflow and Table 4.1 provides a summary of methods for mapping the spatial distribution of oil.

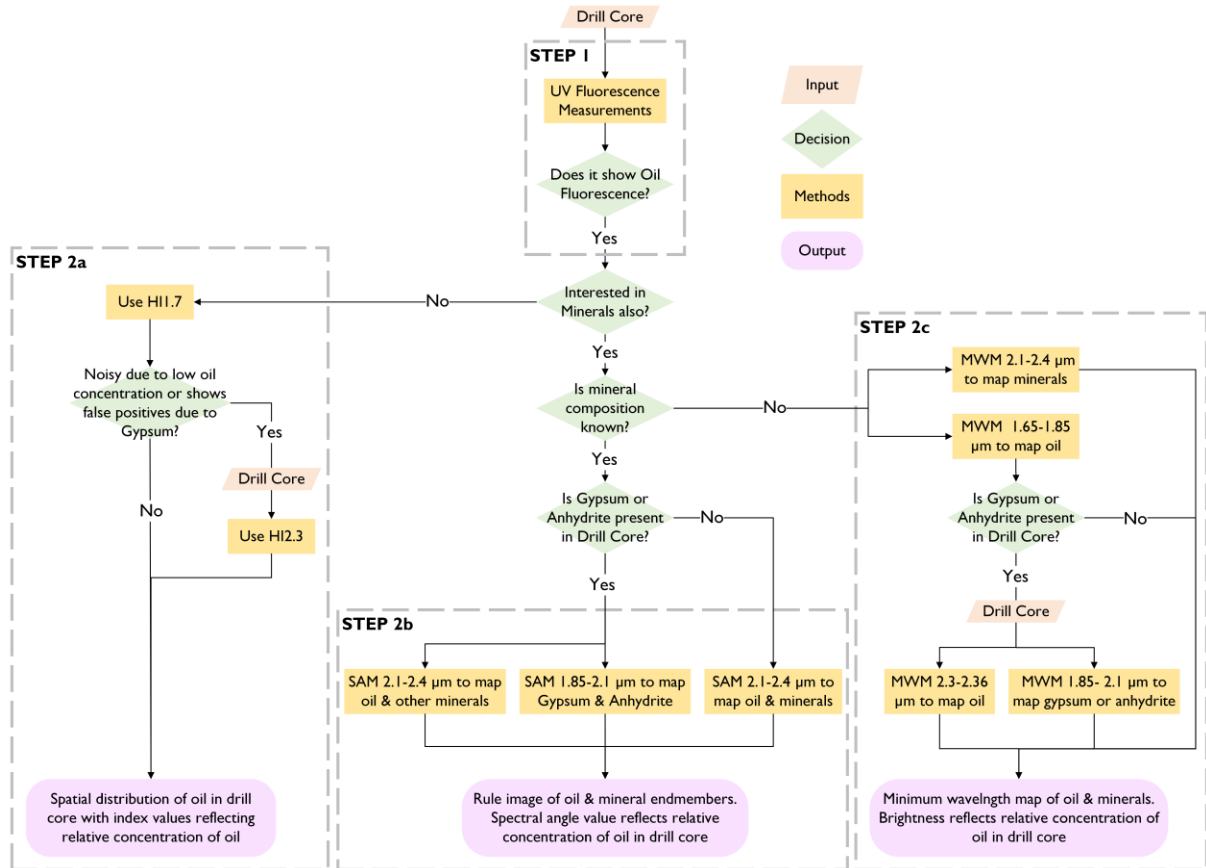


Figure 4.1 Flowchart of the workflow to detect (step 1) and map (step 2) the oil in drill cores.

Step 1:

UV fluorescence analysis proved effective in detecting the presence of both transparent and heavy oils in the respective drill cores, highlighting its utility across a spectrum of oil types. This approach laid the first step in confirming the presence of oil in the drill cores.

Step 2:

Step 2a should be used when only the spatial distribution of oil in the drill core is of interest. To delineate the spatial distribution of both oil and minerals within the drill core, either Step 2b or Step 2c can be used.

Step 2a:

The Hydrocarbon Index emerged as a robust approach for datasets primarily focused on oil spatial distribution. This method offered computational efficiency while specifically targeting the spatial distribution and concentration of oil. The choice between using the 1.7 μm or 2.3 μm absorption features in the Hydrocarbon Index depended on the oil concentration in the core and its mineral composition. HI1.7 is advantageous when oil concentration is high, resulting in a deep absorption feature, while the 2.3 μm absorption feature may have reached saturation. HI1.7 is also suitable when no overlapping minerals like gypsum and anhydrite are present. On the other hand, HI2.3 is preferable when the oil concentration in the drill core is low, such that the 2.3 μm absorption feature is not saturated and is deeper than the 1.7 μm feature. This index is also suitable in the presence of minerals like gypsum and anhydrite. However, the suitability of this feature in the presence of overlapping minerals like dolomite and chlorite still requires further investigation.

Step 2b:

Using SAM requires an understanding of the mineral composition of the drill cores beforehand. The 2.1 μm to 2.4 μm range is suitable for mapping the spatial distribution of oil in the drill core, as oil in this range shows high spectral angle values with the minerals present in the drill core. Gypsum and anhydrite can be differentiated from oil by mapping them in the 1.85 μm to 2.1 μm range. Other minerals like illite, muscovite, kaolinite, and calcite can be mapped in the range of 2.1 μm to 2.4 μm . However, chlorite and dolomite do not show high spectral values in this range. The suitability of using SAM in the range of 2.1 μm to 2.4 μm in the presence of chlorite and dolomite will require further examination.

Step 2c:

The Minimum Wavelength Mapper can also be used to map the oil and minerals in the drill cores. This method, however, requires prior knowledge of the absorption features of oil and minerals, as the output of the Minimum Wavelength Mapper is a map that indicates the wavelength values corresponding to the minima of the absorption features in the wavelength ranges specified by the user. These wavelengths from the minimum wavelength map must then be compared with the minimum wavelength values of characteristic absorption features of minerals to accurately determine their spatial distribution.

The wavelength ranges of 1.65 μm to 1.85 μm and 2.1 μm to 2.4 μm proved effective in mapping the oil, specifically the range of 2.3 μm to 2.36 μm . Gypsum and anhydrite can be mapped within the 1.85 μm to 2.1 μm range, while minerals such as illite, muscovite, and kaolinite can be mapped within the 2.1 μm to 2.4 μm range, specifically between 2.185 μm and 2.225 μm . However, calcite has overlapping features with oil and cannot be mapped in an oil-bearing drill core using this method. Although Figure 3.10 shows that the minimum wavelengths of chlorite and dolomite do not overlap with those of oil, their influence in mixed spectra requires further research.

Finally, the mapping methods discussed can be used to estimate the relative concentration of the oil within the drill core. The value of the Hydrocarbon Index reflects the relative concentration of oil in the drill core. For SAM, the spectral angle value of the rule image reflects the relative concentration of oil in the drill core, where smaller angles refer to higher concentrations. For the Minimum Wavelength Mapper, the feature depth bands can be used to indicate the relative concentration of oil in the drill core, with brighter values referring to higher concentrations.

While this study also aimed to classify the oil in the drill core in the VNIR and SWIR ranges based on the functional groups present, it was found that this was not feasible with the two drill cores used. In the SWIR range, the hetero-compounds show minor absorption features as overtones and combinations of N-H and O-H bonds. These minor absorption features are present at around 1.4 μm and 1.9 μm and are thus easily masked out by the OH or water absorption features of minerals and oil present in the drill core. Additionally, quartz and halite neither have distinct absorption features in the SWIR range nor do they exhibit 100% reflectance and, therefore, mask or diminish the already minor features of oil.

In conclusion, this study demonstrates the potential of a prototype workflow for mapping hyperspectral images of drill cores, focusing on the accurate detection and mapping of oil and minerals. UV fluorescence analysis effectively detected both transparent and heavy oils, serving as a crucial initial step in confirming oil presence. The Hydrocarbon Index provided a computationally efficient method for mapping oil, with specific wavelength features suited to different concentrations and mineral compositions. The Spectral Angle Mapper and Minimum Wavelength Mapper both offered robust spatial distribution mapping of oil and minerals, with the Spectral Angle Mapper requiring prior knowledge of endmembers and the Minimum Wavelength Mapper necessitating an understanding of absorption features. A limitation of this

workflow arises when drill cores contain minerals like chlorite and dolomite. While Section 3.1.4 shows that the minimum wavelengths of chlorite and dolomite do not overlap with those of oil, their influence in mixed spectra could be further investigated by analysing the mixed spectra from a drill core containing both oil and these minerals or by mixing powdered samples of the minerals with oil. This aspect, however, was not covered in this study.

Table 4.1 Summary of the methods used to map the spatial distribution of oil in a drill core. Green indicates suitable for mapping while red indicates not suitable for mapping for the given method, wavelength range, oil concentration and drill core mineral composition. Yellow indicates the suitability needs to be tested, which was not covered in this study.

Method	Absorption feature/range	Low Oil Concentration	High Oil Concentration	Presence of gypsum or anhydrite in the core	Presence of chlorite or dolomite in the core
Hydrocarbon Index	1.7 μm	Shallow feature, noisy	Deep feature	Overlap with oil feature	No overlap with oil feature
	2.3 μm	Deeper than 1.7 feature	If saturated	No overlap with oil feature	Probable overlap with oil feature
Spectral Angle Mapper (oil endmember)	1.65 μm to 1.85 μm range	Low pixel purity	High pixel purity	Low Spectral Angle value	High Spectral Angle value
	2.1 μm to 2.4 μm range	High pixel purity	If saturated	High Spectral Angle value	Low Spectral Angle value
Minimum Wavelength Mapper	1.65 μm to 1.85 μm range	Shallow feature	Deep feature	Overlap with oil feature	No overlap with oil feature
	2.1 μm to 2.4 μm range	Deeper than 1.7 feature	If saturated	No overlap, but gypsum feature deeper	No overlap with oil feature
	2.3 μm to 2.36 μm range	Deeper than 1.7 feature	If saturated	No overlap with oil feature	No overlap with oil feature

5. CONCLUSION

This section presents the conclusions of this study and provides recommendations for further research.

5.1. Conclusion

This research aims to measure and characterise the spectral properties of crude oil in the VNIR, SWIR and TIR range, integrate this into a prototype workflow and further apply this workflow to detect, map, and classify crude oil and minerals using the hyperspectral images of drill cores from the Dutch region.

The study characterized heavy, light, and very light oils used in this study through TIR, SWIR, and VNIR spectral analyses, along with UV fluorescence analysis. Across the TIR range, all oils exhibited absorption features attributed to C-H bonds from aliphatic and aromatic compounds, as well as bonds from various functional groups such as C=O, C-O, O-H, and N-H. Heavy oil additionally displayed water absorption features in this range. In the SWIR range, distinct C-H absorption features were evident, though water absorption often obscures other functional groups. Differentiating oil types in the SWIR range primarily relied on mean reflectance/transmittance values, with very light oil showing the highest transmittance, light oil showing intermediate transmittance, and heavy oil showing the lowest reflectance. The VNIR range further differentiated the oils: very light oil appeared transparent with no absorption, light oil exhibited a steep absorption slope, and heavy oil displayed a gentler slope. Finally, UV fluorescence analysis provided a rapid, non-destructive method for detecting oil presence.

Increasing oil thickness correlated with decreased mean transmittance values and increased absorption feature depth, facilitating the estimation of oil concentration in drill cores. However, saturation at 2.308 μm posed challenges in high oil concentration scenarios. Longer wavelength features, such as 2.308 μm , were more prominent due to stronger combination bands and first overtones, making them preferable for oil concentration mapping, though overlaps with mineral absorption features must be considered.

Comparison of absorption features of oil and mineral from typical hydrocarbon-bearing Dutch drill cores identified specific spectral ranges conducive to distinguishing oils from minerals, particularly 1.65 μm to 1.85 μm and 2.1 μm to 2.4 μm , which highlighted distinctive oil absorption features like 1.724 μm and 2.308 μm .

The mapping techniques used to map the oil and minerals in the drill core proved effective in revealing their spatial distribution in both the drill core with transparent oil and the drill core with heavy oil. This study utilized the Hydrocarbon Index, initially developed for HyMAP data, to map the oil in the drill cores. The Hydrocarbon Index was applied to the 1.7 μm absorption feature and then further modified to include the oil absorption feature at 2.3 μm . The modified Hydrocarbon Index, HI2.3, demonstrated a clearer and more accurate spatial distribution of oil compared to the original HI1.7.

This study also applied the Spectral Angle Mapper over four specific wavelength ranges, contrasting with previous studies that utilized the full spectral range. This targeted approach increased the sensitivity and accuracy of the method by focusing on ranges where the diagnostic absorption features of oil and minerals are most prominent. By narrowing the spectral analysis, SAM effectively differentiated the oil and minerals across various spectral ranges. Notably, the 2.1 μm to 2.4 μm range proved particularly effective for mapping oil and minerals in the drill core. Gypsum was mapped in the 1.85 μm to 2.1 μm range. This targeted application of SAM underscores its utility in improving the precision of oil and mineral mapping.

This study introduced the Minimum Wavelength Mapper as an innovative approach for mapping oil in drill cores. It was applied across four primary spectral ranges, with further subdivision of the final range into smaller intervals. These analyses enabled a thorough examination of mineral and oil distributions within both Drill Core 1 and Drill Core 2. Specifically, the ranges of 1.65 μm to 1.85 μm and 2.3 μm to 2.36 μm proved effective for mapping oil despite variations in spectra containing both gypsum and oil. By focusing on the interpolated wavelengths and depths of absorption features in the spectra, this method provided a more accurate understanding of mapping the oil and minerals in the drill core.

Finally, the study attempted to classify the oil in the drill core based on the functional groups present in the VNIR and SWIR ranges. While the absorption features due to C-H bonds from aliphatics and aromatics cause the diagnostic absorption features of oil, the absorption features due to the hetero-compounds cause minor absorption features. The absorption features of OH and water present in the minerals of the drill core easily mask these minor absorption features. Similarly, the water present in the oil can mask these features. Even in the absence of these interfering features, for oil present in a sandstone drill core, the quartz is not 100% reflective and, therefore, diminishes or masks the already minor features of oil due to the hetero-compounds. Thus, determining the functional groups present in the oil was not possible for the two drill cores used in this study.

Overall, this study demonstrates that oil and minerals can be mapped in oil bearing drill cores from the Netherlands, which contain lighter oil and minerals like gypsum and carbonates, whose absorption features lie close to that of oil. This study also shows that the oil present in the drill core cannot be classified based on its functional groups using the VNIR and SWIR spectra of the oil from the drill core. However, the relative concentration of the oil within the drill core can be determined by analysing the depth of the oil features using mapping techniques such as Hydrocarbon Index, Spectral Angle Mapper and Minimum Wavelength Mapper, which were used in this study.

5.2. Recommendations

The UV fluorescence analysis demonstrated its utility in detecting oil within the drill core. However, the 3-watt UV source used in this study proved insufficient for illumination, resulting in point illuminations with intensities too low to be captured effectively. Future studies should consider using a higher wattage UV source to address this limitation. A more powerful UV source would provide brighter illumination across the entire core, enabling the Specim VNIR camera to capture the spatial variation in the fluorescence intensity. Thus, the enhanced illumination would also allow for a better comparison between fluorescence mapping and other spectral mapping techniques, leading to more robust and reliable conclusions about the oil distribution.

6. ETHICAL CONSIDERATIONS, RISKS AND CONTINGENCIES

No reasonably predicted or anticipated adverse effects are expected to be experienced by any party during the research or as a result of its findings. The author is aware of the current policy in the Netherlands of reducing the use of fossil fuels in the energy transition framework. While preparing this work, the author used ChatGPT, and Grammarly to refine the language and grammar. After using this tool/service, the author reviewed and edited the content as needed and takes full responsibility for the content of the work.

LIST OF REFERENCES

- Ali, H. N. (2017). Fundamentals of Petroleum Geology. In *Springer Handbooks of Petroleum Technology* (pp. 321–357). Springer. https://doi.org/10.1007/978-3-319-49347-3_9
- Altawell, N. (2021). Crude oil. In *Rural Electrification* (pp. 39–80). Elsevier. <https://doi.org/10.1016/B978-0-12-822403-8.00003-5>
- Alves, J. C. L., & Poppi, R. J. (2015). Near-Infrared Spectroscopy in Analysis of Crudes and Transportation Fuels. In *Encyclopedia of Analytical Chemistry* (pp. 1–16). Wiley. <https://doi.org/10.1002/9780470027318.a1817.pub2>
- Asadzadeh, S., & Filho, C. R. de S. (2016). A review on spectral processing methods for geological remote sensing. *International Journal of Applied Earth Observation and Geoinformation*, 47, 69–90. <https://doi.org/10.1016/J.JAG.2015.12.004>
- Asadzadeh, S., & Filho, C. R. de S. (2017). Spectral remote sensing for onshore seepage characterization: A critical overview. *Earth-Science Reviews*, 168, 48–72. <https://doi.org/10.1016/j.earscirev.2017.03.004>
- Asemani, M., & Rabbani, A. R. (2020). Detailed FTIR spectroscopy characterization of crude oil extracted asphaltenes: Curve resolve of overlapping bands. *Journal of Petroleum Science and Engineering*, 185. <https://doi.org/10.1016/j.petrol.2019.106618>
- Ashena, R. (2023). Analysis of some case studies and a recommended idea for geothermal energy production from retrofitted abandoned oil and gas wells. *Geothermics*, 108, 102634. <https://doi.org/10.1016/J.GEOTHERMICS.2022.102634>
- Ayyad, M., & Parmigiano, J. (1983). *Helm Field Development Well Completion Report*. <https://www.nlog.nl/brh-web/rest/brh/document/896577072>
- Bakker, W. H. (2024). *nimbakker/hyppy: HypPy3 (hyppy-v3)*. Zenodo. <https://doi.org/10.5281/zenodo.11204368>
- Bakker, W., Ruitenbeek, F. J. A. van, & Werff, H. M. A. van der. (2011). Hyperspectral image mapping by automatic color coding of absorption features. *7th EARSEL Workshop on Imaging Spectroscopy*, 56–57. <https://research.utwente.nl/en/publications/hyperspectral-image-mapping-by-automatic-color-coding-of-absorpti>
- Baldrige, A. M., Hook, S. J., Grove, C. I., & Rivera, G. (2009). The ASTER spectral library version 2.0. *Remote Sensing of Environment*, 113(4), 711–715. <https://doi.org/10.1016/J.RSE.2008.11.007>
- Bouw, S., & Lutgert, J. (2012). Shale Plays in The Netherlands. *Society of Petroleum Engineers - SPE/EAGE European Unconventional Resources Conference and Exhibition 2012*, 623–634. <https://doi.org/10.2118/152644-MS>
- Canadian Association of Petroleum Producers. (2019). *Fracking in Canada | What is Hydraulic Fracturing & Is Fracking Bad?* <https://www.capp.ca/explore/hydraulic-fracturing/>
- Clark, R. N., King, T. V. V., Klejwa, M., Swayze, G. A., & Vergo, N. (1990). High spectral resolution reflectance spectroscopy of minerals. *Journal of Geophysical Research: Solid Earth*, 95(B8), 12653–12680. <https://doi.org/10.1029/JB095IB08P12653>
- Cloutis, E. A. (1989). Spectral Reflectance Properties of Hydrocarbons: Remote-Sensing Implications. *Science*, 245(4914), 165–168. <https://doi.org/10.1126/science.245.4914.165>
- Connan, J. (1984). Biodegradation of Crude Oils in Reservoirs. *Advances in Petroleum Geochemistry*, 1, 299–335. <https://doi.org/10.1016/B978-0-12-032001-1.50011-0>
- de Jager, J., & Geluk, M. (2007). Petroleum Geology. *Geology of the Netherlands*, 241–264. https://www.researchgate.net/publication/327750734_Petroleum_Geology_of_the_Netherlands

- den Hartog Jager, D. G. (1996). Fluvio-marine sequences in the Lower Cretaceous of the West Netherlands Basin: correlation and seismic expression. *Geology of Gas and Oil under the Netherlands*, 229–241. https://doi.org/10.1007/978-94-009-0121-6_19
- Eggertsson, G. H., Lavallée, Y., Kendrick, J. E., & Markússon, S. H. (2020). Improving fluid flow in geothermal reservoirs by thermal and mechanical stimulation: The case of Krafla volcano, Iceland. *Journal of Volcanology and Geothermal Research*, 391, 106351. <https://doi.org/10.1016/J.JVOLGEORES.2018.04.008>
- EIA. (2023). *Monthly Energy Review - May 2023*. <https://www.eia.gov/totalenergy/data/monthly/archive/00352305.pdf>
- Fang, Y., Wang, C., Elsworth, D., & Ishibashi, T. (2017). Seismicity-permeability coupling in the behavior of gas shales, CO₂ storage and deep geothermal energy. *Geomechanics and Geophysics for Geo-Energy and Geo-Resources*, 3(2), 189–198. <https://doi.org/10.1007/s40948-017-0051-9>
- Geluk, M. C. (2000). Late Permian (Zechstein) carbonate-facies maps, the Netherlands. *Netherlands Journal of Geosciences - Geologie En Mijnbouw*, 79(1), 17–27. <https://doi.org/10.1017/S0016774600021545>
- GMEX. (2008). *Spectral Interpretation Field Manual* (3rd ed., Vol. 1). AusSpec International Ltd.
- Groysman, A. (2014). Physico-Chemical Properties and Corrosiveness of Crude Oils and Petroleum Products. *Corrosion in Systems for Storage and Transportation of Petroleum Products and Biofuels*, 1–21. https://doi.org/10.1007/978-94-007-7884-9_1
- Hagemann, H. W., & Hollerbach, A. (1986). The fluorescence behaviour of crude oils with respect to their thermal maturation and degradation. *Organic Geochemistry*, 10(1–3), 473–480. [https://doi.org/10.1016/0146-6380\(86\)90047-1](https://doi.org/10.1016/0146-6380(86)90047-1)
- Hall, C., Tharakan, P., Hallock, J., Cleveland, C., & Jefferson, M. (2003). Hydrocarbons and the evolution of human culture. *Nature*, 426, 318–322. <https://doi.org/10.1038/nature02130>
- Hecker, C., Hook, S., van der Meijde, M., Bakker, W., van Werff, H., Wilbrink, H., van Ruitenbeek, F., de Smeth, B., & van der Meer, F. (2011). Thermal Infrared Spectrometer for Earth Science Remote Sensing Applications—Instrument Modifications and Measurement Procedures. *Sensors 2011, Vol. 11, Pages 10981-10999*, 11(11), 10981–10999. <https://doi.org/10.3390/S111110981>
- Hecker, C., van der Meijde, M., & van der Meer, F. D. (2010). Thermal infrared spectroscopy on feldspars - Successes, limitations and their implications for remote sensing. *Earth-Science Reviews*, 103(1), 60–70. <https://doi.org/10.1016/j.earscirev.2010.07.005>
- Hecker, C., van Ruitenbeek, F. J. A., Bakker, W. H., Fagbohun, B. J., Riley, D., van der Werff, H. M. A., & van der Meer, F. D. (2019). Mapping the wavelength position of mineral features in hyperspectral thermal infrared data. *International Journal of Applied Earth Observation and Geoinformation*, 79, 133–140. <https://doi.org/10.1016/J.JAG.2019.02.013>
- Hou, Y., Li, Y., Li, G., Tong, X., & Wang, Y. (2022). Oil-spill detection sensor using ultraviolet-induced fluorescence for routine surveillance in coastal environments. *Applied Physics B*, 128. <https://doi.org/10.1007/s00340-021-07741-3>
- Hsu, C. S., & Robinson, P. R. (2019). Chemical Composition. *Petroleum Science and Technology*, 39–56. https://doi.org/10.1007/978-3-030-16275-7_3
- Hunt, G. R., & Ashley, R. P. (1979). Spectra of altered rocks in the visible and near infrared. *Economic Geology*, 74(7), 1613–1629. <https://doi.org/10.2113/GSECONGEO.74.7.1613>
- Huntington, J., Mauger, A., Skirrow, R., Bastrakov, E., Connor, P., Mason, P., Keeling, J., Coward, D., Berman, M., Phillips, R., Whitbourn, L., & Heithersay, P. (2006). Automated mineralogical core logging at the Emmie Bluff iron oxide–copper–gold prospect. *MESA Journal*, 41, 38–44. <https://www.ausimm.com/publications/conference-proceedings/pacrim-2004/automated->

mineralogical-logging-of-core-from-the-emmie-bluff-iron-oxide-copper-gold-prospect-south-australia/

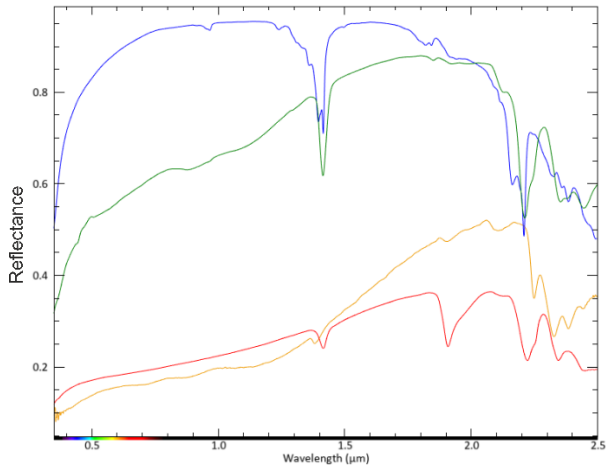
- Insights. (2023). *10 Must uses Of Crude Oil, Life without OIL seems impossible*. <https://insightss.co/10-must-uses-of-crude-oil-life-without-oil-seems-impossible/>
- Irina Smirnova. (1995). Geological and Geomorphological Study of the Amudariya Syncline (Middle Asia) for Petroleum-Bearing Structures Prediction: ABSTRACT. *AAPG Bulletin*, 79. <https://doi.org/10.1306/7834D256-1721-11D7-8645000102C1865D>
- Jiaqi, L. (2018). Application of Quantitative Fluorescence Analysis in Oilfield Development. *IOSR Journal of Engineering (IOSRJEN)*, 08(5), 1–6. https://iosrjen.org/Papers/vol8_issue5/Version-1/A0805010106.pdf
- Kang, M., Boutot, J., McVay, R. C., Roberts, K. A., Jasechko, S., Perrone, D., Wen, T., Lackey, G., Raimi, D., Digiulio, D. C., Shonkoff, S. B. C., William Carey, J., Elliott, E. G., Vorhees, D. J., & Peltz, A. S. (2023). Environmental risks and opportunities of orphaned oil and gas wells in the United States. *Environmental Research Letters*, 18(7), 074012. <https://doi.org/10.1088/1748-9326/ACDAE7>
- Kharrat, A. M., Zacharia, J., Cherian, V. J., & Anyatonwu, A. (2007). Issues with Comparing SARA Methodologies. *Energy & Fuels*, 21(6), 3618–3621. <https://doi.org/10.1021/ef700393a>
- Kiefer, J., & Corsetti, S. (2018). Raman and Infrared Spectroscopy of Crude Oil and its Constituents. In A. Shukla (Ed.), *Analytical Characterization Methods for Crude Oil and Related Products* (pp. 245–269). Wiley. <https://doi.org/10.1002/9781119286325.ch9>
- Kokaly, R. F., Clark, R. N., Swayze, G. A., Livo, K. E., Hoefen, T. M., Pearson, N. C., Wise, R. A., Benzel, W., Lowers, H. A., Driscoll, R. L., Klein, A. J., & Survey, U. S. G. (2017). USGS Spectral Library Version 7. In *Data Series*. <https://doi.org/https://doi.org/10.3133/ds1035>
- Kortekaas, M., Böker, U., van der Kooij, C., & Jaarsma, B. (2018). Lower Triassic reservoir development in the northern Dutch offshore. *Geological Society, London, Special Publications*, 469(1), 149–168. <https://doi.org/10.1144/SP469.19>
- Kühn, F., Oppermann, K., & Hörig, B. (2004). Hydrocarbon Index – an algorithm for hyperspectral detection of hydrocarbons. *International Journal of Remote Sensing*, 25(12), 2467–2473. <https://doi.org/10.1080/01431160310001642287>
- Lammoglia, T., & Filho, C. R. de S. (2011). Spectroscopic characterization of oils yielded from Brazilian offshore basins: Potential applications of remote sensing. *Remote Sensing of Environment*, 115(10), 2525–2535. <https://doi.org/10.1016/j.rse.2011.04.038>
- Linton, P., Kosanke, T., Greene, J., & Porter, B. (2023). The application of hyperspectral core imaging for oil and gas. *Geological Society, London, Special Publications*, 527(1), 95–119. <https://doi.org/10.1144/SP527-2022-2>
- Lyder, D., Feng, J., Rivard, B., Gallie, A., & Cloutis, E. (2010). Remote bitumen content estimation of Athabasca oil sand from hyperspectral infrared reflectance spectra using Gaussian singlets and derivative of Gaussian wavelets. *Fuel*, 89(3), 760–767. <https://doi.org/10.1016/j.fuel.2009.03.027>
- Meerdink, S. K., Hook, S. J., Roberts, D. A., & Abbott, E. A. (2019). The ECOSTRESS spectral library version 1.0. *Remote Sensing of Environment*, 230, 111196. <https://doi.org/10.1016/J.RSE.2019.05.015>
- Mijnlieff, H. F. (2020). Introduction to the geothermal play and reservoir geology of the Netherlands. *Netherlands Journal of Geosciences*, 99. <https://doi.org/10.1017/njg.2020.2>
- Munsterman, D. K., Verreussel, R. M. C. H., Mijnlieff, H. F., Witmans, N., Kerstholt-Boegehold, S., & Abbink, O. A. (2012). Revision and update of the Callovian-Ryazanian Stratigraphic Nomenclature in the northern Dutch offshore, i.e. Central Graben Subgroup and Scruff Group. *Netherlands Journal of Geosciences*, 91(4), 555–590. <https://doi.org/10.1017/S001677460000038X>

- Nian, Y. Le, & Cheng, W. L. (2018). Insights into geothermal utilization of abandoned oil and gas wells. *Renewable and Sustainable Energy Reviews*, 87, 44–60. <https://doi.org/10.1016/J.RSER.2018.02.004>
- Olivarius, M., Weibel, R., Friis, H., Boldreel, L. O., Keulen, N., & Thomsen, T. B. (2017). Provenance of the Lower Triassic Bunter Sandstone Formation: implications for distribution and architecture of aeolian vs. fluvial reservoirs in the North German Basin. *Basin Research*, 29, 113–130. <https://doi.org/10.1111/BRE.12140>
- Pabón, R. E. C., & Filho, C. R. de S. (2019). Crude oil spectral signatures and empirical models to derive API gravity. *Fuel*, 237, 1119–1131. <https://doi.org/10.1016/j.fuel.2018.09.098>
- Palmer, S. E. (1993). *Effect of Biodegradation and Water Washing on Crude Oil Composition*. 511–533. https://doi.org/10.1007/978-1-4615-2890-6_23
- Peng, S., Mei-ping, S., & Ju-bai, A. (2013). Study of Prediction Models for Oil Thickness Based on Spectral Curve. *Spectroscopy and Spectral Analysis*, 33(07), 1881–1885. <https://www.gpxygpfx.com/EN/abstract/abstract6432.shtml>
- Rivard, B., Lyder, D., Feng, J., Gallie, A., Cloutis, E., Dougan, P., Gonzalez, S., Cox, D., & Lipsett, M. G. (2010). Bitumen content estimation of Athabasca oil sand from broad band infrared reflectance spectra. *The Canadian Journal of Chemical Engineering*, 88(5), 830–838. <https://doi.org/10.1002/CJCE.20343>
- Robbmond, R., Jaggie, F., Taylor, G., & Geerlings, L. (2002). *Final Wellsite Geological Report: Well Q4-10*. <https://www.nlog.nl/brh-web/rest/brh/document/936274268>
- Romdhane, A., Emmel, B., Zonetti, S., Dupuy, B., Gawel, K., Edvardsen, L., & Bhuiyan, M. H. (2022). Screening, Monitoring, and Remediation of Legacy Wells to Improve Reservoir Integrity for Large-Scale CO₂ Storage—An example from the Smeaheia structure in the Northern North Sea. *Frontiers in Energy Research*, 10, 826100. <https://doi.org/10.3389/FENRG.2022.826100/BIBTEX>
- Ryder, A. G. (2005). Analysis of Crude Petroleum Oils Using Fluorescence Spectroscopy. *Reviews in Fluorescence 2005*, 169–198. https://doi.org/10.1007/0-387-23690-2_8
- Scafutto, R. D. M., & Filho, C. R. de S. (2016). Quantitative characterization of crude oils and fuels in mineral substrates using reflectance spectroscopy: Implications for remote sensing. *International Journal of Applied Earth Observation and Geoinformation*, 50, 221–242. <https://doi.org/10.1016/J.JAG.2016.03.017>
- Scafutto, R. D. P. M., Lievens, C., Hecker, C., van der Meer, F. D., & Souza Filho, C. R. de. (2021). Detection of petroleum hydrocarbons in continental areas using airborne hyperspectral thermal infrared data (SEBASS). *Remote Sensing of Environment*, 256, 112323. <https://doi.org/10.1016/J.RSE.2021.112323>
- Schodlok, M. C., Whitbourn, L., Huntington, J., Mason, P., Green, A., Berman, M., Coward, D., Connor, P., Wright, W., Jolivet, M., & Martinez, R. (2016). HyLogger-3, a visible to shortwave and thermal infrared reflectance spectrometer system for drill core logging: functional description. *Australian Journal of Earth Sciences*, 63(8), 929–940. <https://doi.org/10.1080/08120099.2016.1231133>
- Sebborn, Les. K. (1982). *Reservoir Fluid Study for Union Oil Company of Netherlands Inc*. <https://www.nlog.nl/brh-web/rest/brh/document/896577073>
- Selley, R. C., & Sonnenberg, S. A. (2022). Elements of Petroleum Geology. In *Elements of Petroleum Geology* (Fourth Edition). Elsevier. <https://doi.org/10.1016/C2019-0-04461-5>
- Shchepetkina, A., Speta, M., Gingras, M. K., Rivard, B., Pemberton, S. G., & Keighley, D. (2017). Hyperspectral imaging as an aid for facies analysis in massive-appearing sediments: a case study from the middle McMurray Formation. *Bulletin of Canadian Petroleum Geology*, 65(2), 262–278. <https://doi.org/10.2113/gscpgbull.65.2.262>

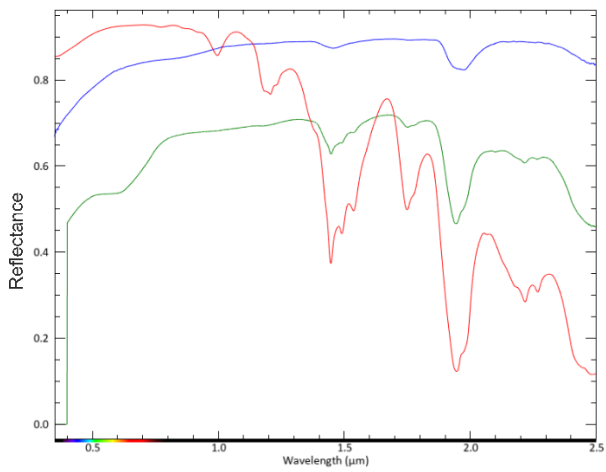
- Sherman, D. M. (1985). The electronic structures of Fe³⁺ coordination sites in iron oxides: Applications to spectra, bonding, and magnetism. *Physics and Chemistry of Minerals*, 12(3), 161–175. <https://doi.org/10.1007/BF00308210/METRICS>
- Smith, B. (1998). Infrared Spectral Interpretation. In *Infrared Spectral Interpretation: A Systematic Approach*. CRC Press. <https://doi.org/10.1201/9780203750841>
- Speta, M. (2016). *Hyperspectral imaging for the characterization of Athabasca oil sands core* [Doctoral dissertation Thesis, University of Alberta]. <https://doi.org/10.7939/R3280541K>
- Speta, M., Gingras, M. K., & Rivard, B. (2016). Shortwave Infrared Hyperspectral Imaging: A Novel Method For Enhancing the Visibility of Sedimentary And Biogenic Features In Oil-Saturated Core. *Journal of Sedimentary Research*, 86(7), 830–842. <https://doi.org/10.2110/jsr.2016.54>
- Speta, M., Rivard, B., & Feng, J. (2018). Shortwave infrared (1.0–2.5 μm) hyperspectral imaging of the Athabasca West Grand Rapids Formation oil sands. *AAPG Bulletin*, 102(09), 1671–1683. <https://doi.org/10.1306/01081817264>
- Speta, M., Rivard, B., Feng, J., Lipsett, M., & Gingras, M. (2013). Hyperspectral imaging for the characterization of athabasca oil sands drill core. *2013 IEEE International Geoscience and Remote Sensing Symposium - IGARSS*, 2184–2187. <https://doi.org/10.1109/IGARSS.2013.6723248>
- Speta, M., Rivard, B., Feng, J., Lipsett, M., & Gingras, M. (2015). Hyperspectral imaging for the determination of bitumen content in Athabasca oil sands core samples. *AAPG Bulletin*, 99(07), 1245–1259. <https://doi.org/10.1306/03021514121>
- Steffens, J., Landulfo, E., Courrol, L. C., & Guardani, R. (2011). Application of fluorescence to the study of crude petroleum. *Journal of Fluorescence*, 21(3), 859–864. <https://doi.org/10.1007/S10895-009-0586-4>
- Stuart, B. H. (2004). Infrared Spectroscopy: Fundamentals and Applications. In *Infrared Spectroscopy: Fundamentals and Applications*. Wiley. <https://doi.org/10.1002/0470011149>
- Tissot, B. P., & Welte, D. H. (1984). Petroleum Formation and Occurrence. In *Petroleum Formation and Occurrence* (Second Edition). Springer Berlin Heidelberg. <https://doi.org/10.1007/978-3-642-87813-8>
- van Ruitenbeek, F. J. A., Bakker, W. H., van der Werff, H. M. A., Zegers, T. E., Oosthoek, J. H. P., Omer, Z. A., Marsh, S. H., & van der Meer, F. D. (2014). Mapping the wavelength position of deepest absorption features to explore mineral diversity in hyperspectral images. *Planetary and Space Science*, 101, 108–117. <https://doi.org/10.1016/j.pss.2014.06.009>
- Verweij, H. J. M. (2003). *Fluid flow systems analysis on geological timescales in onshore and offshore Netherlands. With special reference to the Broad Fourteens Basin Fluid flow systems analysis on geological timescales in onshore and offshore Netherlands* [Doctoral dissertation Thesis, Vrije Universiteit Amsterdam]. <https://research.vu.nl/en/publications/fluid-flow-systems-analysis-on-geological-timescales-in-onshore-a>
- Verweij, H. J. M., & Simmelink, H. J. (2002). Geodynamic and hydrodynamic evolution of the Broad Fourteens Basin (The Netherlands) in relation to its petroleum systems. *Marine and Petroleum Geology*, 19(3), 339–359. [https://doi.org/10.1016/S0264-8172\(02\)00021-1](https://doi.org/10.1016/S0264-8172(02)00021-1)
- Verweij, H. J. M., Simmelink, H. J., Van Balen, R. T., & David, P. (2003). History of petroleum systems in the southern part of the Broad Fourteens Basin. *Netherlands Journal of Geosciences - Geologie En Mijnbouw*, 82(1), 71–90. <https://doi.org/10.1017/S0016774600022800>

APPENDIX

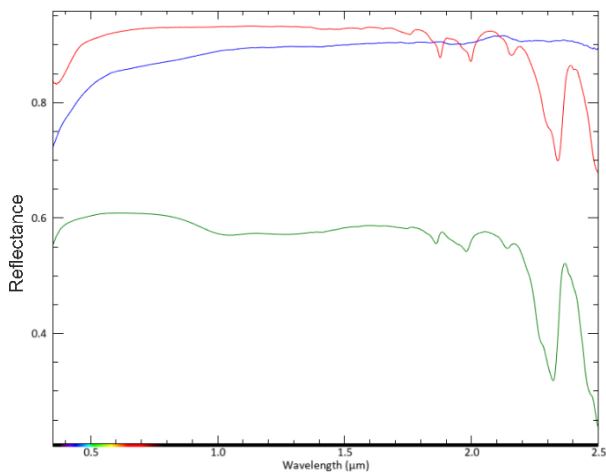
Annex 1: Spectra of Other Minerals from USGS and ECOSTRESS spectral libraries.



Spectra of illite (red), muscovite (green), kaolinite (blue) and chlorite (yellow).



Spectra of gypsum (red), anhydrite (green) and halite (blue).



Spectra of calcite (red), dolomite (green) and quartz (blue).

Four deepest absorption features of the oil and minerals in the respective ranges.

1100-1650				
	First	Second	Third	Fourth
Oil	1.193	1.209	1.391	1.412
Illite	1.415			
Muscovite	1.414			
Kaolinite	1.415	1.396	1.360	1.240
Chlorite	1.381			
Gypsum	1.446	1.490	1.536	1.206
Anhydrite	1.447	1.489	1.538	
Calcite				
Dolomite				
Halite				

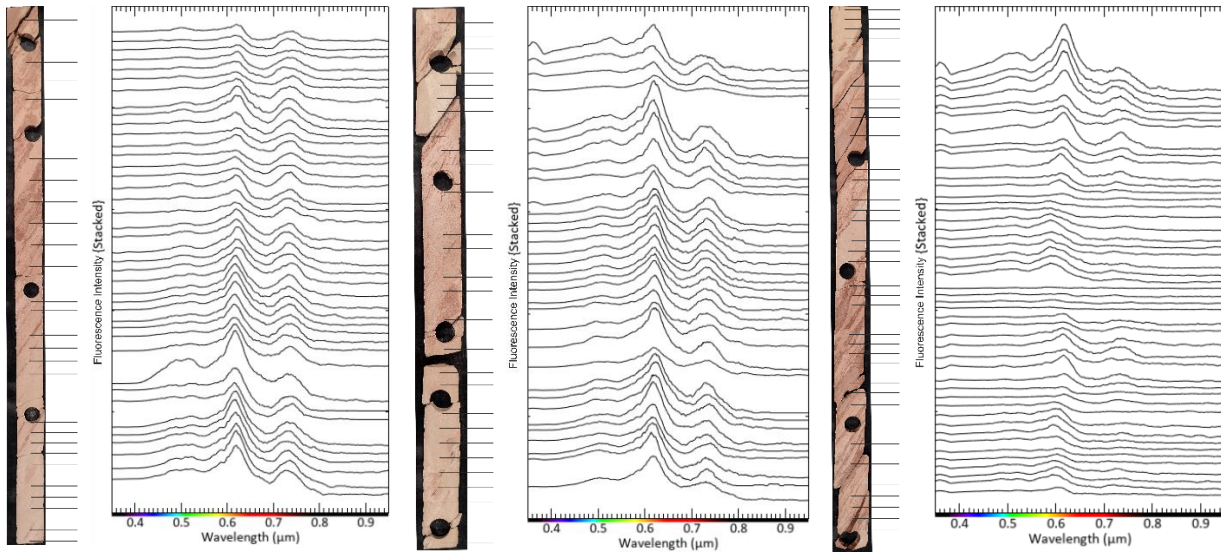
1650-1850				
	First	Second	Third	Fourth
Oil	1.724	1.761	1.704	1.796
Illite				
Muscovite				
Kaolinite	1.820	1.843		
Chlorite				
Gypsum	1.749			
Anhydrite	1.750			
Calcite				
Dolomite				
Halite				

1850-2100				
	First	Second	Third	Fourth
Oil	2.008			
Illite	1.908			
Muscovite	1.851	1.922		
Kaolinite	1.913	1.819		
Chlorite	1.904			
Gypsum	1.946	2.067		
Anhydrite	1.947	2.069		
Calcite	1.997	1.876		
Dolomite	1.979	1.861		
Halite	1.971			

2100-2460				
	First	Second	Third	Fourth
Oil	2.308	2.347	2.399	2.457
Illite	2.222	2.345	2.437	2.132
Muscovite	2.211	2.353	2.443	2.374
Kaolinite	2.208	2.162	2.384	2.359
Chlorite	2.326	2.385	2.248	2.441
Gypsum	2.217	2.268		
Anhydrite	2.218	2.269		
Calcite	2.340	2.158		
Dolomite	2.322	2.141		
Halite				

Annex 2: UV Fluorescence Measurements

Drill Core 1

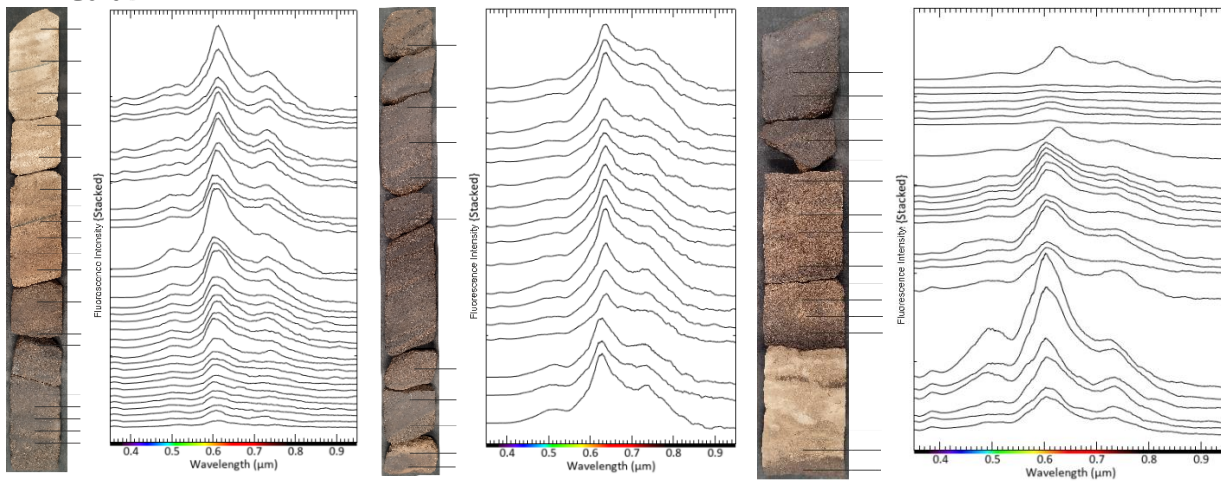


2668 m to 2669 m

2669 m to 2670 m

2670 m to 2671 m

Drill Core 2



1247 m to 1248 m

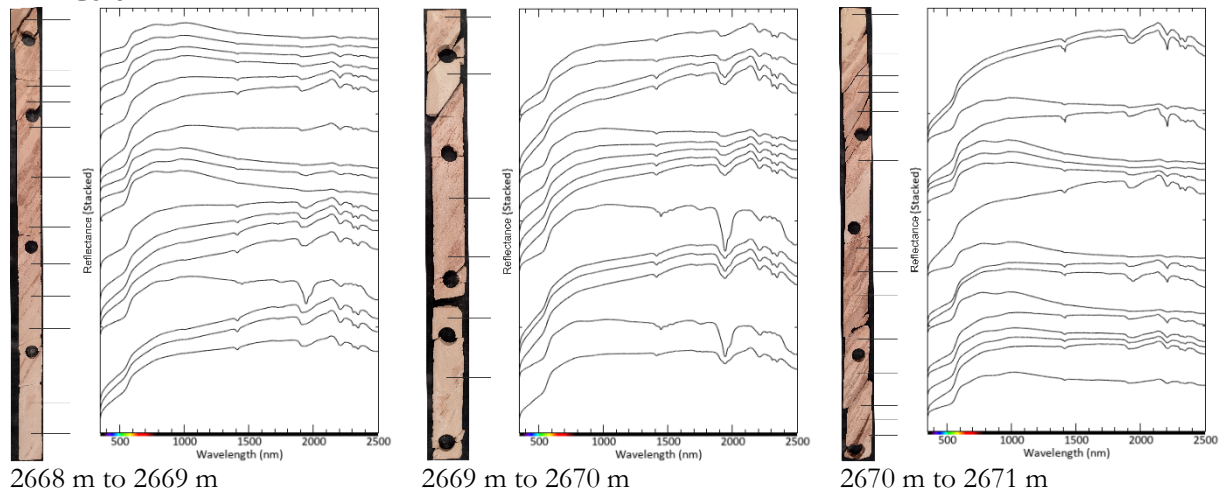
1248 m to 1249 m

1249 m to 1250 m

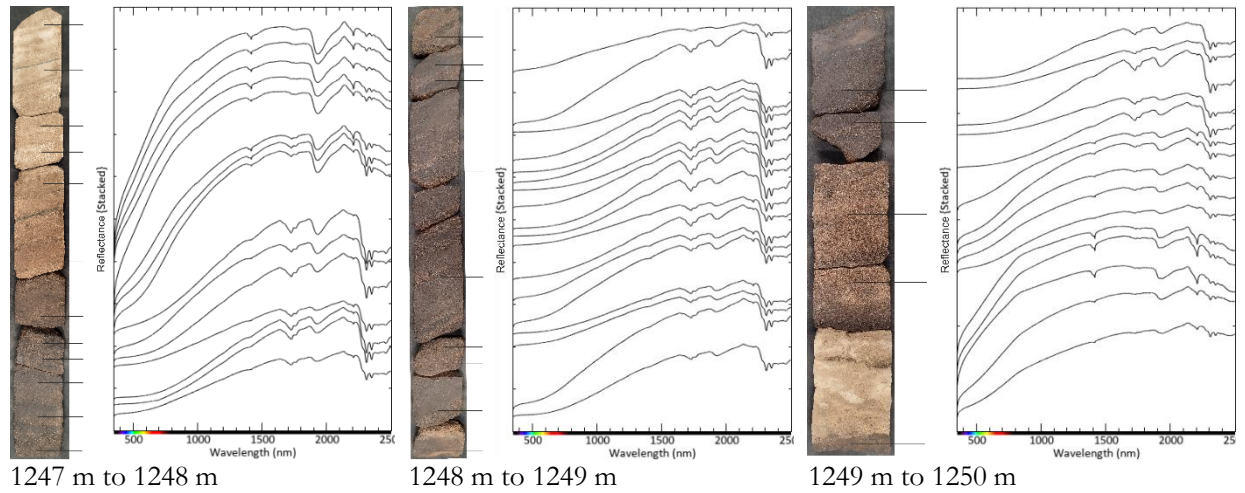
The indications on the drill core mark the region from where the spectra were recorded.

Annex 3: Point Spectroscopy Measurements

Drill Core 1



Drill Core 2



The indications on the drill core mark the region from where the spectra were recorded.

Annex 4: Spectral Angle Matrix for the range of 1.1 μm to 2.4 μm .

